

Wave propagation in three-dimensional fractional viscoelastic infinite solid body

Sladjan Jelić¹ Dušan Zorica^{2 3 *}

January 29, 2024

Abstract

In order to analyze the wave propagation in three-dimensional isotropic and viscoelastic body, the Cauchy initial value problem on unbounded domain is considered for the wave equation written as a system of fractional partial differential equations consisting of equation of motion of three-dimensional solid body, equation of strain, as well as of the constitutive equation, obtained by generalizing the classical Hooke's law of three-dimensional isotropic and elastic body by replacing Lamé coefficients with the relaxation moduli to account for different memory kernels corresponding to the propagation of compressive and shear waves. By the use of the method of integral transforms, namely Laplace and Fourier transforms, the displacement field, as a solution of the Cauchy initial value problem, is expressed through Green's functions corresponding to both compressive and shear wave propagation. Two approaches are adopted in solving the Cauchy problem: in the first one the displacement field is expressed through the scalar and vector fields, obtained as solutions of wave equations which are consequences of decoupling the wave equation for displacement field, while in the second approach the displacement field is obtained by the action of the resolvent tensor on the initial conditions. Fractional anti-Zener and Zener model I⁺ID.ID, as well as fractional Burgers model VII, as representatives of models yielding infinite and finite wave propagation speed, are used in numerical calculations and graphical representations of Green's functions and its short and large time asymptotic behavior.

Key words: wave propagation in three-dimensional isotropic and viscoelastic body, compressive and shear waves, thermodynamically consistent fractional models of viscoelastic body, relaxation moduli as memory functions generalizing Lamé coefficients

1 Introduction

The wave equation for three-dimensional isotropic and elastic body, written in terms of displacement field $\mathbf{u} = \mathbf{u}(\mathbf{r}, t)$, which is calculated at the point determined by the radius vector $\mathbf{r} \in \mathbb{R}^3$ at time instant $t > 0$, takes the form

$$\frac{\mu}{\varrho} \Delta \mathbf{u}(\mathbf{r}, t) + \frac{\lambda + \mu}{\varrho} \text{grad div } \mathbf{u}(\mathbf{r}, t) + \mathbf{f}_b(\mathbf{r}, t) = \partial_{tt}^2 \mathbf{u}(\mathbf{r}, t), \quad (1)$$

representing an equation obtained by reduction of the system of equations consisting of the equation of motion of deformable solid body

$$\frac{1}{\varrho} \text{div } \hat{\boldsymbol{\sigma}}(\mathbf{r}, t) + \mathbf{f}_b(\mathbf{r}, t) = \partial_{tt}^2 \mathbf{u}(\mathbf{r}, t), \quad (2)$$

equation of infinitesimal strain

$$\hat{\boldsymbol{\varepsilon}}(\mathbf{r}, t) = \frac{1}{2} \left(\text{grad } \mathbf{u}(\mathbf{r}, t) + (\text{grad } \mathbf{u}(\mathbf{r}, t))^T \right), \quad (3)$$

and Hooke's law

$$\hat{\boldsymbol{\sigma}}(\mathbf{r}, t) = \lambda \text{tr} \hat{\boldsymbol{\varepsilon}}(\mathbf{r}, t) \hat{\mathbf{I}} + 2\mu \hat{\boldsymbol{\varepsilon}}(\mathbf{r}, t) \quad (4)$$

as a constitutive equation, where λ and μ are Lamé coefficients corresponding to an isotropic and elastic body, ϱ is material density, while \mathbf{f}_b are body forces per unit mass, $\hat{\boldsymbol{\sigma}}$ is the Cauchy stress tensor, $\hat{\boldsymbol{\varepsilon}}$ is the infinitesimal strain tensor, and $\hat{\mathbf{I}}$ is the identity tensor. The wave equation (1), rewritten as

$$c_c^2 \text{grad div } \mathbf{u}(\mathbf{r}, t) - c_s^2 \text{curl curl } \mathbf{u}(\mathbf{r}, t) + \mathbf{f}_b(\mathbf{r}, t) = \partial_{tt}^2 \mathbf{u}(\mathbf{r}, t), \quad (5)$$

¹ Department of Physics, Faculty of Sciences, University of Novi Sad, Trg D. Obradovića 4, 21000 Novi Sad, Serbia, sladjan.jelic@df.uns.ac.rs

² Department of Physics, Faculty of Sciences, University of Novi Sad, Trg D. Obradovića 4, 21000 Novi Sad, Serbia, dušan.zorica@df.uns.ac.rs

³ Mathematical Institute, Serbian Academy of Arts and Sciences, Kneza Mihaila 36, 11000 Belgrade, Serbia, dušan_zorica@mi.sanu.ac.rs

* Corresponding author

in terms of speeds of compressive and shear waves $c_c = \sqrt{\frac{\lambda+2\mu}{\rho}}$ and $c_s = \sqrt{\frac{\mu}{\rho}}$ respectively, decomposes by the application of divergence and curl operators into two three-dimensional wave equations

$$c_c^2 \Delta \varphi(\mathbf{r}, t) - \partial_{tt}^2 \varphi(\mathbf{r}, t) = -\operatorname{div} \mathbf{f}_b(\mathbf{r}, t), \quad \text{with} \quad \varphi(\mathbf{r}, t) = \operatorname{div} \mathbf{u}(\mathbf{r}, t), \quad (6)$$

$$c_s^2 \Delta \boldsymbol{\Omega}(\mathbf{r}, t) - \partial_{tt}^2 \boldsymbol{\Omega}(\mathbf{r}, t) = -\operatorname{curl} \mathbf{f}_b(\mathbf{r}, t), \quad \text{with} \quad \boldsymbol{\Omega}(\mathbf{r}, t) = \operatorname{curl} \mathbf{u}(\mathbf{r}, t), \quad (7)$$

governing the propagation of compressive and shear waves respectively, see [2].

The reflection of three-dimensional elastic waves is considered in [40] by analyzing the wave equations for both scalar and vector fields in the case when there are no body forces, while three-dimensional elastic wave propagation is analyzed in [22, 29, 43] using cylindrical coordinates. Further considerations of wave propagation in periodic media are contained in [9, 10, 11].

Coupling the mechanical and thermal effects by considering wave propagation in three-dimensional thermo-elastic media is conducted in [35] by examining the propagation of plane-waves and considering the wave equations for scalar and vector fields, while in [12] the wave propagation is considered in thermo-elastic cylindrical media. Further, the reflection of three-dimensional plane waves in a highly anisotropic thermo-elastic material is analyzed in [36]. Numerical methods are used in [4] and [28] for description of shock wave propagation, as well as for three-dimensional elastic wave propagation on unbounded domain.

Aiming to generalize the classical three-dimensional wave equation for isotropic and elastic body, given by (1) or equivalently by (5), to the three-dimensional wave equation for isotropic and viscoelastic body, the approach arising from the considerations of one-dimensional viscoelastic body is adopted, where the stress, instead by Hooke's law $\sigma = E\varepsilon$, with E being the Young modulus, can be expressed in terms of strain through the relaxation modulus σ_{sr} as

$$\sigma(t) = \frac{d}{dt} (\sigma_{sr}(t) *_t \varepsilon(t)) = \frac{d}{dt} \int_0^t \sigma_{sr}(t-t') \varepsilon(t') dt', \quad (8)$$

where $*_t$ denotes the convolution in time, thus having different material properties of viscoelastic body accounted by the choice of different relaxation moduli. Note, the relaxation modulus is a function accounting for the time evolution of stress having the strain in the constitutive equation assumed as the Heaviside step function. Namely, the classical Hooke's law (4), being of the form

$$\begin{aligned} \sigma_{11} &= (\lambda + 2\mu) \varepsilon_{11} + \lambda \varepsilon_{22} + \lambda \varepsilon_{33}, & \text{i.e.,} & \quad \frac{1}{\rho} \sigma_{11} = c_c^2 \varepsilon_{11} + (c_c^2 - 2c_s^2) \varepsilon_{22} + (c_c^2 - 2c_s^2) \varepsilon_{33}, \\ \sigma_{22} &= \lambda \varepsilon_{11} + (\lambda + 2\mu) \varepsilon_{22} + \lambda \varepsilon_{33}, & \text{i.e.,} & \quad \frac{1}{\rho} \sigma_{22} = (c_c^2 - 2c_s^2) \varepsilon_{11} + c_c^2 \varepsilon_{22} + (c_c^2 - 2c_s^2) \varepsilon_{33}, \\ \sigma_{33} &= \lambda \varepsilon_{11} + \lambda \varepsilon_{22} + (\lambda + 2\mu) \varepsilon_{33}, & \text{i.e.,} & \quad \frac{1}{\rho} \sigma_{33} = (c_c^2 - 2c_s^2) \varepsilon_{11} + (c_c^2 - 2c_s^2) \varepsilon_{22} + c_c^2 \varepsilon_{33}, \\ \sigma_{12} &= 2\mu \varepsilon_{12}, & \text{i.e.,} & \quad \frac{1}{\rho} \sigma_{12} = 2c_s^2 \varepsilon_{12}, \\ \sigma_{13} &= 2\mu \varepsilon_{13}, & \text{i.e.,} & \quad \frac{1}{\rho} \sigma_{13} = 2c_s^2 \varepsilon_{13}, \\ \sigma_{23} &= 2\mu \varepsilon_{23}, & \text{i.e.,} & \quad \frac{1}{\rho} \sigma_{23} = 2c_s^2 \varepsilon_{23}, \end{aligned}$$

is generalized by employing two different relaxation moduli $\sigma_{sr}^{(c)}$ and $\sigma_{sr}^{(s)}$ instead of speeds of compressive and shear waves, c_c and c_s , yielding

$$\begin{aligned} \sigma_{11} &= \partial_t \left(\sigma_{sr}^{(c)} *_t \varepsilon_{11} \right) + \partial_t \left(\sigma_{sr}^{(c,s)} *_t \varepsilon_{22} \right) + \partial_t \left(\sigma_{sr}^{(c,s)} *_t \varepsilon_{33} \right), & \sigma_{12} &= 2\partial_t \left(\sigma_{sr}^{(s)} *_t \varepsilon_{12} \right), \\ \sigma_{22} &= \partial_t \left(\sigma_{sr}^{(c,s)} *_t \varepsilon_{11} \right) + \partial_t \left(\sigma_{sr}^{(c)} *_t \varepsilon_{22} \right) + \partial_t \left(\sigma_{sr}^{(c,s)} *_t \varepsilon_{33} \right), & \sigma_{13} &= 2\partial_t \left(\sigma_{sr}^{(s)} *_t \varepsilon_{13} \right), \\ \sigma_{33} &= \partial_t \left(\sigma_{sr}^{(c,s)} *_t \varepsilon_{11} \right) + \partial_t \left(\sigma_{sr}^{(c,s)} *_t \varepsilon_{22} \right) + \partial_t \left(\sigma_{sr}^{(c)} *_t \varepsilon_{33} \right), & \sigma_{23} &= 2\partial_t \left(\sigma_{sr}^{(s)} *_t \varepsilon_{23} \right), \end{aligned}$$

with $\sigma_{sr}^{(c,s)} = \sigma_{sr}^{(c)} - 2\sigma_{sr}^{(s)}$, and reducing to

$$\hat{\boldsymbol{\sigma}}(\mathbf{r}, t) = \partial_t \left(\sigma_{sr}^{(c,s)}(t) *_t \operatorname{tr} \hat{\boldsymbol{\varepsilon}}(\mathbf{r}, t) \right) \hat{\mathbf{I}} + 2\partial_t \left(\sigma_{sr}^{(s)}(t) *_t \hat{\boldsymbol{\varepsilon}}(\mathbf{r}, t) \right), \quad (9)$$

thus generalizing the characteristics of compressive and shear wave propagation by taking into account viscous properties of isotropic body besides the elastic ones, implying different type of compressive and shear excitation propagation. The constitutive equation of three-dimensional viscoelastic body (9) is further used along with the

equation of motion of deformable solid body (2) and strain (3) in order to formulate and solve the corresponding wave equation.

Linear fractional-order models of one-dimensional viscoelastic body, taking the most general form

$$\sum_{k=1}^{N_1} a_k {}_0I_t^{\alpha_k} \sigma(t) + \sum_{k=1}^{N_2} b_k {}_0D_t^{\beta_k} \sigma(t) = \sum_{k=1}^{M_1} c_k {}_0I_t^{\mu_k} \varepsilon(t) + \sum_{k=1}^{M_2} d_k {}_0D_t^{\nu_k} \varepsilon(t), \quad (10)$$

containing non-negative model parameters a_k, b_k, c_k, d_k , as well as fractional integration and differentiation orders $\alpha_k, \beta_k, \mu_k, \nu_k$, that can belong to both intervals $(0, 1)$ and $(1, 2)$, are among the constitutive models that yield stress expressed in terms of strain through the relaxation modulus according to expression (8), where the fractional integral of order $\mu > 0$ and Riemann-Liouville fractional derivative of order $n + \nu$, with $n \in \mathbb{N}_0$ and $\nu \in (0, 1)$, appearing in (10), are respectively defined by

$$\begin{aligned} {}_0I_t^\mu f(t) &= \frac{t^{\mu-1}}{\Gamma(\mu)} * f(t) = \frac{1}{\Gamma(\mu)} \int_0^t \frac{f(t')}{(t-t')^{1-\mu}} dt' \quad \text{and} \\ {}_0D_t^{n+\nu} f(t) &= \frac{d^{n+1}}{dt^{n+1}} {}_0I_t^{1-\nu} f(t) = \frac{d^{n+1}}{dt^{n+1}} \left(\frac{t^{-\nu}}{\Gamma(1-\nu)} * f(t) \right), \end{aligned}$$

see [17]. Namely, the application of Laplace transform with respect to time, defined by

$$\tilde{f}(s) = \mathcal{L}[f(t)](s) = \int_0^\infty f(t) e^{-st} dt, \quad \text{Re } s > 0, \quad (11)$$

according to the Laplace transforms of fractional integral and Riemann-Liouville fractional derivative

$$\mathcal{L}[{}_0I_t^\mu f(t)](s) = \frac{1}{s^\mu} \tilde{f}(s), \quad \mu > 0 \quad \text{and} \quad (12)$$

$$\mathcal{L}[{}_0D_t^{n+\nu} f(t)](s) = s^{n+\nu} \hat{f}(s) - \sum_{k=0}^n \left[\frac{d^k}{dt^k} {}_0I_t^{1-\nu} f(t) \right]_{t=0} s^{n-k} = s^{n+\nu} \hat{f}(s), \quad \nu \in (0, 1), \quad (13)$$

obtained assuming that function f is bounded at zero, transforms the constitutive model (10) into

$$\Phi_\sigma(s) \tilde{\sigma}(s) = \Phi_\varepsilon(s) \tilde{\varepsilon}(s), \quad \text{yielding} \quad \tilde{E}(s) = \frac{\tilde{\sigma}(s)}{\tilde{\varepsilon}(s)} = \frac{\Phi_\varepsilon(s)}{\Phi_\sigma(s)}, \quad \text{with} \quad (14)$$

$$\Phi_\sigma(s) = \sum_{k=1}^{N_1} a_k \frac{1}{s^{\alpha_k}} + \sum_{k=1}^{N_2} b_k s^{\beta_k} \quad \text{and} \quad \Phi_\varepsilon(s) = \sum_{k=1}^{M_1} c_k \frac{1}{s^{\mu_k}} + \sum_{k=1}^{M_2} d_k s^{\nu_k}, \quad (15)$$

where \tilde{E} denotes the complex modulus, implying the relaxation modulus in Laplace domain to be of the form

$$\tilde{\sigma}_{sr}(s) = \frac{1}{s} \frac{\Phi_\varepsilon(s)}{\Phi_\sigma(s)} = \frac{1}{s} \tilde{E}(s), \quad (16)$$

according to the constitutive model in Laplace domain (14)₁, since the Laplace transform of strain assumed as the Heaviside function H is $\tilde{\varepsilon}(x, s) = \mathcal{L}[H(t)](s) = \frac{1}{s}$, so that the constitutive model in Laplace domain (14)₁ is rewritten as

$$\tilde{\sigma}(s) = s \tilde{\sigma}_{sr}(s) \tilde{\varepsilon}(s),$$

becoming

$$\begin{aligned} \sigma(t) &= \mathcal{L}^{-1}[s \tilde{\sigma}_{sr}(s)](t) * \varepsilon(t) = (\sigma_{sr/g} \delta(t) + \dot{\sigma}_{sr}(t)) * \varepsilon(t), \quad \text{i.e.,} \\ \sigma(t) &= \sigma_{sr/g} \varepsilon(t) + \dot{\sigma}_{sr}(t) * \varepsilon(t), \end{aligned} \quad (17)$$

where the glass modulus, defined by

$$\sigma_{sr/g} = \sigma_{sr}(0) = \lim_{s \rightarrow \infty} s \tilde{\sigma}_{sr}(s),$$

is obtained according to the Tauberian theorem, implying the final form

$$\sigma(t) = \sigma_{sr/g} \varepsilon(t) + \frac{d}{dt} (\sigma_{sr}(t) * \varepsilon(t)) - \sigma_{sr/g} \varepsilon(t) = \frac{d}{dt} (\sigma_{sr}(t) * \varepsilon(t))$$

of the constitutive equation (17), according to the derivative of a convolution

$$\frac{d}{dt} (f(t) * g(t)) = \dot{f}(t) * g(t) + f(0) g(t).$$

Actually, the glass modulus proves to be connected with the wave propagation speed by

$$c = \sqrt{\frac{\sigma_{sr/g}}{\rho}}, \quad (18)$$

which is accounted for one-dimensional wave equations in [21], obtained for linear fractional constitutive equations containing Riemann-Liouville derivatives of orders in interval $(0, 1)$, and further extended in [18] for the case of distributed-order models, where the integration is performed with respect to orders of fractional derivatives in interval $(0, 1)$, as well as extending to thermodynamically consistent fractional Burgers models containing fractional derivatives of orders in interval $(1, 2)$ as well, having the wave propagation considered on infinite domain in [27] and on finite domain in [13]. Micro-local analysis of the fractional Zener and distributed-order wave equations, yielding support of fundamental solution in the cone defined by wave propagation speed, is conducted in [5, 6].

Linear fractional-order models containing only Riemann-Liouville fractional derivatives of orders in interval $(0, 1)$, obtained from the constitutive model (10) for $a_k = 0$, with $k = 1, \dots, N_1$, and $c_k = 0$, with $k = 1, \dots, M_1$, thus taking the form

$$\sum_{i=1}^n a_i {}_0D_t^{\alpha_i} \sigma(x, t) = \sum_{j=1}^m b_j {}_0D_t^{\beta_j} \varepsilon(x, t), \quad (19)$$

prove to have four thermodynamically consistent cases

$$\sum_{i=1}^n a_i {}_0D_t^{\alpha_i} \sigma(t) = \sum_{i=1}^n b_i {}_0D_t^{\alpha_i} \varepsilon(t), \quad (20)$$

$$\sum_{i=1}^n a_i {}_0D_t^{\alpha_i} \sigma(t) = \sum_{i=1}^n b_i {}_0D_t^{\alpha_i} \varepsilon(t) + \sum_{i=n+1}^m b_i {}_0D_t^{\beta_i} \varepsilon(t), \quad (21)$$

$$\sum_{i=1}^{n-m} a_i {}_0D_t^{\alpha_i} \sigma(t) + \sum_{i=n-m+1}^n a_i {}_0D_t^{\alpha_i} \sigma(t) = \sum_{j=1}^m b_j {}_0D_t^{\alpha_{n-m+j}} \varepsilon(t), \quad (22)$$

$$\sum_{i=1}^n a_i {}_0D_t^{\alpha_i} \sigma(t) = \sum_{j=1}^m b_j {}_0D_t^{\beta_j} \varepsilon(t), \quad (23)$$

as derived in [3] and listed in Supplementary material. By examining the large-time asymptotics of creep compliance, one finds that models belonging to Case I and II, given by (20) and (21), display solid-like behavior, since the creep compliance takes the finite value for infinite time, while models belonging to Case III and IV, given by (22) and (23), display fluid-like behavior, since the creep compliance tends to infinity as time tends to infinity. On the other hand, models belonging to Case I and III yield finite wave propagation speed, since the relaxation modulus tends to a finite value as time tends to zero, while models belonging to Case II and IV yield infinite wave propagation speed, since the relaxation modulus tends to a infinite value as time tends to zero. These model properties are used in [46] in proving dissipativity of fractional wave equations using a priori energy estimates.

On the other hand, the representatives of models containing only Riemann-Liouville fractional derivatives of orders in both intervals $(0, 1)$ and $(1, 2)$ are fractional Burgers models, derived and checked for thermodynamical consistency in [24], which group into two thermodynamically consistent classes

$$\begin{aligned} \left(1 + a_1 {}_0D_t^\alpha + a_2 {}_0D_t^\beta + a_3 {}_0D_t^\gamma\right) \sigma(x, t) &= \left(b_1 {}_0D_t^\mu + b_2 {}_0D_t^{\mu+\eta}\right) \varepsilon(x, t) \quad \text{and} \\ \left(1 + a_1 {}_0D_t^\alpha + a_2 {}_0D_t^\beta + a_3 {}_0D_t^{\beta+\eta}\right) \sigma(x, t) &= \left(b_1 {}_0D_t^\beta + b_2 {}_0D_t^{\beta+\eta}\right) \varepsilon(x, t), \end{aligned} \quad (24)$$

such that for models of the first class the highest fractional differentiation order of strain is $\mu + \eta \in [1, 2]$, with $\eta \in \{\alpha, \beta\}$, while the highest fractional differentiation order of stress is either $\gamma \in [0, 1]$ in the case of Model I, with $0 \leq \alpha \leq \beta \leq \gamma \leq \mu \leq 1$ and $\eta \in \{\alpha, \beta, \gamma\}$, or $\gamma \in [1, 2]$ in the case of Models II - V, with $0 \leq \alpha \leq \beta \leq \mu \leq 1$ and $(\eta, \gamma) \in \{(\alpha, 2\alpha), (\alpha, \alpha + \beta), (\beta, \alpha + \beta), (\beta, 2\beta)\}$, while for models of the second class it holds $0 \leq \alpha \leq \beta \leq 1$ and $\beta + \eta \in [1, 2]$, with $\eta = \alpha$, in the case of Model VI; $\eta = \beta$ in the case of Model VII; and $\alpha = \eta = \beta$, $\bar{a}_1 = a_1 + a_2$, and $\bar{a}_2 = a_3$ in the case of Model VIII, see Supplementary material for details.

In constitutive equations of Models I - V, the orders of fractional derivatives are ordered from lowest to highest, separately for those in the interval $[0, 1]$ and separately for those in the interval $[1, 2]$. Model I contains only one derivative acting on strain having order in interval $[1, 2]$, obtained as a sum of the highest differentiation order in interval $[0, 1]$ and any of the other three differentiation orders. Models II - V contain two fractional derivatives having orders in interval $[0, 1]$ and another one having order in interval $[1, 2]$, all acting on stress, where the highest order is obtained either as a sum of the orders in interval $[0, 1]$ or as a double value of any

of them. Moreover, Models II - V contain one fractional derivative of order in interval $[0, 1]$ and one of order in interval $[1, 2]$, both acting on strain, where the second one is obtained as a sum of the first one and any remaining order up to one.

Models VI and VII contain two fractional derivatives of orders in interval $[0, 1]$ and another one of order in interval $[1, 2]$, all acting on stress, as well as one fractional derivative of order in interval $[0, 1]$ and one of order in interval $[1, 2]$, both acting on strain, such that the highest orders of fractional derivatives acting on strain coincide with the highest orders of fractional derivatives acting on stress regardless of the interval they belong to. Fractional derivative orders in interval $[1, 2]$ are obtained either as a sum of orders from interval $[0, 1]$, or as a double value of the higher one. Model VIII contains the same two fractional derivatives acting on both stress and strain, the first one having order in the interval $[\frac{1}{2}, 1]$ and the second one having the order obtained as a double value of the first one.

In [25], the responses of fractional Burgers models are examined in creep and stress relaxation tests, so that the considerations of large-time asymptotics of creep compliance categorize these models into fluid-like models, since the equilibrium compliance tends to infinity, while the considerations of short-time asymptotic behavior of relaxation modulus separate these models into two classes, such that the mechanical disturbance propagation speed has an infinite value for models of the first class, since the glass modulus has an infinite value, while the propagation speed of mechanical disturbance for models of the second class has a finite value, since the glass modulus has a finite value, as well.

Model	Constitutive equation
ID.ID	$(a_1 {}_0I_t^\alpha + a_2 {}_0D_t^\beta) \sigma(t) = (b_1 {}_0I_t^\mu + a_2 {}_0D_t^{\alpha+\beta-\mu}) \varepsilon(t)$
ID.DD⁺	$(a_1 {}_0I_t^\alpha + a_2 {}_0D_t^\beta) \sigma(t) = (b_1 {}_0D_t^\mu + b_2 {}_0D_t^{\alpha+\beta+\mu}) \varepsilon(t)$
IID.IID	$(a_1 {}_0I_t^\alpha + a_2 {}_0I_t^\beta + a_3 {}_0D_t^\gamma) \sigma(t) = (b_1 {}_0I_t^{\alpha+\gamma-\eta} + b_2 {}_0I_t^{\beta+\gamma-\eta} + b_3 {}_0D_t^\eta) \varepsilon(t)$
IDD.IDD	$(a_1 {}_0I_t^\alpha + a_2 {}_0D_t^\beta + a_3 {}_0D_t^\gamma) \sigma(t) = (b_1 {}_0I_t^\mu + b_2 {}_0D_t^{\alpha+\beta-\mu} + b_3 {}_0D_t^{\alpha+\gamma-\mu}) \varepsilon(t)$
IID.IDD	$(a_1 {}_0I_t^\alpha + a_2 {}_0I_t^\beta + a_3 {}_0D_t^\gamma) \sigma(t) = (b_1 {}_0I_t^\mu + b_2 {}_0D_t^\nu + b_3 {}_0D_t^{\alpha+\gamma-\mu}) \varepsilon(t)$
I⁺ID.I⁺ID	$(a_1 {}_0I_t^{1+\alpha} + a_2 {}_0I_t^{\frac{1+\alpha-\gamma}{2}} + a_3 {}_0D_t^\gamma) \sigma(t) = (b_1 {}_0I_t^{1+\mu} + b_2 {}_0I_t^{\frac{1+\mu-(\alpha+\gamma-\mu)}{2}} + b_3 {}_0D_t^{\alpha+\gamma-\mu}) \varepsilon(t)$
IDD⁺.IDD⁺	$(a_1 {}_0I_t^\alpha + a_2 {}_0D_t^{\frac{1+\gamma-\alpha}{2}} + a_3 {}_0D_t^{1+\gamma}) \sigma(t) = (b_1 {}_0I_t^{\alpha+\gamma-\eta} + b_2 {}_0D_t^{\frac{1+\eta-(\alpha+\gamma-\eta)}{2}} + b_3 {}_0D_t^{1+\eta}) \varepsilon(t)$
I⁺ID.IDD⁺	$(a_1 {}_0I_t^{1+\alpha} + a_2 {}_0I_t^{\frac{1+\alpha-\gamma}{2}} + a_3 {}_0D_t^\gamma) \sigma(t) = (b_1 {}_0I_t^{\alpha+\gamma-\eta} + b_2 {}_0D_t^{\frac{1+\eta-(\alpha+\gamma-\eta)}{2}} + b_3 {}_0D_t^{1+\eta}) \varepsilon(t)$
IID.ID	$(a_1 {}_0I_t^{\alpha+\beta-\gamma} + a_2 {}_0I_t^\nu + a_3 {}_0D_t^\gamma) \sigma(t) = (b_1 {}_0I_t^\alpha + b_2 {}_0D_t^\beta) \varepsilon(t)$
IDD.DD⁺	$(a_1 {}_0I_t^\alpha + a_2 {}_0D_t^\beta + a_3 {}_0D_t^\gamma) \sigma(t) = (b_1 {}_0D_t^\mu + b_2 {}_0D_t^{\alpha+\beta+\mu}) \varepsilon(t)$
I⁺ID.ID	$(a_1 {}_0I_t^{\alpha+\beta+\nu} + a_2 {}_0I_t^\nu + a_3 {}_0D_t^{\alpha+\beta-\nu}) \sigma(t) = (b_1 {}_0I_t^\alpha + b_2 {}_0D_t^\beta) \varepsilon(t)$
IDD⁺.DD⁺	$(a_1 {}_0I_t^\alpha + a_2 {}_0D_t^\beta + a_3 {}_0D_t^{\alpha+2\beta}) \sigma(t) = (b_1 {}_0D_t^\mu + b_2 {}_0D_t^{\alpha+\beta+\mu}) \varepsilon(t)$
ID.IDD	$(a_1 {}_0I_t^\mu + a_2 {}_0D_t^\nu) \sigma(t) = (b_1 {}_0I_t^\alpha + b_2 {}_0D_t^\beta + b_3 {}_0D_t^{\mu+\nu-\alpha}) \varepsilon(t)$
ID.DDD⁺	$(a_1 {}_0I_t^\alpha + a_2 {}_0D_t^\beta) \sigma(t) = (b_1 {}_0D_t^\mu + b_2 {}_0D_t^\nu + b_3 {}_0D_t^{\alpha+\beta+\nu}) \varepsilon(t)$
ID.IDD⁺	$(a_1 {}_0I_t^\alpha + a_2 {}_0D_t^\beta) \sigma(t) = (b_1 {}_0I_t^{\alpha+\beta-\nu} + b_2 {}_0D_t^\nu + b_3 {}_0D_t^{\alpha+\beta+\nu}) \varepsilon(t)$

Table 1: Symmetric and asymmetric fractional anti-Zener and Zener constitutive models.

The linear fractional-order models containing both fractional integrals and Riemann-Liouville fractional derivatives of orders in both intervals $(0, 1)$ and $(1, 2)$ are fractional anti-Zener and Zener constitutive mod-

els, derived and checked for thermodynamical consistency in [15], grouping into the classes of symmetric and asymmetric models, where the symmetric models have the same number of operators, either fractional integrals and/or Riemann-Liouville fractional derivatives, acting on both stress and strain, see Table 1 for the list of models and Supplementary material for details. It is proved in [14] that fractional anti-Zener and Zener models describe fluid-like solid body having the wave propagation speed infinite. Moreover, in [14] energy balance properties of viscoelastic body are examined a priori by splitting the power per unit volume into a term being a time derivative of a quantity that can be interpreted as the energy per unit volume and a term representing dissipated power per unit volume. These results are applied in [16] for investigating the energy balance properties of a fractional anti-Zener and Zener type body subject to a harmonic strain.

Fractional generalization of the wave equation for damped waves is conducted in [20], while considering the three-dimensional deformable body, fractional Zener wave equation is considered in [23], while in [26] existence and uniqueness of solution to the three-dimensional fractional Zener wave equation is proved. Numerical methods, including finite element analysis, are used in [30, 34] in order to analyze transient wave processes in linearly viscoelastic solids, while in [33, 37, 39, 45] different numerical methods are employed in order to obtain solutions to proposed models. Also, different methods for the discretization of stochastic fractional wave equation are used in [19].

Various applications of viscoelastic wave equations include modeling of ultrasonic waves used to estimate the distribution of a damage in a material, see [31], three-dimensional solid thermoviscoelastic material, see [32], wave propagation after a tsunami, see [38], seismic waves, see [41], stratified porous media, as done in [44], and many others.

In order to examine the torsional waves characteristic for human cervical tissue, a three-dimensional wave equation is examined in [7], while the research about ultrasound waves traveling through biological tissues is carried out in [8]. In [42], considering shear modulus, three-dimensional wave propagation is analyzed in viscoelastic materials, having importance in, for example, modeling human tissues.

2 Displacement field

The method of integral transforms, Fourier transform with respect to spatial coordinates, defined by

$$\bar{f}(\mathbf{k}) = \mathcal{F}[f(\mathbf{r})](\mathbf{k}) = \int_{\mathbb{R}^3} f(\mathbf{r}) e^{-i\mathbf{k}\cdot\mathbf{r}} d_r V, \quad \mathbf{k} \in \mathbb{R}^3,$$

and Laplace transform with respect to time, defined by (11), is used in order to solve the Cauchy initial-value problem for the three-dimensional wave equation of viscoelastic body, considered as the system of equations consisting of the equation of motion of deformable solid body (2), strain (3), and constitutive equation (9), where the relaxation moduli $\sigma_{sr}^{(c)}$ and $\sigma_{sr}^{(s)}$ define material response of viscoelastic body, i.e., in order to solve the system of equations

$$\frac{1}{\rho} \operatorname{div} \hat{\boldsymbol{\sigma}}(\mathbf{r}, t) + \mathbf{f}_b(\mathbf{r}, t) = \partial_{tt}^2 \mathbf{u}(\mathbf{r}, t), \quad (25)$$

$$\hat{\boldsymbol{\varepsilon}}(\mathbf{r}, t) = \frac{1}{2} \left(\operatorname{grad} \mathbf{u}(\mathbf{r}, t) + (\operatorname{grad} \mathbf{u}(\mathbf{r}, t))^T \right), \quad (26)$$

$$\hat{\boldsymbol{\sigma}}(\mathbf{r}, t) = \partial_t \left(\sigma_{sr}^{(c,s)}(t) *_t \operatorname{tr} \hat{\boldsymbol{\varepsilon}}(\mathbf{r}, t) \right) \hat{\mathbf{I}} + 2\partial_t \left(\sigma_{sr}^{(s)}(t) *_t \hat{\boldsymbol{\varepsilon}}(\mathbf{r}, t) \right), \quad (27)$$

on $\mathbf{r} \in \mathbb{R}^3$, for $t > 0$, subject to initial conditions

$$\mathbf{u}(\mathbf{r}, 0) = \mathbf{u}_0(\mathbf{r}) \quad \text{and} \quad \partial_t \mathbf{u}(\mathbf{r}, 0) = \mathbf{v}_0(\mathbf{r}) \quad (28)$$

and assuming that all components of displacement field, as well as of the Cauchy stress tensor, vanish as any of the coordinates tend to both positive and negative infinity. Namely, the application of Fourier and Laplace transforms, applied to the previously mentioned system of equations, yields

$$\frac{1}{\rho} i\mathbf{k} \bar{\hat{\boldsymbol{\sigma}}}(\mathbf{k}, s) + \bar{\mathbf{f}}_b(\mathbf{k}, s) = s^2 \bar{\hat{\mathbf{u}}}(\mathbf{k}, s) - s\bar{\mathbf{u}}_0(\mathbf{k}) - \bar{\mathbf{v}}_0(\mathbf{k}), \quad (29)$$

$$\bar{\hat{\boldsymbol{\varepsilon}}}(\mathbf{k}, s) = \frac{1}{2} \left(i\mathbf{k} \otimes \bar{\hat{\mathbf{u}}}(\mathbf{k}, s) + \bar{\hat{\mathbf{u}}}(\mathbf{k}, s) \otimes i\mathbf{k} \right), \quad (30)$$

$$\bar{\hat{\boldsymbol{\sigma}}}(\mathbf{k}, s) = s\bar{\sigma}_{sr}^{(c,s)}(s) \left(i\mathbf{k} \cdot \bar{\hat{\mathbf{u}}}(\mathbf{k}, s) \right) \hat{\mathbf{I}} + 2s\bar{\sigma}_{sr}^{(s)}(s) \bar{\hat{\boldsymbol{\varepsilon}}}(\mathbf{k}, s), \quad (31)$$

since $\mathcal{F}[\nabla](\mathbf{k}) = i\mathbf{k}$ implies $\mathcal{F}[\operatorname{div} \hat{\boldsymbol{\sigma}}(\mathbf{r}, t)](\mathbf{k}) = \mathcal{F}[\nabla \hat{\boldsymbol{\sigma}}(\mathbf{r}, t)](\mathbf{k}) = i\mathbf{k} \bar{\hat{\boldsymbol{\sigma}}}(\mathbf{k}, t)$, $\mathcal{F}[\operatorname{grad} \mathbf{u}(\mathbf{r}, t)](\mathbf{k}) = \mathcal{F}[\nabla \otimes \mathbf{u}(\mathbf{r}, t)](\mathbf{k}) = i\mathbf{k} \otimes \bar{\hat{\mathbf{u}}}(\mathbf{k}, t)$, and $\mathcal{F}[\operatorname{tr} \hat{\boldsymbol{\varepsilon}}(\mathbf{r}, t)](\mathbf{k}) = \mathcal{F}[\operatorname{div} \mathbf{u}(\mathbf{r}, t)](\mathbf{k}) = \mathcal{F}[\nabla \cdot \mathbf{u}(\mathbf{r}, t)](\mathbf{k}) = i\mathbf{k} \cdot \bar{\hat{\mathbf{u}}}(\mathbf{k}, t)$,

where \otimes is used to denote the dyadic product, while the system of equations (29) - (31) reduced to a single equation containing the displacement field in Fourier and Laplace domain becomes

$$\begin{aligned} & \frac{s\tilde{\sigma}_{sr}^{(c,s)}(s)}{\rho} \mathbf{i}\mathbf{k} (\mathbf{i}\mathbf{k} \cdot \bar{\mathbf{u}}(\mathbf{k}, s)) + \frac{s\tilde{\sigma}_{sr}^{(s)}(s)}{\rho} \mathbf{i}\mathbf{k} (\mathbf{i}\mathbf{k} \otimes \bar{\mathbf{u}}(\mathbf{k}, s)) \\ & \quad + \frac{s\tilde{\sigma}_{sr}^{(s)}(s)}{\rho} \mathbf{i}\mathbf{k} (\bar{\mathbf{u}}(\mathbf{k}, s) \otimes (\mathbf{i}\mathbf{k})) - s^2 \bar{\mathbf{u}}(\mathbf{k}, s) = -s\bar{\mathbf{u}}_0(\mathbf{k}) - \bar{\mathbf{v}}_0(\mathbf{k}) - \bar{\mathbf{f}}_b(\mathbf{k}, s), \\ & \left(\left(\frac{s\tilde{\sigma}_{sr}^{(s)}(s)}{\rho} k^2 + s^2 \right) \hat{\mathbf{I}} + \frac{s(\sigma_{sr}^{(c)}(s) - \sigma_{sr}^{(s)}(s))}{\rho} (\mathbf{k} \otimes \mathbf{k}) \right) \bar{\mathbf{u}}(\mathbf{k}, s) = s\bar{\mathbf{u}}_0(\mathbf{k}) + \bar{\mathbf{v}}_0(\mathbf{k}) + \bar{\mathbf{f}}_b(\mathbf{k}, s), \end{aligned} \quad (32)$$

since $\mathbf{i}\mathbf{k} (\mathbf{i}\mathbf{k} \otimes \bar{\mathbf{u}}(\mathbf{k}, s)) = (\mathbf{i}\mathbf{k})^2 \bar{\mathbf{u}}(\mathbf{k}, s)$, $\mathbf{i}\mathbf{k} (\bar{\mathbf{u}}(\mathbf{k}, s) \otimes (\mathbf{i}\mathbf{k})) = (\mathbf{i}\mathbf{k} \cdot \bar{\mathbf{u}}(\mathbf{k}, s)) \mathbf{i}\mathbf{k} = \mathbf{i}\mathbf{k} (\bar{\mathbf{u}}(\mathbf{k}, s) \cdot (\mathbf{i}\mathbf{k})) = ((\mathbf{i}\mathbf{k}) \otimes (\mathbf{i}\mathbf{k})) \bar{\mathbf{u}}(\mathbf{k}, s)$, which can be considered as the wave equation of viscoelastic body in Fourier and Laplace domain.

2.1 Displacement field via functions φ and Ω

The classical three-dimensional wave equations (6) and (7), describing the compressive and shear wave propagation and expressed in terms of $\varphi(\mathbf{r}, t) = \text{div } \mathbf{u}(\mathbf{r}, t)$ and $\Omega(\mathbf{r}, t) = \text{curl } \mathbf{u}(\mathbf{r}, t)$ as unknown functions, are generalized for the viscoelastic body and the solution to the wave equation of viscoelastic body, i.e., to the system of equations (25) - (27) is calculated by the use of functions φ and Ω , similarly as in the case of classical wave equation.

The generalization of the wave equation (6) is obtained as follows: by applying the scalar product of wave vector $\mathbf{i}\mathbf{k}$ with the wave equation of viscoelastic body in Fourier and Laplace domain (32), one obtains

$$\begin{aligned} & \left(\frac{s\tilde{\sigma}_{sr}^{(c)}(s)}{\rho} k^2 + s^2 \right) (\mathbf{i}\mathbf{k} \cdot \bar{\mathbf{u}}(\mathbf{k}, s)) = \mathbf{i}\mathbf{k} \cdot (s\bar{\mathbf{u}}_0(\mathbf{k}) + \bar{\mathbf{v}}_0(\mathbf{k}) + \bar{\mathbf{f}}_b(\mathbf{k}, s)), \quad \text{i.e.,} \\ & -\tilde{c}_c^2(s) k^2 (\mathbf{i}\mathbf{k} \cdot \bar{\mathbf{u}}(\mathbf{k}, s)) - \mathbf{i}\mathbf{k} \cdot (s^2 \bar{\mathbf{u}}(\mathbf{k}, s) - s\bar{\mathbf{u}}_0(\mathbf{k}) - \bar{\mathbf{v}}_0(\mathbf{k})) = -\mathbf{i}\mathbf{k} \cdot \bar{\mathbf{f}}_b(\mathbf{k}, s), \end{aligned} \quad (33)$$

since $\mathbf{i}\mathbf{k} \cdot ((\mathbf{k} \otimes \mathbf{k}) \bar{\mathbf{u}}(\mathbf{k}, s)) = \mathbf{i}\mathbf{k} \cdot (\mathbf{k} (\mathbf{k} \cdot \bar{\mathbf{u}}(\mathbf{k}, s))) = k^2 (\mathbf{i}\mathbf{k} \cdot \bar{\mathbf{u}}(\mathbf{k}, s))$, where

$$\tilde{c}_c(s) = \sqrt{\frac{s\tilde{\sigma}_{sr}^{(c)}(s)}{\rho}} \quad (34)$$

is the memory function corresponding to compressive waves, so that after application of the inverse Fourier and Laplace transforms, with $\mathcal{F}[\Delta](\mathbf{k}) = \mathcal{F}[\nabla \cdot \nabla](\mathbf{k}) = (\mathbf{i}\mathbf{k})^2 = -k^2$, the previous expression becomes

$$\begin{aligned} & \tilde{c}_c^2(s) \Delta \text{div } \tilde{\mathbf{u}}(\mathbf{r}, s) - \text{div} (s^2 \tilde{\mathbf{u}}(\mathbf{r}, s) - s\mathbf{u}_0(\mathbf{r}) - \mathbf{v}_0(\mathbf{r})) = -\text{div } \bar{\mathbf{f}}_b(\mathbf{r}, s), \quad \text{i.e.,} \\ & \Delta (\mathcal{L}^{-1} [\tilde{c}_c^2(s) \tilde{\varphi}(\mathbf{r}, s)](\mathbf{r}, t)) - \partial_{tt}^2 \varphi(\mathbf{r}, t) = -\text{div } \mathbf{f}_b(\mathbf{r}, t), \quad \text{with } \varphi(\mathbf{r}, t) = \text{div } \mathbf{u}(\mathbf{r}, t), \end{aligned} \quad (35)$$

reducing to either

$$\frac{\dot{\sigma}_{sr}^{(c)}(t)}{\rho} *_t \Delta \varphi(\mathbf{r}, t) + \frac{\sigma_{sr/g}^{(c)}}{\rho} \Delta \varphi(\mathbf{r}, t) - \partial_{tt}^2 \varphi(\mathbf{r}, t) = -\text{div } \mathbf{f}_b(\mathbf{r}, t), \quad (36)$$

if glass modulus $\sigma_{sr/g}^{(c)} = \sigma_{sr}^{(c)}(0)$ is finite and therefore compressive wave propagation speed $c_c = \sqrt{\frac{\sigma_{sr/g}^{(c)}}{\rho}}$ as well, due to

$$\mathcal{L}^{-1} [\tilde{c}_c^2(s) \tilde{\varphi}(\mathbf{r}, s)](\mathbf{r}, t) = \mathcal{L}^{-1} \left[\frac{s\tilde{\sigma}_{sr}^{(c)}(s)}{\rho} \tilde{\varphi}(\mathbf{r}, s) \right](\mathbf{r}, t) = \left(\frac{1}{\rho} \dot{\sigma}_{sr}^{(c)}(t) + \frac{1}{\rho} \sigma_{sr/g}^{(c)} \delta(t) \right) *_t \varphi(\mathbf{r}, t), \quad (37)$$

or reducing to

$$\frac{\sigma_{sr}^{(c)}(t)}{\rho} *_t \Delta \partial_t \varphi(\mathbf{r}, t) + \frac{\sigma_{sr}^{(c)}(t)}{\rho} \Delta \varphi_0(\mathbf{r}) - \partial_{tt}^2 \varphi(\mathbf{r}, t) = -\text{div } \mathbf{f}_b(\mathbf{r}, t), \quad (38)$$

with $\varphi_0(\mathbf{r}) = \varphi(\mathbf{r}, 0)$, if glass modulus is infinite, so as the compressive wave propagation speed, due to

$$\mathcal{L}^{-1} [\tilde{c}_c^2(s) \tilde{\varphi}(\mathbf{r}, s)](\mathbf{r}, t) = \mathcal{L}^{-1} \left[\frac{\tilde{\sigma}_{sr}^{(c)}(s)}{\rho} s \tilde{\varphi}(\mathbf{r}, s) \right](\mathbf{r}, t) = \frac{1}{\rho} \sigma_{sr}^{(c)}(t) *_t (\partial_t \varphi(\mathbf{r}, t) + \varphi_0(\mathbf{r}) \delta(t)). \quad (39)$$

Hence, the general form of wave equation expressed in terms of function φ is given by (35), while its specific form when compressive wave propagation speed is finite is given by (36), while wave equation (38) corresponds to the case when compressive wave propagation speed is infinite. Each of the previously mentioned wave equations requires initial conditions

$$\varphi_0(\mathbf{r}) = \varphi(\mathbf{r}, 0) = \operatorname{div} \mathbf{u}(\mathbf{r}, 0) = \operatorname{div} \mathbf{u}_0(\mathbf{r}) \quad \text{and} \quad \dot{\varphi}_0(\mathbf{r}) = \partial_t \varphi(\mathbf{r}, 0) = \operatorname{div} \partial_t \mathbf{u}(\mathbf{r}, 0) = \operatorname{div} \mathbf{v}_0(\mathbf{r}), \quad (40)$$

arising from the initial conditions on displacement field (28).

On the other hand, the generalization of the wave equation (7) is obtained as follows: the vector product of wave vector $\mathbf{i}\mathbf{k}$ with the wave equation of viscoelastic body in Fourier and Laplace domain (32) implies

$$\begin{aligned} \left(\frac{s\tilde{\sigma}_{sr}^{(s)}(s)}{\varrho} k^2 + s^2 \right) (\mathbf{i}\mathbf{k} \times \bar{\mathbf{u}}(\mathbf{k}, s)) &= \mathbf{i}\mathbf{k} \times \left(s\bar{\mathbf{u}}_0(\mathbf{k}) + \bar{\mathbf{v}}_0(\mathbf{k}) + \bar{\mathbf{f}}_b(\mathbf{k}, s) \right), \quad \text{i.e.,} \\ -\tilde{c}_s^2(s) k^2 (\mathbf{i}\mathbf{k} \times \bar{\mathbf{u}}(\mathbf{k}, s)) - \mathbf{i}\mathbf{k} \times (s^2 \bar{\mathbf{u}}(\mathbf{k}, s) - s\bar{\mathbf{u}}_0(\mathbf{k}) - \bar{\mathbf{v}}_0(\mathbf{k})) &= -\mathbf{i}\mathbf{k} \times \bar{\mathbf{f}}_b(\mathbf{k}, s), \end{aligned} \quad (41)$$

since $\mathbf{i}\mathbf{k} \times ((\mathbf{k} \otimes \mathbf{k}) \bar{\mathbf{u}}(\mathbf{k}, s)) = \mathbf{i}\mathbf{k} \times (\mathbf{k} (\mathbf{k} \cdot \bar{\mathbf{u}}(\mathbf{k}, s))) = \mathbf{0}$, where

$$\tilde{c}_s(s) = \sqrt{\frac{s\tilde{\sigma}_{sr}^{(s)}(s)}{\varrho}} \quad (42)$$

is the memory function corresponding to shear waves, so that the previous expression is transformed into

$$\begin{aligned} \tilde{c}_s^2(s) \Delta (\operatorname{curl} \bar{\mathbf{u}}(\mathbf{r}, s)) - \operatorname{curl} (s^2 \bar{\mathbf{u}}(\mathbf{r}, s) - s\mathbf{u}_0(\mathbf{r}) - \mathbf{v}_0(\mathbf{r})) &= -\operatorname{curl} \bar{\mathbf{f}}_b(\mathbf{r}, s), \quad \text{i.e.,} \\ \Delta \left(\mathcal{L}^{-1} \left[\tilde{c}_s^2(s) \bar{\mathbf{\Omega}}(\mathbf{r}, s) \right] (\mathbf{r}, t) \right) - \partial_{tt}^2 \mathbf{\Omega}(\mathbf{r}, t) &= -\operatorname{curl} \mathbf{f}_b(\mathbf{r}, t), \quad \text{with} \quad \mathbf{\Omega}(\mathbf{r}, t) = \operatorname{curl} \mathbf{u}(\mathbf{r}, t), \end{aligned} \quad (43)$$

after application of the inverse Fourier and Laplace transforms, reducing to either

$$\frac{\dot{\sigma}_{sr}^{(s)}(t)}{\varrho} *_t \Delta \mathbf{\Omega}(\mathbf{r}, t) + \frac{\sigma_{sr/g}^{(s)}}{\varrho} \Delta \mathbf{\Omega}(\mathbf{r}, t) - \partial_{tt}^2 \mathbf{\Omega}(\mathbf{r}, t) = -\operatorname{curl} \mathbf{f}_b(\mathbf{r}, t), \quad (44)$$

if glass modulus $\sigma_{sr/g}^{(s)} = \sigma_{sr}^{(s)}(0)$ is finite and therefore shear wave propagation speed $c_s = \sqrt{\frac{\sigma_{sr/g}^{(s)}}{\varrho}}$ as well, see (37), or to

$$\frac{\sigma_{sr}^{(s)}(t)}{\varrho} *_t \Delta \partial_t \mathbf{\Omega}(\mathbf{r}, t) + \frac{\sigma_{sr}^{(s)}(t)}{\varrho} \Delta \mathbf{\Omega}_0(\mathbf{r}) - \partial_{tt}^2 \mathbf{\Omega}(\mathbf{r}, t) = -\operatorname{curl} \mathbf{f}_b(\mathbf{r}, t), \quad (45)$$

with $\mathbf{\Omega}_0(\mathbf{r}) = \mathbf{\Omega}(\mathbf{r}, 0)$, if glass modulus is infinite, so as the shear wave propagation speed. Hence, the general form of wave equation expressed in terms of function $\mathbf{\Omega}$ is given by (43), while its specific form when shear wave propagation speed is finite is given by (44), while wave equation (45) corresponds to the case when shear wave propagation speed is infinite. Each of the previously mentioned wave equations requires initial conditions

$$\mathbf{\Omega}_0(\mathbf{r}) = \mathbf{\Omega}(\mathbf{r}, 0) = \operatorname{curl} \mathbf{u}(\mathbf{r}, 0) = \operatorname{curl} \mathbf{u}_0(\mathbf{r}) \quad \text{and} \quad \dot{\mathbf{\Omega}}_0(\mathbf{r}) = \partial_t \mathbf{\Omega}(\mathbf{r}, 0) = \operatorname{curl} \partial_t \mathbf{u}(\mathbf{r}, 0) = \operatorname{curl} \mathbf{v}_0(\mathbf{r}), \quad (46)$$

arising from the initial conditions on displacement field (28).

Wave equations for compressive waves (36) and (38), as well as wave equations for shear waves (44) and (45), generalize classical wave equations (6) and (7). In particular, wave propagation speeds of compressive and shear waves in the Laplace transform of wave equations (6) and (7) are replaced by different memory functions (34) and (42) depending on the selected model of viscoelastic body through the relaxation modulus. Rewriting compressive and shear wave equations in Fourier and Laplace domain (33) and (41) in the form

$$\begin{aligned} (\tilde{c}_c^2(s) k^2 + s^2) \bar{\varphi}(\mathbf{k}, s) &= s\bar{\varphi}_0(\mathbf{k}) + \bar{\varphi}_0(\mathbf{k}) + \mathbf{i}\mathbf{k} \cdot \bar{\mathbf{f}}_b(\mathbf{k}, s), \\ (\tilde{c}_s^2(s) k^2 + s^2) \bar{\mathbf{\Omega}}(\mathbf{k}, s) &= s\bar{\mathbf{\Omega}}_0(\mathbf{k}) + \bar{\mathbf{\Omega}}_0(\mathbf{k}) + \mathbf{i}\mathbf{k} \times \bar{\mathbf{f}}_b(\mathbf{k}, s), \end{aligned}$$

with initial data

$$\begin{aligned} \bar{\varphi}_0(\mathbf{k}) &= \mathbf{i}\mathbf{k} \cdot \bar{\mathbf{u}}_0(\mathbf{k}) \quad \text{and} \quad \bar{\varphi}_0(\mathbf{k}) = \mathbf{i}\mathbf{k} \cdot \bar{\mathbf{v}}_0(\mathbf{k}), \quad \text{as well as} \\ \bar{\mathbf{\Omega}}_0(\mathbf{k}) &= \mathbf{i}\mathbf{k} \times \bar{\mathbf{u}}_0(\mathbf{k}) \quad \text{and} \quad \bar{\mathbf{\Omega}}_0(\mathbf{k}) = \mathbf{i}\mathbf{k} \times \bar{\mathbf{v}}_0(\mathbf{k}), \end{aligned}$$

see (40) and (46), for the solution of these wave equations one has

$$\bar{\varphi}(\mathbf{k}, s) = \bar{G}^{(c)}(k, s) \left(s\bar{\varphi}_0(\mathbf{k}) + \bar{\varphi}_0(\mathbf{k}) + \mathbf{i}\mathbf{k} \cdot \bar{\mathbf{f}}_b(\mathbf{k}, s) \right), \quad \text{with} \quad \bar{G}^{(c)}(k, s) = \frac{1}{\tilde{c}_c^2(s) k^2 + s^2}, \quad (47)$$

$$\bar{\bar{\boldsymbol{\Omega}}}(\mathbf{k}, s) = \bar{\bar{G}}^{(s)}(k, s) \left(s\bar{\boldsymbol{\Omega}}_0(\mathbf{k}) + \bar{\boldsymbol{\Omega}}_0(\mathbf{k}) + i\mathbf{k} \times \bar{\bar{\mathbf{f}}}_b(\mathbf{k}, s) \right), \quad \text{with} \quad \bar{\bar{G}}^{(s)}(k, s) = \frac{1}{\tilde{c}_s^2(s) k^2 + s^2}, \quad (48)$$

where $\bar{\bar{G}}^{(c)}$ and $\bar{\bar{G}}^{(s)}$ are Green's functions in Fourier and Laplace domain corresponding to compressive and shear waves respectively, implying the solution to compressive and shear wave equations (35) and (43) in the form

$$\varphi(\mathbf{r}, t) = \partial_t G^{(c)}(r, t) *_r \varphi_0(\mathbf{r}) + G^{(c)}(r, t) *_r \dot{\varphi}_0(\mathbf{r}) + G^{(c)}(r, t) *_r \text{div} \mathbf{f}_b(\mathbf{r}, t), \quad (49)$$

$$\boldsymbol{\Omega}(\mathbf{r}, t) = \partial_t G^{(s)}(r, t) *_r \boldsymbol{\Omega}_0(\mathbf{r}) + G^{(s)}(r, t) *_r \dot{\boldsymbol{\Omega}}_0(\mathbf{r}) + G^{(s)}(r, t) *_r \text{curl} \mathbf{f}_b(\mathbf{r}, t), \quad (50)$$

if $G^{(c)}(r, 0) = G^{(s)}(r, 0) = 0$.

Once the functions φ and $\boldsymbol{\Omega}$ are known, see expressions (49) and (50), the displacement field \mathbf{u} can be determined from the wave equation of viscoelastic body in Fourier and Laplace domain (32), which transforms into

$$\begin{aligned} \tilde{c}_s^2(s) k^2 \bar{\bar{\mathbf{u}}}(\mathbf{k}, s) + (\tilde{c}_c^2(s) - \tilde{c}_s^2(s)) (\mathbf{k} \otimes \mathbf{k}) \bar{\bar{\mathbf{u}}}(\mathbf{k}, s) + s^2 \bar{\bar{\mathbf{u}}}(\mathbf{k}, s) &= s\bar{\mathbf{u}}_0(\mathbf{k}) + \bar{\mathbf{v}}_0(\mathbf{k}) + \bar{\bar{\mathbf{f}}}_b(\mathbf{k}, s), \\ \tilde{c}_s^2(s) i\mathbf{k} \times \bar{\bar{\boldsymbol{\Omega}}}(\mathbf{k}, s) - \tilde{c}_c^2(s) i\mathbf{k} \bar{\bar{\varphi}}(\mathbf{k}, s) + s^2 \bar{\bar{\mathbf{u}}}(\mathbf{k}, s) &= s\bar{\mathbf{u}}_0(\mathbf{k}) + \bar{\mathbf{v}}_0(\mathbf{k}) + \bar{\bar{\mathbf{f}}}_b(\mathbf{k}, s), \end{aligned}$$

due to the memory functions (34) and (42), as well as due to $k^2 \bar{\bar{\mathbf{u}}}(\mathbf{k}, s) = \mathbf{k}(\mathbf{k} \cdot \bar{\bar{\mathbf{u}}}(\mathbf{k}, s)) - \mathbf{k} \times (\mathbf{k} \times \bar{\bar{\mathbf{u}}}(\mathbf{k}, s)) = -i\mathbf{k} \bar{\bar{\varphi}}(\mathbf{k}, s) + i\mathbf{k} \times \bar{\bar{\boldsymbol{\Omega}}}(\mathbf{k}, s)$ and $(\mathbf{k} \otimes \mathbf{k}) \bar{\bar{\mathbf{u}}}(\mathbf{k}, s) = \mathbf{k}(\mathbf{k} \cdot \bar{\bar{\mathbf{u}}}(\mathbf{k}, s)) = -i\mathbf{k} \bar{\bar{\varphi}}(\mathbf{k}, s)$, yielding

$$\bar{\bar{\mathbf{u}}}(\mathbf{k}, s) = \frac{1}{s} \bar{\mathbf{u}}_0(\mathbf{k}) + \frac{1}{s^2} \bar{\mathbf{v}}_0(\mathbf{k}) + \frac{1}{s^2} \left(\bar{\bar{\mathbf{f}}}_b(\mathbf{k}, s) + \tilde{c}_c^2(s) i\mathbf{k} \bar{\bar{\varphi}}(\mathbf{k}, s) - \tilde{c}_s^2(s) i\mathbf{k} \times \bar{\bar{\boldsymbol{\Omega}}}(\mathbf{k}, s) \right),$$

which implies the displacement field in the form

$$\mathbf{u}(\mathbf{r}, t) = \mathbf{u}_0(\mathbf{r}) + \mathbf{v}_0(\mathbf{r}) t + t *_t \left(\mathbf{f}_b(\mathbf{r}, t) + \mathcal{L}^{-1} [\tilde{c}_c^2(s) \text{grad} \tilde{\varphi}(\mathbf{r}, s)](\mathbf{r}, t) - \mathcal{L}^{-1} [\tilde{c}_s^2(s) \text{curl} \tilde{\boldsymbol{\Omega}}(\mathbf{r}, s)](\mathbf{r}, t) \right)$$

after performing the inverse Fourier and Laplace transforms and becoming

$$\begin{aligned} \mathbf{u}(\mathbf{r}, t) &= \mathbf{u}_0(\mathbf{r}) + \mathbf{v}_0(\mathbf{r}) t \\ &+ t *_t \left(\mathbf{f}_b(\mathbf{r}, t) + \begin{cases} \frac{1}{\varrho} \dot{\sigma}_{sr}^{(c)}(t) *_t \text{grad} \varphi(\mathbf{r}, t) + \frac{1}{\varrho} \sigma_{sr/g}^{(c)} \text{grad} \varphi(\mathbf{r}, t), & \text{if } \sigma_{sr/g}^{(c)} \text{ is finite,} \\ \frac{1}{\varrho} \sigma_{sr}^{(c)}(t) *_t (\partial_t \text{grad} \varphi(\mathbf{r}, t)) + \frac{1}{\varrho} \sigma_{sr}^{(c)}(t) \text{grad} \varphi_0(\mathbf{r}), & \text{if } \sigma_{sr/g}^{(c)} \text{ is infinite,} \\ \frac{1}{\varrho} \dot{\sigma}_{sr}^{(s)}(t) *_t \text{curl} \boldsymbol{\Omega}(\mathbf{r}, t) + \frac{1}{\varrho} \sigma_{sr/g}^{(s)} \text{curl} \boldsymbol{\Omega}(\mathbf{r}, t), & \text{if } \sigma_{sr/g}^{(s)} \text{ is finite,} \\ \frac{1}{\varrho} \sigma_{sr}^{(s)}(t) *_t (\partial_t \text{curl} \boldsymbol{\Omega}(\mathbf{r}, t)) + \frac{1}{\varrho} \sigma_{sr}^{(s)}(t) \text{curl} \boldsymbol{\Omega}_0(\mathbf{r}), & \text{if } \sigma_{sr/g}^{(s)} \text{ is infinite,} \end{cases} \right) \end{aligned} \quad (51)$$

when material properties are taken into account, see (37) and (39), so that expression (51) contains four possible forms of the displacement field, due to the possibility of compressive and shear waves to have finite, determined by

$$c_c = \sqrt{\frac{\sigma_{sr/g}^{(c)}}{\varrho}} \quad \text{and} \quad c_s = \sqrt{\frac{\sigma_{sr/g}^{(s)}}{\varrho}},$$

or infinite wave propagation speeds.

Determining the displacement field via the expression (51), which is apparently complicated, requires very complex and demanding calculations, further complicated by including the expressions for scalar and vector fields φ and $\boldsymbol{\Omega}$, given by (49) and (50), which are also elaborate expressions. Moreover, the form of displacement field depends on the models of a viscoelastic body taken into account, having four different forms depending on the finiteness of the wave propagation speed. Therefore, the expression (51) is certainly demanding for both analytical and numerical calculations.

2.2 Displacement field via resolvent tensor \hat{R}

Rather than using (51), which requires laborious and tedious calculations in order to determine the displacement field as a solution to the Cauchy initial-value problem for the wave equation of viscoelastic body, i.e., to the system of equations (25) - (27) subject to initial conditions (28), the approach of resolvent tensor calculation is adopted, so that the resolvent tensor applied to the initial conditions and body force as prescribed forcing,

yields the displacement field. Namely, the wave equation of viscoelastic body in Fourier and Laplace domain (32), rewritten as

$$\bar{\bar{\mathbf{R}}}^{-1}(\mathbf{k}, s) \bar{\bar{\mathbf{u}}}(\mathbf{k}, s) = s\bar{\mathbf{u}}_0(\mathbf{k}) + \bar{\mathbf{v}}_0(\mathbf{k}) + \bar{\bar{\mathbf{f}}}_b(\mathbf{k}, s), \quad (52)$$

where the inverse tensor of the resolvent tensor in Fourier and Laplace domain takes the form

$$\begin{aligned} \bar{\bar{\mathbf{R}}}^{-1}(\mathbf{k}, s) &= (\tilde{c}_s^2(s) k^2 + s^2) \hat{\mathbf{I}} + (\tilde{c}_c^2(s) - \tilde{c}_c^2(s)) (\mathbf{k} \otimes \mathbf{k}) \\ &= \frac{1}{\bar{\bar{G}}^{(s)}(k, s)} \left(\hat{\mathbf{I}} - \frac{\mathbf{k} \otimes \mathbf{k}}{k^2} \right) + \frac{1}{\bar{\bar{G}}^{(c)}(k, s)} \frac{\mathbf{k} \otimes \mathbf{k}}{k^2}, \end{aligned} \quad (53)$$

according to memory functions (34) and (42), as well as according to Green's functions (47)₂ and (48)₂, implies the displacement field in Fourier and Laplace domain

$$\bar{\bar{\mathbf{u}}}(\mathbf{k}, s) = \bar{\bar{\mathbf{R}}}(\mathbf{k}, s) \left(s\bar{\mathbf{u}}_0(\mathbf{k}) + \bar{\mathbf{v}}_0(\mathbf{k}) + \bar{\bar{\mathbf{f}}}_b(\mathbf{k}, s) \right), \quad (54)$$

transforming into

$$\mathbf{u}(\mathbf{r}, t) = \partial_t \hat{\mathbf{R}}(\mathbf{r}, t) *_r \mathbf{u}_0(\mathbf{r}) + \hat{\mathbf{R}}(\mathbf{r}, t) *_r \mathbf{v}_0(\mathbf{r}) + \hat{\mathbf{R}}(\mathbf{r}, t) *_r \mathbf{f}_b(\mathbf{r}, t), \quad (55)$$

assuming $\hat{\mathbf{R}}(\mathbf{r}, 0) = 0$, after the Fourier and Laplace transforms inversions are performed, so that it is necessary to determine the resolvent tensor $\hat{\mathbf{R}}$ and its first derivative with respect to time.

In order to do so, the first step is to find the resolvent tensor in Fourier and Laplace domain $\bar{\bar{\mathbf{R}}}$ in the form

$$\bar{\bar{\mathbf{R}}}(\mathbf{k}, s) = \bar{\bar{G}}^{(s)}(k, s) \left(\hat{\mathbf{I}} - \frac{\mathbf{k} \otimes \mathbf{k}}{k^2} \right) + \bar{\bar{G}}^{(c)}(k, s) \frac{\mathbf{k} \otimes \mathbf{k}}{k^2}, \quad (56)$$

through its inverse counterpart $\bar{\bar{\mathbf{R}}}^{-1}$, given by (53), since $\bar{\bar{\mathbf{R}}}(\mathbf{k}, s) \bar{\bar{\mathbf{R}}}^{-1}(\mathbf{k}, s) = \hat{\mathbf{I}}$, due to $\frac{\mathbf{k} \otimes \mathbf{k}}{k^2} \frac{\mathbf{k} \otimes \mathbf{k}}{k^2} = \frac{\mathbf{k} \otimes \mathbf{k}}{k^2}$, so that (56) transforms into

$$\begin{aligned} \bar{\bar{\mathbf{R}}}(\mathbf{k}, s) &= \bar{\bar{G}}^{(s)}(k, s) \hat{\mathbf{I}} - \frac{1}{k^2} \bar{\bar{G}}^{(s)}(k, s) (\mathbf{k} \otimes \mathbf{k}) + \frac{1}{k^2} \bar{\bar{G}}^{(c)}(k, s) (\mathbf{k} \otimes \mathbf{k}) \\ &= \bar{\bar{G}}^{(s)}(k, s) \hat{\mathbf{I}} + \frac{\tilde{c}_s^2(s)}{s^2} (\mathbf{k} \otimes \mathbf{k}) \bar{\bar{G}}^{(s)}(k, s) - \frac{\tilde{c}_c^2(s)}{s^2} (\mathbf{k} \otimes \mathbf{k}) \bar{\bar{G}}^{(c)}(k, s) \end{aligned}$$

using $\frac{1}{k^2} \bar{\bar{G}}^{(x)}(k, s) = \frac{1}{k^2} \frac{1}{\tilde{c}_x^2(s) k^2 + s^2} = \frac{1}{s^2} \frac{1}{k^2} - \frac{\tilde{c}_x^2(s)}{s^2} \frac{1}{\tilde{c}_x^2(s) k^2 + s^2} = \frac{1}{s^2} \frac{1}{k^2} - \frac{\tilde{c}_x^2(s)}{s^2} \bar{\bar{G}}^{(x)}(k, s)$.

In the second step, the inversion of Fourier transform in the previous expression yields the resolvent tensor in Laplace domain $\tilde{\mathbf{R}}$, taking the form

$$\tilde{\mathbf{R}}(\mathbf{r}, s) = \tilde{G}^{(s)}(r, s) \hat{\mathbf{I}} - \frac{\tilde{c}_s^2(s)}{s^2} (\nabla \otimes \nabla) \tilde{G}^{(s)}(r, s) + \frac{\tilde{c}_c^2(s)}{s^2} (\nabla \otimes \nabla) \tilde{G}^{(c)}(r, s) \quad (57)$$

since $\mathcal{F}[\nabla \otimes \nabla](\mathbf{k}) = i\mathbf{k} \otimes i\mathbf{k} = -(\mathbf{k} \otimes \mathbf{k})$, where Green's function in Laplace domain is obtained as

$$\tilde{G}^{(x)}(r, s) = \mathcal{F}^{-1} \left[\bar{\bar{G}}^{(x)}(k, s) \right] (r, s) = \frac{1}{4\pi r \tilde{c}_x^2(s)} e^{-\frac{rs}{\tilde{c}_x(s)}}, \quad x \in \{c, s\}, \quad (58)$$

by calculating the inverse Fourier transform

$$\begin{aligned} \tilde{G}^{(x)}(r, s) &= \frac{1}{(2\pi)^3} \int_{\mathbb{R}^3} \bar{\bar{G}}^{(x)}(k, s) e^{i\mathbf{k} \cdot \mathbf{r}} d\mathbf{k} V \\ &= \frac{1}{(2\pi)^3} \int_0^{2\pi} \int_0^\pi \int_0^\infty \frac{1}{\tilde{c}_x^2(s) k^2 + s^2} e^{-ikr \cos \theta} k^2 \sin \theta dk d\theta d\varphi \\ &= \frac{1}{(2\pi)^2 r} \int_0^\infty \frac{k}{\tilde{c}_x^2(s) k^2 + s^2} dk \int_{-kr}^{kr} e^{-ip} dp \\ &= \frac{1}{2\pi^2 r} \int_0^\infty \frac{k \sin(kr)}{\tilde{c}_x^2(s) k^2 + s^2} dk \\ &= \frac{1}{2\pi^2 r \tilde{c}_x^2(s)} \int_0^\infty \frac{q \sin q}{q^2 + \left(\frac{rs}{\tilde{c}_x(s)}\right)^2} dq \end{aligned}$$

$$= \frac{1}{4\pi r \tilde{c}_x^2(s)} e^{-\frac{rs}{\tilde{c}_x(s)}},$$

using the integral

$$\int_0^\infty \frac{q \sin q}{q^2 + \lambda} dq = \frac{\pi}{2} e^{-\sqrt{\lambda}}, \quad \text{if } \text{Re } \lambda > 0,$$

obtained by the integration in complex plane, with Green's functions in Fourier and Laplace domain $\tilde{G}^{(x)}$, given by (47)₂ and (48)₂. The condition $\text{Re } \lambda > 0$ implies $\text{Re } \frac{s^2}{\tilde{c}_x^2(s)} > 0$ for $\text{Re } s > 0$, whose validity is checked in Appendix C. The terms $(\nabla \otimes \nabla) \tilde{G}^{(x)}(r, s)$, $x \in \{c, s\}$, occurring in (57), are calculated as

$$\begin{aligned} (\nabla \otimes \nabla) \tilde{G}^{(x)}(r, s) &= \frac{1}{r} \partial_r \left(\frac{1}{r} \partial_r \tilde{G}^{(x)}(r, s) \right) (\mathbf{r} \otimes \mathbf{r}) + \frac{1}{r} \partial_r \tilde{G}^{(x)}(r, s) \hat{\mathbf{I}} \\ &= \left(\frac{3}{r^2} + \frac{3}{r} \frac{s}{\tilde{c}_x(s)} + \frac{s^2}{\tilde{c}_x^2(s)} \right) \tilde{G}^{(x)}(r, s) \frac{\mathbf{r} \otimes \mathbf{r}}{r^2} - \frac{1}{r} \left(\frac{1}{r} + \frac{s}{\tilde{c}_x(s)} \right) \tilde{G}^{(x)}(r, s) \hat{\mathbf{I}}, \end{aligned}$$

using $(\nabla \otimes \nabla) f(r) = \nabla \otimes (\nabla f(r)) = \text{grad grad } f(r) = \text{grad} \left(\frac{df(r)}{dr} \text{grad } r \right) = \text{grad} \left(\frac{df(r)}{dr} \frac{\mathbf{r}}{r} \right) = \text{grad} \left(\frac{1}{r} \frac{df(r)}{dr} \right) \otimes \mathbf{r} + \frac{1}{r} \frac{df(r)}{dr} \hat{\mathbf{I}} = \frac{1}{r} \frac{d}{dr} \left(\frac{1}{r} \frac{df(r)}{dr} \right) (\mathbf{r} \otimes \mathbf{r}) + \frac{1}{r} \frac{df(r)}{dr} \hat{\mathbf{I}}$, as well as using

$$\partial_r \tilde{G}^{(x)}(r, s) = - \left(\frac{1}{r} + \frac{s}{\tilde{c}_x(s)} \right) \tilde{G}^{(x)}(r, s),$$

see Green's function in Laplace domain given by (58), transforming (57) into

$$\begin{aligned} \tilde{\mathbf{R}}(\mathbf{r}, s) &= \tilde{G}^{(c)}(r, s) \frac{\mathbf{r} \otimes \mathbf{r}}{r^2} + \tilde{G}^{(s)}(r, s) \left(\hat{\mathbf{I}} - \frac{\mathbf{r} \otimes \mathbf{r}}{r^2} \right) \\ &\quad + \frac{1}{r} \left(\frac{\tilde{c}_s^2(s)}{s^2} \left(\frac{1}{r} + \frac{s}{\tilde{c}_s(s)} \right) \tilde{G}^{(s)}(r, s) - \frac{\tilde{c}_c^2(s)}{s^2} \left(\frac{1}{r} + \frac{s}{\tilde{c}_c(s)} \right) \tilde{G}^{(c)}(r, s) \right) \left(\hat{\mathbf{I}} - 3 \frac{\mathbf{r} \otimes \mathbf{r}}{r^2} \right), \end{aligned}$$

i.e.,

$$\tilde{\mathbf{R}}(\mathbf{r}, s) = \tilde{G}^{(c)}(r, s) \frac{\mathbf{r} \otimes \mathbf{r}}{r^2} + \tilde{G}^{(s)}(r, s) \left(\hat{\mathbf{I}} - \frac{\mathbf{r} \otimes \mathbf{r}}{r^2} \right) - \frac{1}{r} \left(\partial_r \tilde{g}^{(s)}(r, s) - \partial_r \tilde{g}^{(c)}(r, s) \right) \left(\hat{\mathbf{I}} - 3 \frac{\mathbf{r} \otimes \mathbf{r}}{r^2} \right), \quad (59)$$

where functions $\tilde{g}^{(x)}$, $x \in \{c, s\}$, defined by

$$\tilde{g}^{(x)}(r, s) = \frac{\tilde{c}_x^2(s)}{s^2} \tilde{G}^{(x)}(r, s) = \frac{1}{4\pi r} \frac{1}{s^2} e^{-\frac{rs}{\tilde{c}_x(s)}}, \quad (60)$$

see also (58), imply

$$\partial_r \tilde{g}^{(x)}(r, s) = - \frac{\tilde{c}_x^2(s)}{s^2} \left(\frac{1}{r} + \frac{s}{\tilde{c}_x(s)} \right) \tilde{G}^{(x)}(r, s).$$

In order to find the resolvent tensor $\hat{\mathbf{R}}$, in the final step, it is necessary to invert the Laplace transform of Green's functions in Laplace domain $\tilde{G}^{(x)}$, see (58), as well as of functions $\tilde{g}^{(x)}$, $x \in \{c, s\}$, see (60), so that the resolvent tensor in Laplace domain (59) transforms into

$$\hat{\mathbf{R}}(\mathbf{r}, t) = G^{(c)}(r, t) \frac{\mathbf{r} \otimes \mathbf{r}}{r^2} + G^{(s)}(r, t) \left(\hat{\mathbf{I}} - \frac{\mathbf{r} \otimes \mathbf{r}}{r^2} \right) - \frac{1}{r} \left(\partial_r g^{(s)}(r, t) - \partial_r g^{(c)}(r, t) \right) \left(\hat{\mathbf{I}} - 3 \frac{\mathbf{r} \otimes \mathbf{r}}{r^2} \right), \quad (61)$$

or equivalently into

$$\begin{aligned} \hat{\mathbf{R}}(\mathbf{r}, t) &= G^{(c)}(r, t) \begin{bmatrix} \mathbf{e}_r \\ \mathbf{0} \\ \mathbf{0} \end{bmatrix}^T + G^{(s)}(r, t) \begin{bmatrix} \mathbf{0} \\ \mathbf{e}_\theta \\ \mathbf{e}_\varphi \end{bmatrix}^T - \frac{1}{r} \left(\partial_r g^{(s)}(r, t) - \partial_r g^{(c)}(r, t) \right) \begin{bmatrix} -2\mathbf{e}_r \\ \mathbf{e}_\theta \\ \mathbf{e}_\varphi \end{bmatrix}^T, \quad \text{i.e.,} \\ \hat{\mathbf{R}}(\mathbf{r}, t) &= \begin{bmatrix} G^{(c)}(r, t) \mathbf{e}_r \\ G^{(s)}(r, t) \mathbf{e}_\theta \\ G^{(s)}(r, t) \mathbf{e}_\varphi \end{bmatrix}^T - \frac{1}{r} \left(\partial_r g^{(s)}(r, t) - \partial_r g^{(c)}(r, t) \right) \begin{bmatrix} -2\mathbf{e}_r \\ \mathbf{e}_\theta \\ \mathbf{e}_\varphi \end{bmatrix}^T, \quad (62) \end{aligned}$$

where \mathbf{e}_r , \mathbf{e}_θ , and \mathbf{e}_φ are unit vectors of the spherical coordinate system, due to the diagonalization of tensors appearing in the resolvent tensor (61), namely due to

$$\frac{\mathbf{r} \otimes \mathbf{r}}{r^2} = \begin{bmatrix} 1 & 0 & 0 \\ 0 & 0 & 0 \\ 0 & 0 & 0 \end{bmatrix} = \begin{bmatrix} \mathbf{e}_r \\ \mathbf{0} \\ \mathbf{0} \end{bmatrix}^T$$

implying

$$\hat{\mathbf{I}} - \frac{\mathbf{r} \otimes \mathbf{r}}{r^2} = \begin{bmatrix} 0 & 0 & 0 \\ 0 & 1 & 0 \\ 0 & 0 & 1 \end{bmatrix} = \begin{bmatrix} \mathbf{0} \\ \mathbf{e}_\theta \\ \mathbf{e}_\varphi \end{bmatrix}^T \quad \text{and} \quad \hat{\mathbf{I}} - 3 \frac{\mathbf{r} \otimes \mathbf{r}}{r^2} = \begin{bmatrix} -2 & 0 & 0 \\ 0 & 1 & 0 \\ 0 & 0 & 1 \end{bmatrix} = \begin{bmatrix} -2\mathbf{e}_r \\ \mathbf{e}_\theta \\ \mathbf{e}_\varphi \end{bmatrix}^T,$$

since the eigenvalue problem

$$\frac{\mathbf{r} \otimes \mathbf{r}}{r^2} \mathbf{u} = \lambda \hat{\mathbf{I}} \mathbf{u}$$

yields eigenvalues $\lambda_1 = 1$ and $\lambda_{2,3} = 0$, with eigenvectors $\mathbf{u}^{(1)} = \frac{\mathbf{r}}{r} = \mathbf{e}_r$ and $\mathbf{r} \cdot \mathbf{u}^{(2,3)} = 0$, implying $r\mathbf{u}^{(1)} \cdot \mathbf{u}^{(2,3)} = 0$, i.e., $r\mathbf{e}_r \cdot \mathbf{u}^{(2,3)} = 0$, so that eigenvectors $\mathbf{u}^{(2,3)}$ can be identified as the unit vectors \mathbf{e}_θ and \mathbf{e}_φ .

The simple matrix form of resolvent tensor (62) clearly shows that the compressive wave progresses in the direction of a radius vector, depending on its intensity, while the shear wave progresses in the plane perpendicular to the direction of a radius vector, see the first term in (62), while the second term in (62) accounts for the additional contributions.

2.3 Green's functions

Green's functions $G^{(x)}$, $x \in \{c, s\}$, appearing in the resolvent tensor (61) and (62), take similar but different forms depending on the wave propagation speed character, while functions $g^{(x)}$ have the same form regardless of the wave speed. Namely, by examining the short-time asymptotics of Green's function, one finds that Green's function is actually a distribution in the case when wave propagation speed is finite, which implies that one has to regularize Green's function in Laplace domain in order to be able to apply Laplace inversion formula and obtain Green's function at arbitrary time instant, while in the case when wave propagation speed is infinite, no regularization of Green's function is needed, since its short-time asymptotics implies that Green's function is a function. Short- and large-time asymptotics of Green's function are obtained from the asymptotics of Green's function in Laplace domain, governed by the behavior of memory function $\tilde{c}_x(s)$ as $s \rightarrow \infty$ and $s \rightarrow 0$, respectively, which is established in Appendix A.

If wave propagation speed is finite, i.e., if glass modulus $\sigma_{sr/g}^{(x)}$ attains a finite value, then Green's function is actually a distribution, which is apparent from the asymptotics of Green's function in Laplace domain (58), being of the form

$$\tilde{G}^{(x)}(r, s) \sim \frac{1}{4\pi r c_x^2} e^{-\frac{rs}{c_x}}, \quad \text{as } s \rightarrow \infty,$$

thus implying the asymptotics of Green's function in time domain

$$G^{(x)}(r, t) \sim \frac{1}{4\pi r c_x^2} \delta\left(t - \frac{r}{c_x}\right), \quad \text{as } t \rightarrow 0, \quad (63)$$

where δ is a Dirac delta distribution, which is obtained according to the theorem that if $\tilde{f}(s) \sim \tilde{g}(s)$ as $s \rightarrow \infty$, then $f(t) \sim g(t)$ as $t \rightarrow 0$, since the asymptotics of memory function \tilde{c}_x , according to (84), yields

$$\tilde{c}_x(s) \sim \kappa, \quad \text{as } s \rightarrow \infty,$$

with κ given in Tables 5, 6, 7, and 8, on one hand, while the expressions for memory functions (34) and (42) and calculations in Appendix B.1 yield

$$\tilde{c}_x(s) = \sqrt{\frac{s \tilde{\sigma}_{sr}^{(x)}(s)}{\varrho}} \sim \sqrt{\frac{\sigma_{sr/g}^{(x)}}{\varrho}} = c_x, \quad \text{as } s \rightarrow \infty$$

on the other hand, see also (18). Note, calculation of Green's function, conducted in Appendix B.1, implies that Green's function has non-zero values if $r < c_x t$, with c_x taken as above. Therefore, materials described by Case I and III of linear fractional-order models containing derivatives of orders in interval $(0, 1)$, as well as fractional Burgers models belonging to the second class, have finite speed of mechanical disturbance propagation.

If wave propagation speed is finite, then Green's function in time domain is obtained via regularization in Laplace domain

$$\tilde{G}_\varepsilon^{(x)}(r, s) = \tilde{G}^{(x)}(r, s) \tilde{\delta}_\varepsilon(s) \quad (64)$$

implying

$$G^{(x)}(r, t) = \lim_{\varepsilon \rightarrow 0} G_\varepsilon^{(x)}(r, t) = G^{(x)}(r, t) *_t \lim_{\varepsilon \rightarrow 0} \delta_\varepsilon(t) = G^{(x)}(r, t) *_t \delta(t), \quad (65)$$

where the regularization of Dirac delta distribution is chosen as

$$\delta_\varepsilon(t) = \frac{\varepsilon}{2t\sqrt{\pi t}} e^{-\frac{\varepsilon^2}{4t}}, \quad \text{with } \tilde{\delta}_\varepsilon(s) = e^{-\varepsilon\sqrt{s}}, \quad (66)$$

since $\lim_{\varepsilon \rightarrow 0} \delta_\varepsilon(t) = \delta(t)$, due to $\tilde{\delta}_\varepsilon(s) \Big|_{\varepsilon=0} = e^{-\varepsilon\sqrt{s}} \Big|_{\varepsilon=0} = 1 = \mathcal{L}[\delta(t)]$. The regularized Green's function is obtained according to

$$\begin{aligned} G_\varepsilon^{(x)}(r, t) &= \mathcal{L}^{-1} \left[\tilde{G}^{(x)}(r, s) \tilde{\delta}_\varepsilon(s) \right] (r, t) \\ &= \mathcal{L}^{-1} \left[\frac{1}{4\pi r \tilde{c}_x^2(s)} e^{-\frac{rs}{\tilde{c}_x(s)}} e^{-\varepsilon\sqrt{s}} \right] (r, t) \\ &= \mathcal{L}^{-1} \left[\frac{1}{4\pi r} \varrho \frac{\Phi_\sigma(s)}{\Phi_\varepsilon(s)} e^{-rs\sqrt{\varrho}} \sqrt{\frac{\Phi_\sigma(s)}{\Phi_\varepsilon(s)}} e^{-\varepsilon\sqrt{s}} \right] (r, t), \end{aligned} \quad (67)$$

see expressions (58), (34), (42), and (16), as well as Appendix B.1 for calculations, taking the explicit form

$$\begin{aligned} G_\varepsilon^{(x)}(r, t) &= \frac{1}{4\pi^2 r} \int_0^\infty \frac{1}{|\tilde{c}_x^2(\rho e^{i\varphi_0})|} e^{\rho t \cos \varphi_0 - \frac{r\rho}{|\tilde{c}_x(\rho e^{i\varphi_0})|} \cos(\varphi_0 - \arg \tilde{c}_x(\rho e^{i\varphi_0})) - \varepsilon\sqrt{\rho} \cos \frac{\varphi_0}{2}} \\ &\quad \times \sin \left(\rho t \sin \varphi_0 - \frac{r\rho}{|\tilde{c}_x(\rho e^{i\varphi_0})|} \sin(\varphi_0 - \arg \tilde{c}_x(\rho e^{i\varphi_0})) + \varphi_0 - \arg \tilde{c}_x^2(\rho e^{i\varphi_0}) - \varepsilon\sqrt{\rho} \sin \frac{\varphi_0}{2} \right) d\rho, \end{aligned} \quad (68)$$

if $r < c_x t$, with $c_x = \sqrt{\frac{\sigma_{sr/g}^{(x)}}{\varrho}}$, while if $r > c_x t$, then

$$G_\varepsilon^{(x)}(r, t) = 0,$$

where $\varphi_0 = \pi$ if function Φ_σ (function Φ_ε) either has no zeros or has a negative real zero, while $\varphi_0 = \arg s_0$ if s_0 and its complex conjugate \bar{s}_0 are zeros of function Φ_σ (function Φ_ε). Note, the constant c_x represents the speed of compressive/shear wave propagation, see (18), and it originates from the asymptotics (84) of the memory function \tilde{c}_x , being connected with constant κ in cases when $\delta = 0$, see Tables 5, 6, 7, and 8, by $c_x = \kappa$.

The integral representation of the asymptotics of regularized Green's function (68) is calculated in Appendix B.3 in the form

$$G_{\varepsilon, \text{asy}}^{(x)}(r, t) = \frac{1}{4\pi^2 r \kappa^2} \int_0^\infty e^{-\rho(t - \frac{r}{\kappa})} \sin(\varepsilon\sqrt{\rho}) d\rho, \quad (69)$$

according to (67), since $\tilde{c}_x(s) \sim \kappa$, as $s \rightarrow \infty$.

On the other hand, if wave propagation speed is infinite, i.e., if glass modulus $\sigma_{sr/g}^{(x)}$ tends to infinity, then no regularization of Green's function is needed, which is apparent from the asymptotics of Green's function in Laplace domain (58), being of the form

$$\tilde{G}^{(x)}(r, s) \sim \frac{1}{4\pi \kappa^2 r} \frac{1}{s^\delta} e^{-\frac{r}{\kappa} s^{1-\frac{\delta}{2}}}, \quad \text{as } s \rightarrow \infty, \quad (70)$$

thus, according to the same theorem as above, implying the short-time asymptotics of Green's function

$$G^{(x)}(r, t) \sim \frac{1}{4\pi^2 \kappa^2 r} \int_0^\infty \frac{1}{\rho^\delta} e^{-\rho \left(t - \frac{r}{\kappa} \rho^{-\frac{\delta}{2}} \cos \frac{\delta\pi}{2} \right)} \sin \left(\frac{r}{\kappa} \rho^{1-\frac{\delta}{2}} \sin \frac{\delta\pi}{2} + \delta\pi \right) d\rho, \quad \text{as } t \rightarrow 0, \quad (71)$$

calculated in Appendix B.3, since

$$\tilde{c}_x(s) = \sqrt{\frac{s \tilde{\sigma}_{sr}^{(x)}(s)}{\varrho}} \sim \kappa s^{\frac{\delta}{2}}, \quad \text{as } s \rightarrow \infty, \quad \text{with } \delta \in (0, 1),$$

see also (84) as well as Tables 5, 6, 7, and 8 for values of κ and δ . Therefore, materials described by Case II and IV of linear fractional-order models containing derivatives of orders in interval $(0, 1)$, fractional Burgers models belonging to the first class, as well as all fractional anti-Zener and Zener models have infinite speed of mechanical disturbance propagation.

Green's function, appearing in the resolvent tensor (61) and (62), is given by (68) on the domain $r > 0$ and $t > 0$, for $\varepsilon = 0$, i.e., by

$$G^{(x)}(r, t) = G_\varepsilon^{(x)}(r, t) \Big|_{\varepsilon=0}. \quad (72)$$

Note, calculation of Green's function, conducted in Appendix B.1, implies that Green's function has non-zero values for all points in space $r > 0$ at any time instant $t > 0$, and moreover the large-time asymptotics, as proved below, implies that Green's function tends to zero as a power-type function for any $r > 0$.

In order to investigate the large-time asymptotics of Green's function, one again starts from Green's function in Laplace domain (58) and asymptotics of memory function \tilde{c}_x , taking the form

$$\tilde{c}_x(s) \sim \begin{cases} \kappa, \\ \kappa s^{\frac{\delta}{2}}, & \delta \in (0, 1), \end{cases} \quad \text{for } s \rightarrow 0,$$

see also (84), as well as Tables 5, 6, 7, and 8 for values of κ and δ , implying, by (58), the asymptotics of Green's function in Laplace domain

$$\tilde{G}^{(x)}(r, s) \sim \begin{cases} \frac{1}{4\pi r \kappa^2} e^{-\frac{rs}{\kappa}} \sim \frac{1}{4\pi r \kappa^2}, \\ \frac{1}{4\pi r \kappa^2} \frac{1}{s^\delta} e^{-\frac{r}{\kappa} s^{1-\frac{\delta}{2}}} \sim \frac{1}{4\pi r \kappa^2} \frac{1}{s^\delta}, & \delta \in (0, 1), \end{cases} \quad \text{as } s \rightarrow 0.$$

According to the theorem that if $\tilde{f}(s) \sim \tilde{g}(s)$ as $s \rightarrow 0$, then $f(t) \sim g(t)$ as $t \rightarrow \infty$, one obtains large-time asymptotics of Green's function in the form

$$G^{(x)}(r, t) \sim \begin{cases} \frac{1}{4\pi r \kappa^2} \delta(t) = 0, \\ \frac{1}{4\pi r \kappa^2} \frac{t^{-(1-\delta)}}{\Gamma(\delta)} \rightarrow 0, & \delta \in (0, 1), \end{cases} \quad \text{as } t \rightarrow \infty. \quad (73)$$

Function $g^{(x)}$, appearing in the resolvent tensor (61) and (62), given in the form

$$\begin{aligned} g^{(x)}(r, t) &= \int_0^t \mathfrak{g}^{(x)}(r, t') dt', \quad \text{where} \\ \mathfrak{g}^{(x)}(r, t) &= \frac{1}{4\pi^2 r} \left(\varphi_0 + \int_0^\infty \frac{1}{\rho} e^{\rho t \cos \varphi_0 - \frac{r\rho}{|\tilde{c}_x(\rho e^{i\varphi_0})|} \cos(\varphi_0 - \arg \tilde{c}_x(\rho e^{i\varphi_0}))} \right. \\ &\quad \left. \times \sin \left(\rho t \sin \varphi_0 - \frac{r\rho}{|\tilde{c}_x(\rho e^{i\varphi_0})|} \sin(\varphi_0 - \arg \tilde{c}_x(\rho e^{i\varphi_0})) \right) d\rho \right). \end{aligned} \quad (74)$$

with φ_0 taken as above, is calculated in Appendix B.2 according to

$$g^{(x)}(r, t) = \mathcal{L}^{-1} \left[\frac{1}{s} \tilde{\mathfrak{g}}^{(x)}(r, s) \right] (r, t), \quad \text{with } \tilde{\mathfrak{g}}^{(x)}(r, s) = \frac{1}{4\pi r} \frac{1}{s} e^{-\frac{rs}{\tilde{c}_x(s)}}, \quad (75)$$

see also expression (60) for function $\tilde{g}^{(x)}$.

In the case of classical wave equation (5), considered on unbounded domain and subject to initial conditions (28), which corresponds to the propagation of a mechanical disturbance in an isotropic and elastic three-dimensional body, the resolvent tensor takes the form

$$\begin{aligned} \hat{\mathbf{R}}(\mathbf{r}, s) &= \frac{1}{4\pi r c_c} \delta(c_c t - r) \frac{\mathbf{r} \otimes \mathbf{r}}{r^2} + \frac{1}{4\pi r c_s} \delta(c_s t - r) \left(\hat{\mathbf{I}} - \frac{\mathbf{r} \otimes \mathbf{r}}{r^2} \right) \\ &\quad + \frac{t}{4\pi r^3} \left(H\left(t - \frac{r}{c_s}\right) - H\left(t - \frac{r}{c_c}\right) \right) \left(\hat{\mathbf{I}} - 3 \frac{\mathbf{r} \otimes \mathbf{r}}{r^2} \right), \end{aligned}$$

according to (61), since classical Green's functions $G^{(x)}$, as well as functions $g^{(x)}$, $x \in \{c, s\}$, are obtained as

$$G^{(x)}(r, t) = \frac{1}{4\pi r c_x^2} \delta\left(t - \frac{r}{c_x}\right) = \frac{1}{4\pi r c_x} \delta(c_x t - r), \quad (76)$$

due to $\delta(cr) = \frac{1}{|c|} \delta(r)$, as well as

$$g^{(x)}(r, t) = \frac{1}{4\pi r} \left(t - \frac{r}{c_x}\right) H\left(t - \frac{r}{c_x}\right) \quad \text{with} \quad \partial_r g^{(x)}(r, t) = -\frac{t}{4\pi r^2} H\left(t - \frac{r}{c_x}\right),$$

due to $r\delta(r) = 0$, by inverting the Laplace transforms of classical Green's functions in Laplace domain

$$\tilde{G}^{(x)}(r, s) = \frac{1}{4\pi r c_x^2} e^{-\frac{rs}{c_x}},$$

as well as of functions

$$\tilde{g}^{(x)}(r, s) = \frac{1}{4\pi r} \frac{1}{s^2} e^{-\frac{rs}{c_x}},$$

since (58) and (60) define classical Green's function in Laplace domain and function $\tilde{g}^{(x)}$ if, instead of the memory functions \tilde{c}_x , the constant speed of the wave propagation c_x is substituted. This simple substitution is possible since the generalized wave equations (35) and (43) become classical wave equations (6) and (7) using the mentioned substitution.

3 Numerical examples

Linear fractional-order models, fractional Burgers models, and fractional anti-Zener and Zener models can be classified into two groups depending on whether they model a viscoelastic material with infinite or finite wave propagation speed, as it is stated in Introduction. Case II and IV of linear fractional-order models, fractional Burgers models of the first class (Models I - V), and all fractional anti-Zener and Zener models describe materials with infinite wave propagation speed, while Case I and III of linear fractional-order models and fractional Burgers models of the second class (Models VI - VIII) describe materials with finite wave propagation speed. Fractional anti-Zener and Zener model $I^+ID.ID$, as well as fractional Burgers model VII, namely

$$\left(a_1 {}_0I_t^{\alpha+\beta+\nu} + a_2 {}_0I_t^\nu + a_3 {}_0D_t^{\alpha+\beta-\nu} \right) \sigma(t) = \left(b_1 {}_0I_t^\alpha + b_2 {}_0D_t^\beta \right) \varepsilon(t), \quad (77)$$

with narrowed thermodynamical restrictions

$$0 \leq \alpha + \beta - \nu \leq 1, \quad 1 \leq \alpha + \beta + \nu \leq 2, \quad \alpha \leq \nu \leq 1 - \beta, \quad (78)$$

$$\begin{aligned} \frac{a_1}{a_2} \left| \frac{\cos \frac{(\alpha+2\beta+\nu)\pi}{2}}{\cos \frac{(\nu-\alpha)\pi}{2}} \right| &\leq \frac{a_1}{a_2} \left| \frac{\cos \frac{(\alpha+2\beta+\nu)\pi}{2}}{\cos \frac{(\nu-\alpha)\pi}{2}} \right| \frac{\sin \frac{(\alpha+2\beta+\nu)\pi}{2}}{\sin \frac{(\nu-\alpha)\pi}{2}} \leq \frac{b_1}{b_2}, \\ \frac{b_1}{b_2} &\leq \frac{a_2}{a_3} \frac{\sin \frac{(\beta+\nu)\pi}{2}}{\sin \frac{(2\alpha+\beta-\nu)\pi}{2}} \frac{\cos \frac{(\beta+\nu)\pi}{2}}{\cos \frac{(2\alpha+\beta-\nu)\pi}{2}} \leq \frac{a_2}{a_3} \frac{\sin \frac{(\beta+\nu)\pi}{2}}{\sin \frac{(2\alpha+\beta-\nu)\pi}{2}}, \end{aligned} \quad (79)$$

and

$$\left(1 + a_1 {}_0D_t^\alpha + a_2 {}_0D_t^\beta + a_3 {}_0D_t^{2\beta} \right) \sigma(t) = \left(b_1 {}_0D_t^\beta + b_2 {}_0D_t^{2\beta} \right) \varepsilon(t), \quad (80)$$

with narrowed thermodynamical restrictions

$$\begin{aligned} 0 \leq \alpha \leq \beta \leq 1, \quad \frac{1}{2} \leq \beta \leq \frac{1+\alpha}{2}, \quad \frac{a_3}{a_2} \leq \frac{b_2}{b_1} \leq a_2 \frac{1}{|\cos(\beta\pi)|}, \\ \frac{a_3}{a_2} \leq \frac{a_2}{2 \cos^2(\beta\pi)} \left(1 - \sqrt{1 - \frac{4a_3 \cos^2(\beta\pi)}{a_2^2}} \right) \leq \frac{b_2}{b_1} \leq \frac{a_2}{|\cos(\beta\pi)|}, \end{aligned}$$

are respectively chosen as representatives of previously mentioned two model classes in order to plot time evolution of spatial profiles of Green's function $G^{(x)}$, $x \in \{c, s\}$ and its asymptotics.

3.1 Green's function $G^{(x)}$ - infinite wave propagation speed

Model parameters corresponding to fractional anti-Zener and Zener model $I^+ID.ID$, see (77), are chosen as in Table 2 in order to plot time evolution of spatial profiles of Green's function $G^{(x)}$, either according to analytical expression (68) with $\varepsilon = 0$ and $\varphi_0 = \pi$, if function

$$\phi_\sigma(s) = a_1 + a_2 s^{\alpha+\beta} + a_3 s^{2(\alpha+\beta)}, \quad (81)$$

see also Table 4, has no zeros, or according to analytical expression (68) with $\varepsilon = 0$ and $\varphi_0 = \arg s_0$, if s_0 and its complex conjugate \bar{s}_0 are zeros of function ϕ_σ , as well as by the numerical Laplace transform inversion using the expression (58) for Green's function in Laplace domain $\tilde{G}^{(x)}$ and fixed Talbot method developed in [1], while expressions (71) for short time asymptotics, as well as (73)₂ for large time asymptotics, are used to produce profiles of the asymptotic behavior of Green's function. Namely, spatial profiles of Green's function $G^{(x)}$ in the case when Green's function in Laplace domain $\tilde{G}^{(x)}$ has no other branch points besides $s = 0$ are presented in Figures 1, 2, and 3, while spatial profiles of Green's function $G^{(x)}$ in the case when $\tilde{G}^{(x)}$ has a pair of complex conjugated branch points s_0 and \bar{s}_0 besides $s = 0$ are shown in Figures 4, 5, 6, and 7.

Case when ϕ_σ has	α	β	ν	a_1	a_2	a_3	b_1	b_2
no zeros	0.35	0.55	0.4	0.05	1.5	0.45	0.7	0.95
a pair of complex conjugated zeros				11	15	20.27	7	9.5

Table 2: Parameters of model $I^+ID.ID$ used for numerical examples.

The spatial profiles of Green's function $G^{(x)}$, corresponding to fractional anti-Zener and Zener model $I^+ \text{ID.ID}$ in the case when Green's function in Laplace domain $\tilde{G}^{(x)}$ has no other branch points besides $s = 0$, are presented in Figure 1 for different time instants, being positive and displaying decreasing character for smaller distances r from the origin, with a pronounced peak for medium values of r , and finally tending to zero for large values of r . More precisely, the spatial profiles tend to infinity as r tends to zero and asymptotically settle to zero for r tending to infinity, presumably since Green's function predominantly behaves as a hyperbolic function $\frac{1}{r}$ for both $r \rightarrow 0$ and $r \rightarrow \infty$, which is supported by the form of the analytical expression (68) for Green's function, as well as by the short and large time asymptotics (71) and (73). The peak, carrying the information about the initial disturbance and resembling to the Dirac delta peak in the case of classical wave propagation, see (76), decreases in height and increases in width as time increases, presumably due to the dissipative character of the model. In particular, Figure 1b shows the matching of the profiles obtained through the analytical expression (68) of Green's function, which are presented by the solid line, with the curves presented by dotted line, which are obtained by the numerical Laplace transform inversion of Green's function in the Laplace domain (58) using the fixed Talbot method.

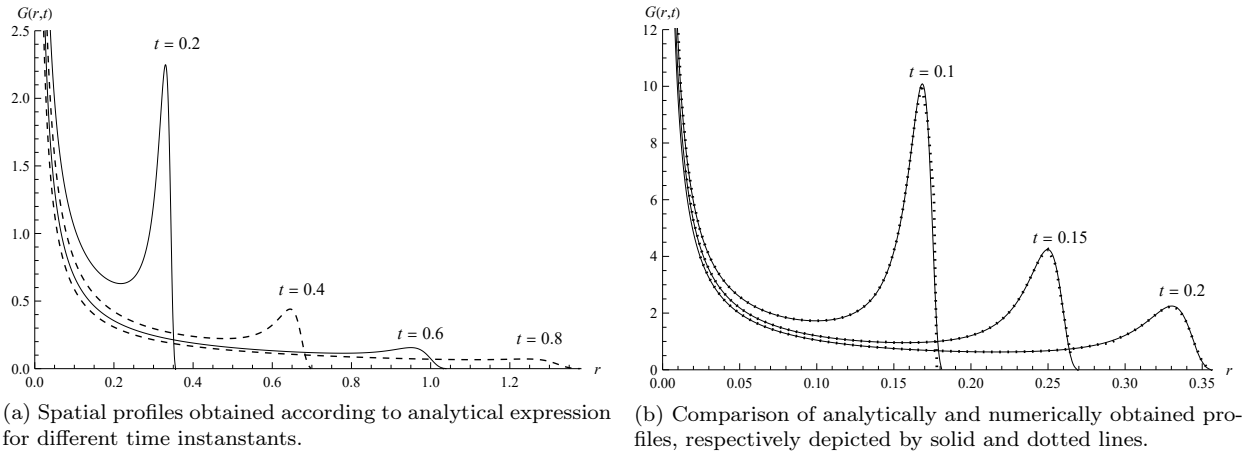


Figure 1: Case of infinite wave propagation speed - spatial profiles of Green's function $G^{(x)}$ corresponding to model $I^+ \text{ID.ID}$ when Green's function in Laplace domain $\tilde{G}^{(x)}$ has no other branch points besides $s = 0$.

Also, it is verified in Figure 2 that the overlap of spatial profile of Green's function, depicted by solid line, with the short time asymptotic profile, depicted by dashed line, becomes better and better as time decreases, where the solid line profiles are obtained according to the analytical expression (68), with $\varepsilon = 0$ and $\varphi_0 = \pi$, while the dotted line profiles are obtained according to the asymptotic expression (71). Similarly, Figure 3 verifies that the overlap of spatial profile of Green's function, depicted by solid line, with the large time asymptotic profile, depicted by dashed line, becomes better and better as time increases, where the expression (73) is used in order to produce large time asymptotic profiles of Green's function.

The spatial profiles that correspond to Green's function $G^{(x)}$ in the case when Green's function in Laplace domain $\tilde{G}^{(x)}$ has a pair of complex conjugated branch points s_0 and \bar{s}_0 besides $s = 0$, obtained according to the expression (68), with $\varepsilon = 0$ and $\varphi_0 = \arg s_0$, and shown in Figure 4a, similarly as in the case when there are no branch points of $\tilde{G}^{(x)}$ besides $s = 0$, tend to infinity as r tends to zero and asymptotically settle to zero for r tending to infinity, again as a hyperbolic function $\frac{1}{r}$ for both $r \rightarrow 0$ and $r \rightarrow \infty$, see (68) and asymptotic expressions (71) and (73)₂. On one hand, Figure 4a presents a single peak for each spatial profile carrying the information about the initial disturbance, resembling to the Dirac delta peak in the case of classical wave propagation, and displaying decrease in height and increase in width as time increases, and on the other hand, Figure 4a shows a good agreement between the solid line curves obtained according to the analytical expression and the dotted line curves obtained by the numerical Laplace transform inversion of Green's function in the Laplace domain (58), similarly as Figure 1b.

Contrary to the case when Green's function in Laplace domain $\tilde{G}^{(x)}$ has no other branch points besides $s = 0$, in which the spatial profiles do not exhibit oscillatory character, in the case when $\tilde{G}^{(x)}$ has a pair of complex conjugated branch points s_0 and \bar{s}_0 besides $s = 0$, for time large enough, Figure 4b clearly shows the damped oscillatory character of the tails of spatial profiles, that is not prominent for smaller values of time, see Figure 4a. The oscillatory character of spatial profiles becomes more pronounced as time becomes larger, as evident from Figure 5, since the number of oscillations increases, so instead of at most one oscillation for time instances $t \leq 15$, see Figures 4b and 5a, there is more than one oscillation, namely a multiplicative factor of an oscillation belonging to a set $\{3/2, 2, 5/2, 3\}$ for respective time instants $t \in \{30, 45, 60, 75\}$, see Figures 5b - 5e. Also, as time increases, the amplitudes of spatial profile tails become smaller, indicating the damping

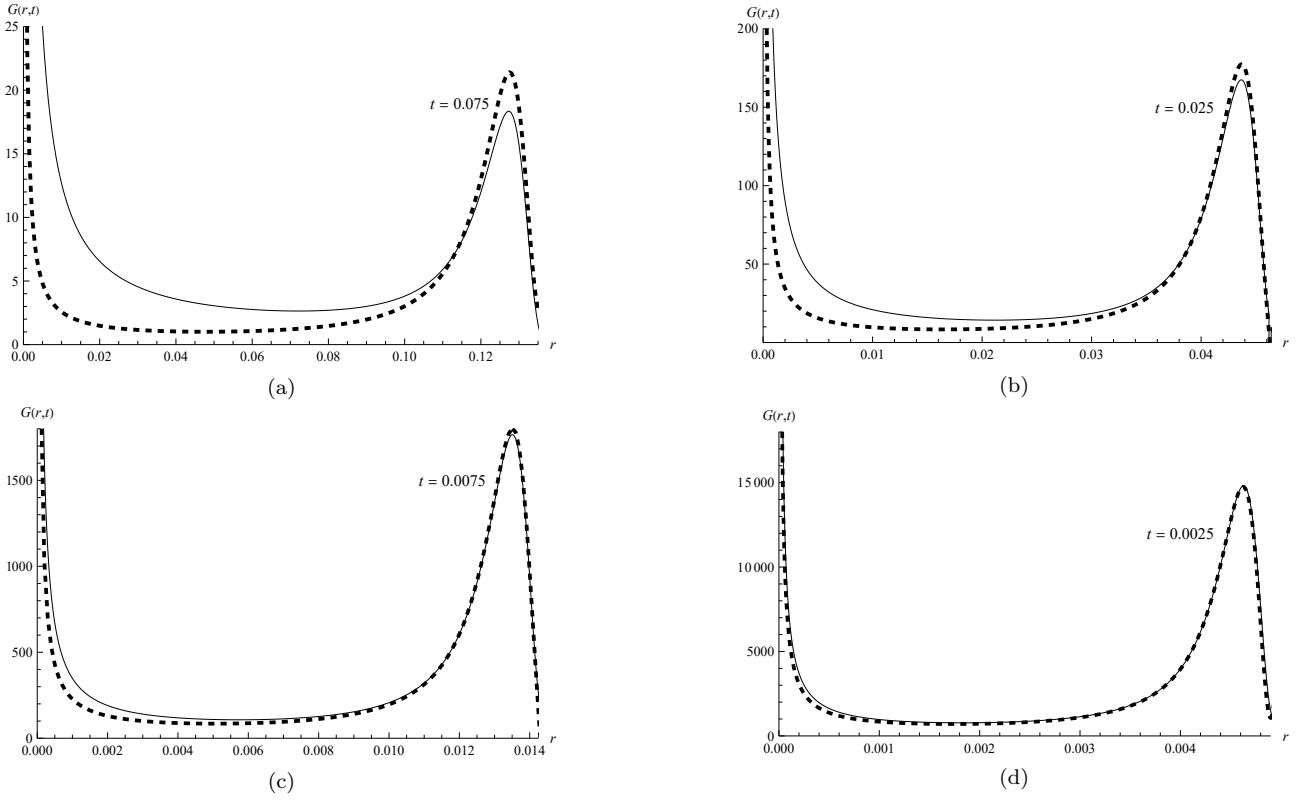


Figure 2: Comparison of spatial profiles of Green's function, depicted by solid lines, with the short time asymptotic profiles, depicted by dashed lines - case when Green's function in Laplace domain $\tilde{G}(x)$ has no other branch points besides $s = 0$.

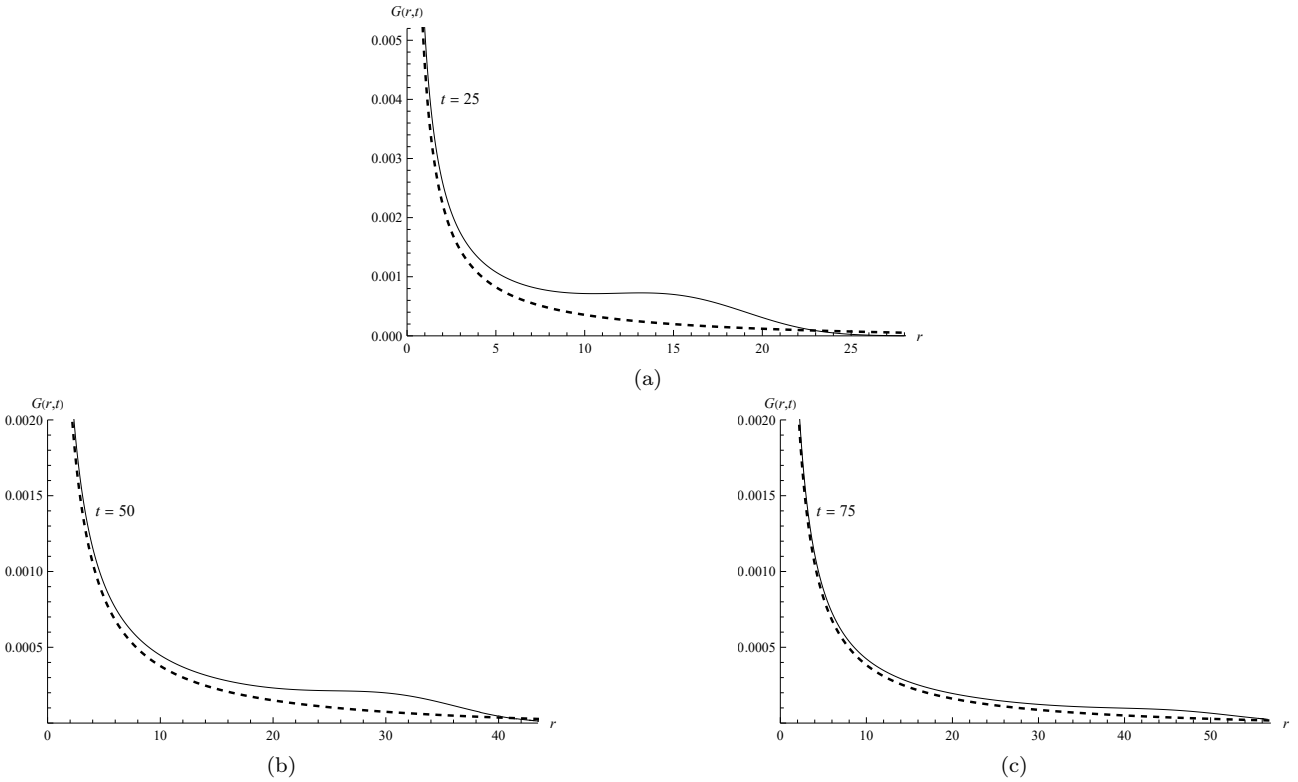
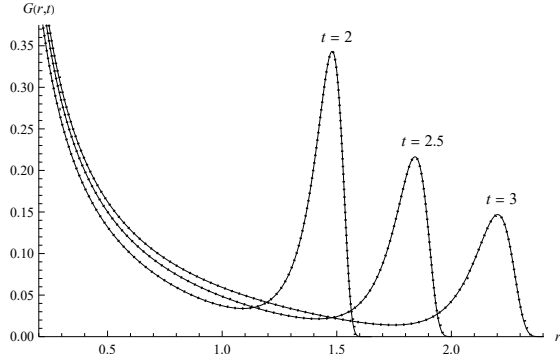
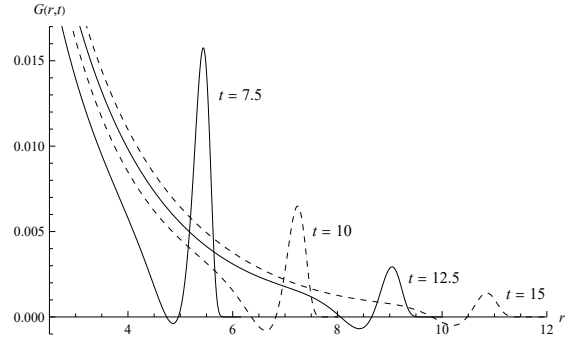


Figure 3: Comparison of spatial profiles of Green's function, depicted by solid lines, with the large time asymptotic profiles, depicted by dashed lines - case when Green's function in Laplace domain $\tilde{G}(x)$ has no other branch points besides $s = 0$.

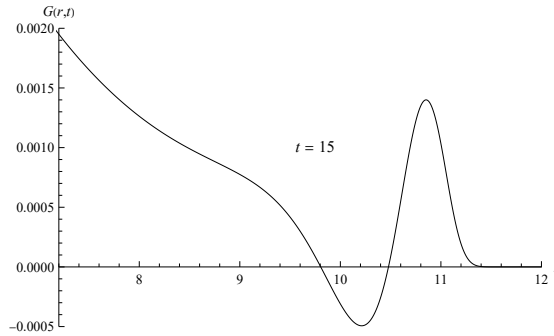


(a) Comparison of analytically and numerically obtained profiles, respectively depicted by solid and dotted lines.

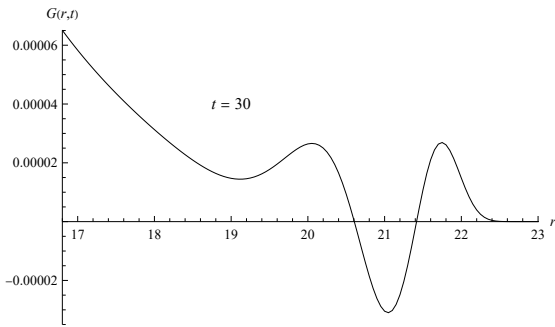


(b) Spatial profiles obtained according to analytical expression for different time instants.

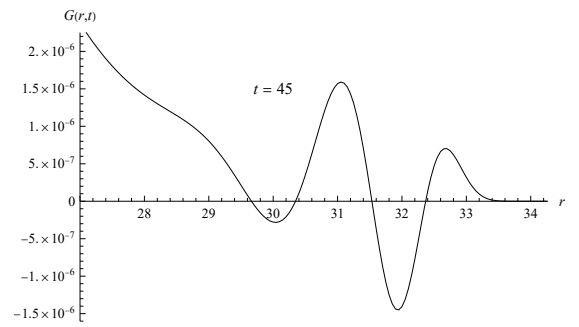
Figure 4: Case of infinite wave propagation speed - spatial profiles of Green's function $G^{(x)}$ corresponding to model $I^+ID.ID$ when Green's function in Laplace domain $\tilde{G}^{(x)}$ has a pair of complex conjugated branch points s_0 and \bar{s}_0 besides $s = 0$.



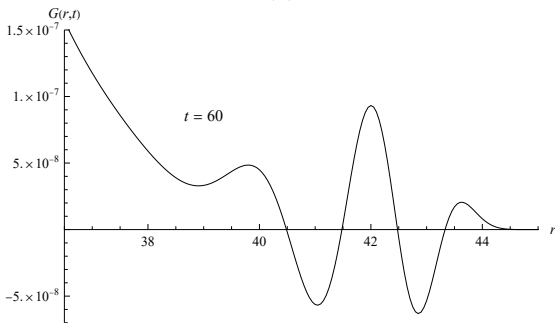
(a)



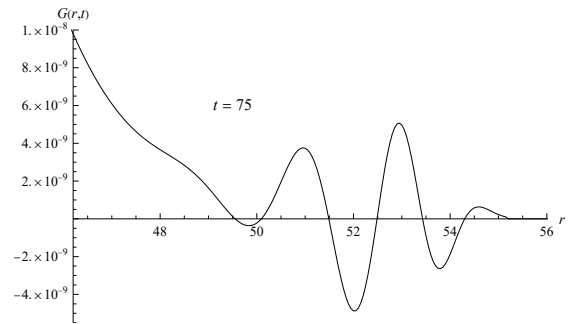
(b)



(c)



(d)



(e)

Figure 5: Case of infinite wave propagation speed - tails of spatial profiles of Green's function $G^{(x)}$ corresponding to model $I^+ID.ID$ when Green's function in Laplace domain $\tilde{G}^{(x)}$ has a pair of complex conjugated branch points s_0 and \bar{s}_0 besides $s = 0$.

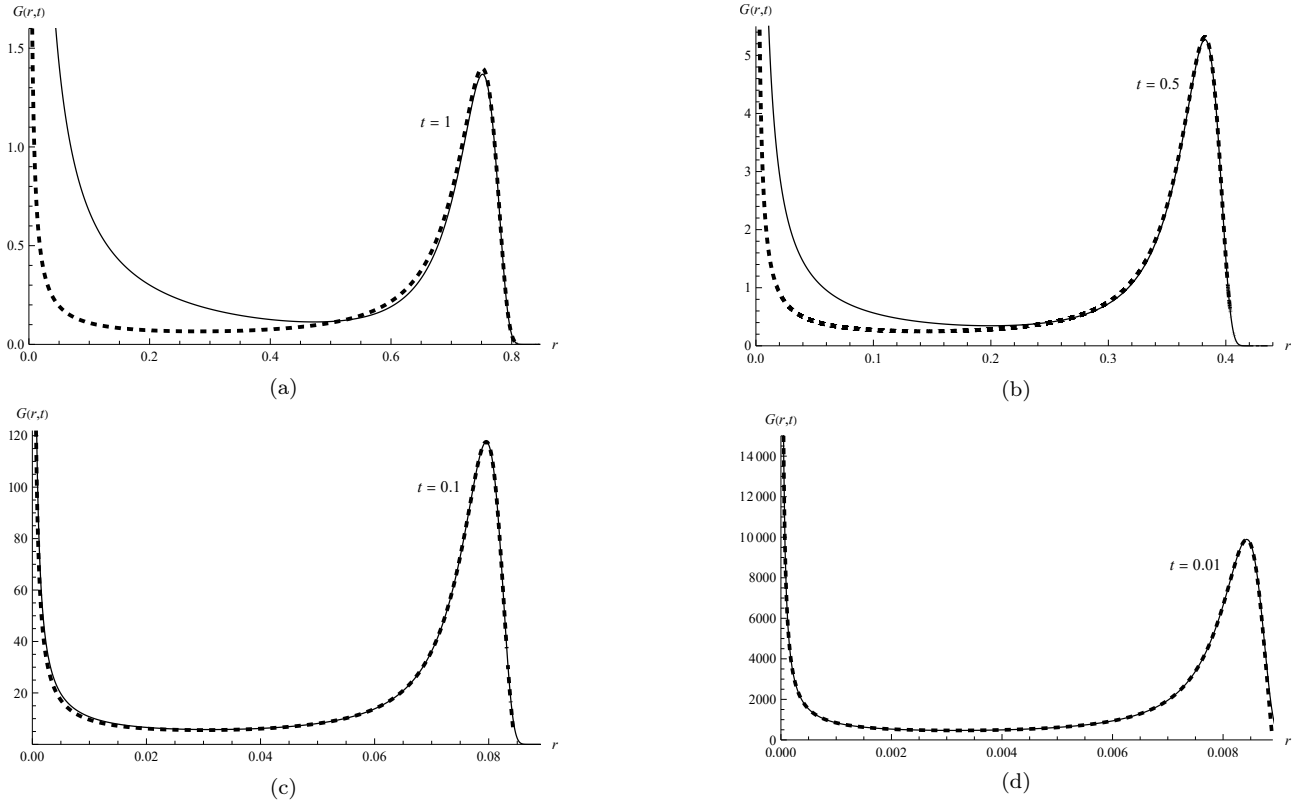


Figure 6: Comparison of spatial profiles of Green's function, depicted by solid lines, with the short time asymptotic profiles, depicted by dashed lines - case when Green's function in Laplace domain $\tilde{G}^{(x)}$ has a pair of complex conjugated branch points s_0 and \bar{s}_0 besides $s = 0$.

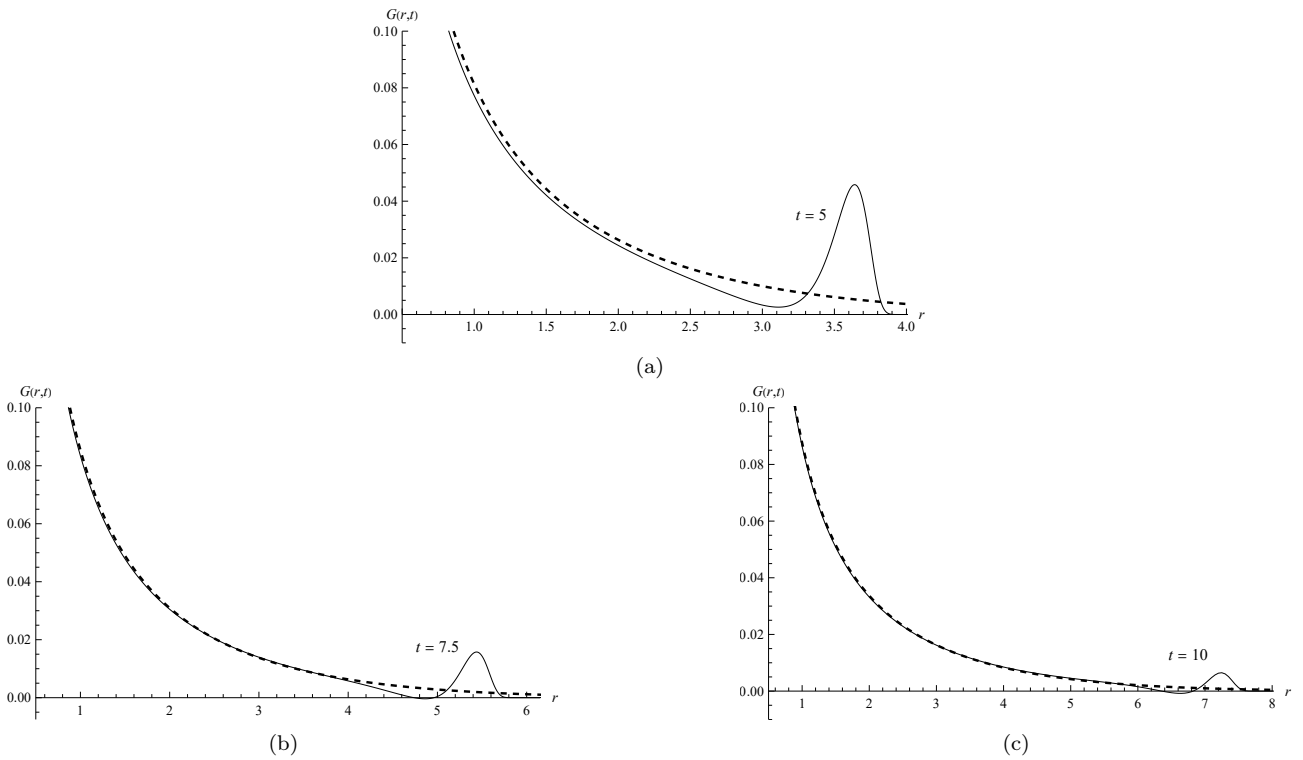


Figure 7: Comparison of spatial profiles of Green's function, depicted by solid lines, with the large time asymptotic profiles, depicted by dashed lines - case when Green's function in Laplace domain $\tilde{G}^{(x)}$ has a pair of complex conjugated branch points s_0 and \bar{s}_0 besides $s = 0$.

in both space and time. Therefore, the damped oscillatory character of Green's function $G^{(x)}$ in both space and time is due to the complex value of branch points of Green's function in Laplace domain $\tilde{G}^{(x)}$, such that, presumably, the real part of branch point s_0 corresponds to the damping, while its imaginary part corresponds to the oscillatory behavior.

On one hand, the expression for Green's function (68) qualitatively corresponds to the short time asymptotic expression (71), which can be observed from Figure 6, since there is a better overlap of the curves corresponding to these expressions as time takes smaller values, while, on the other hand, there is a better overlap of the curves from Figure 7 as time takes larger values, indicating that the expression for Green's function (68) qualitatively turns into the large time asymptotic expression (73) for a sufficiently large time. Although, spatial profiles dominantly behave as the asymptotic curves for small and medium values of r , the tail of the spatial profile is oscillatory, while asymptotic curve is not, however, as can be observed from Figure 5, the oscillation amplitudes decrease as time increases.

3.2 Green's function $G^{(x)}$ - finite wave propagation speed

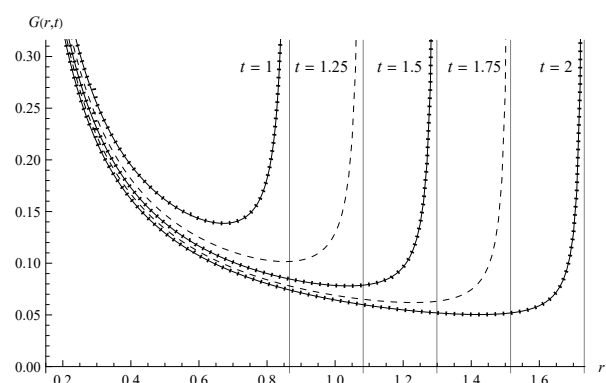
Model parameters corresponding to fractional Burgers model VII, see (80), are chosen as in Table 3 in order to plot time evolution of spatial profiles of Green's function $G^{(x)}$, either according to analytical expression (68) with $\varphi_0 = \pi$, if function Φ_σ , see (99)₁, has no zeros, or according to analytical expression (68) with $\varphi_0 = \arg s_0$, if s_0 and its complex conjugate \bar{s}_0 are zeros of function Φ_σ , as well as by the numerical Laplace transform inversion using the expression (58) for Green's function in Laplace domain $\tilde{G}^{(x)}$, while the expression (69) is used to produce profiles of short time asymptotic behavior of Green's function. Namely, spatial profiles of Green's function $G^{(x)}$ in the case when Green's function in Laplace domain $\tilde{G}^{(x)}$ has no other branch points besides $s = 0$ are presented in Figures 8 and 9, while spatial profiles of Green's function $G^{(x)}$ in the case when $\tilde{G}^{(x)}$ has a pair of complex conjugated branch points s_0 and \bar{s}_0 besides $s = 0$ are shown in Figure 10.

Case when Φ_σ has	a_1	a_2	a_3	b_1	b_2	α	β
no zeros	0.01	4.5	4	1	3	0.7	0.845
a pair of complex conjugated zeros		2.5	5.5		2.21		

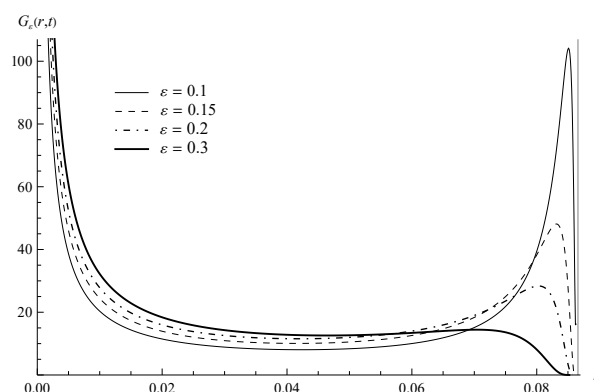
Table 3: Parameters of fractional Burgers model VII used for numerical examples.

The spatial profiles of Green's function $G^{(x)}$, corresponding to the fractional Burgers model VII in the case when Green's function in Laplace domain $\tilde{G}^{(x)}$ has no other branch points besides $s = 0$, are presented for different time instants in Figure 8a by the solid line curves, obtained according to analytical expression (68) with regularization parameter $\varepsilon = 0$, and moreover compared with spatial profiles presented by dotted line curves, obtained by the numerical Laplace transform inversion of Green's function in Laplace domain (58) using the fixed Talbot method. The profiles are positive and decrease from infinity as the distance r increases from zero up to a medium values, presumably since Green's function predominantly behaves as a hyperbolic function $\frac{1}{r}$ for $r \rightarrow 0$. Unlike the case of spatial profiles, corresponding to Green's function when the wave propagation speed is infinite, when there is a peak which translates towards higher values of r as time increases, while reducing in height and gaining in width, see Figures 1 and 4, in the case of fractional Burgers model VII, that assumes a finite value of wave propagation speed $c_x = \frac{1}{\sqrt{g}} \sqrt{\frac{b_2}{a_3}}$, the peak is not observed from medium values of r up to $r = c_x t$, referenced by the vertical line, where the profiles show increasing character towards the infinity. Actually, as indicated by the short time asymptotics of Green's function (63), represented by the Dirac delta distribution centered at $r = c_x t$, the peak should be centered at point $r = c_x t$, which is marked by the vertical line in Figure 8a. However, the peak cannot be observed, since the analytical expression (68) holds true only for $r < c_x t$, so the increase of spatial profile towards the infinity is the peak forming for $r < c_x t$, which cannot be formed for $r \geq c_x t$, and therefore cannot be completely displayed. On the other hand, the expression for regularized Green's function $G_\varepsilon^{(x)}$ allows for the formation of peak at the tail of spatial profile, as can be observed from Figure 8b, from which is obvious that as the regularization parameter ε decreases, the position of peak shifts towards $r = c_x t$, while peak's width decreases and its height increases.

Figure 9 presents the comparison of spatial profiles corresponding to the regularized Green's function $G_\varepsilon^{(x)}$ with the profiles corresponding to the regularization of Dirac delta distribution that represents the short time asymptotics of Green's function, where the expression (68) is used for regularized Green's function calculation, while the expression (69) is used for the calculation of regularized Dirac delta distribution. One can notice that the overlap between the curves corresponding to profiles and asymptotics becomes better as time decreases.

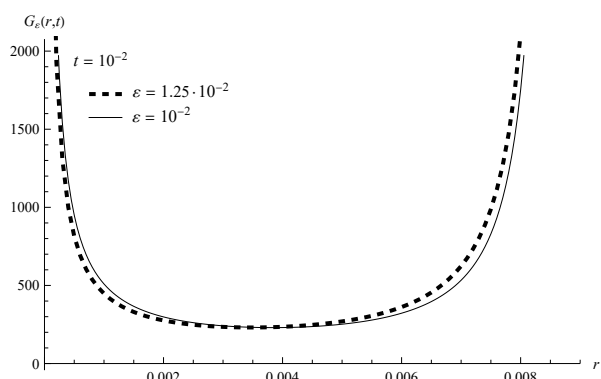


(a) Comparison of analytically and numerically obtained profiles, respectively depicted by solid/dashed and dotted lines.

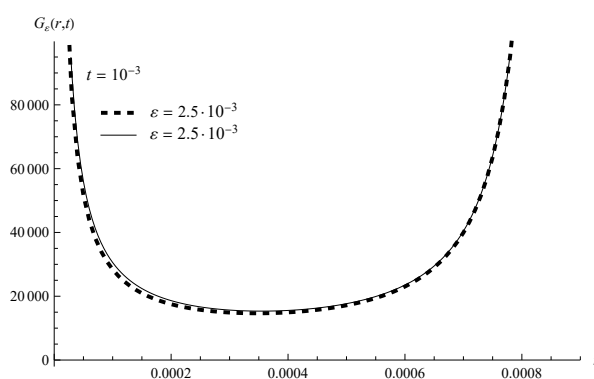


(b) Spatial profiles obtained according to analytical expression for different values of regularization parameter ε at $t = 0.1$.

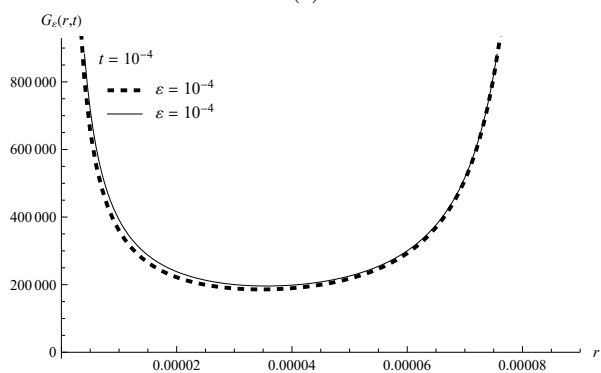
Figure 8: Case of finite wave propagation speed - spatial profiles of Green's function $G^{(x)}$ corresponding to fractional Burgers model VII when Green's function in Laplace domain $\tilde{G}^{(x)}$ has no other branch points besides $s = 0$.



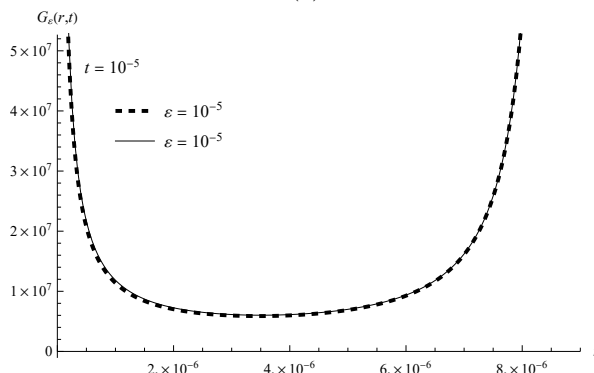
(a)



(b)



(c)



(d)

Figure 9: Comparison of spatial profiles of regularized Green's function, depicted by solid lines, with the short time asymptotic profiles, depicted by dashed lines - case when Green's function in Laplace domain $\tilde{G}^{(x)}$ has no other branch points besides $s = 0$.

Also, note that the regularization parameter ε has sufficiently small value, so that the peak at the tail of profile is not observed.

Contrary to the case when Green's function in Laplace domain $\tilde{G}^{(x)}$ has no other branch points besides $s = 0$, in which, as the distance r increases, the profiles decrease from the infinity up to the point in which the peak located at $r = c_x t$ starts to form, see Figure 8, in the case when Green's function in Laplace domain $\tilde{G}^{(x)}$ has a pair of complex conjugated branch points s_0 and \bar{s}_0 besides $s = 0$ an additional negative peak appears and it precedes the peak forming at $r = c_x t$, as it is obvious from Figure 10. Presumably, the character of spatial profiles is damped oscillatory, similarly as in the case when wave propagation speed is infinite, see Figure 4b, which is not apparent since time is not large enough. More prominent oscillatory character of tails of spatial profiles would be expected for larger times, again similarly as in Figure 5.

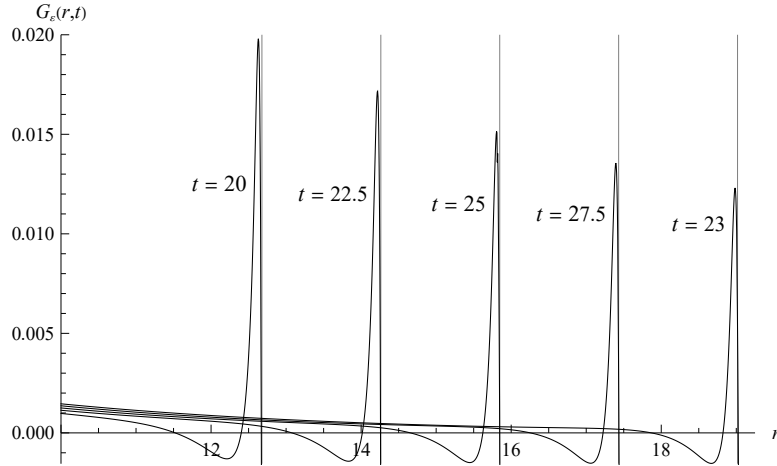


Figure 10: Case of finite wave propagation speed - spatial profiles of regularized Green's function $G_\varepsilon^{(x)}$, $\varepsilon = 0.5$, corresponding to fractional Burgers model VII when Green's function in Laplace domain $\tilde{G}^{(x)}$ has a pair of complex conjugated branch points s_0 and \bar{s}_0 besides $s = 0$.

3.3 Function $g^{(x)}$

Contrary to the case of Green's function, in which it must be taken into account whether the wave propagation speed is infinite or finite, in the case of function $g^{(x)}$, given by the expression (74), wave propagation speed is not important. Spatial profile of function $g^{(x)}$ is obtained using numerical Laplace transform inversion of the expression (75) and depicted by the solid line in Figure 11, displaying quite classical behavior, since it is positive, decreasing, and convex. Moreover, the solid line spatial profile is compared with the spatial profile, represented by dots, that originate from the analytical expression (74). Similarly as Green's function $G^{(x)}$, the function $g^{(x)}$ is also proportional to $\frac{1}{r}$, and therefore the spatial profile starts from infinity for $r \rightarrow 0$ and settles at zero for $r \rightarrow \infty$.

4 Conclusion

The starting point of generalization of the classical Hooke's law (4), describing three-dimensional isotropic and elastic body, to a constitutive model (9), describing three-dimensional isotropic and viscoelastic body, is the constitutive equation of one-dimensional viscoelastic body (8), expressed through the relaxation moduli $\sigma_{sr}^{(c)}$ and $\sigma_{sr}^{(s)}$, used in order to account for different memory kernels corresponding to propagation of compressive (c) and shear (s) waves. Further, in order to describe the wave propagation in three-dimensional isotropic and viscoelastic body, the constitutive model (9) is coupled with the equation of motion of deformable solid body (2) and equation of infinitesimal strain (3), yielding the system of equations (25) - (27), that is subject to initial conditions (28) and solved on unbounded domain for displacement field by the use of Fourier and Laplace transforms. More precisely, the application of Fourier and Laplace transforms to the system of equations (25) - (27), subject to (28), yielded the wave equation of viscoelastic body in Fourier and Laplace domain (32), which is solved for displacement field using two different approaches.

In the first approach, after scalar and vector multiplication of wave vector with the wave equation of viscoelastic body in Fourier and Laplace domain (32) and after performing Laplace and Fourier transforms inversions, wave equations (35) and (43) are obtained, representing the generalization of classical wave equations (6) and (7), where speeds of compressive and shear waves, c_c and c_s , are substituted with the memory kernels \tilde{c}_c and \tilde{c}_s ,

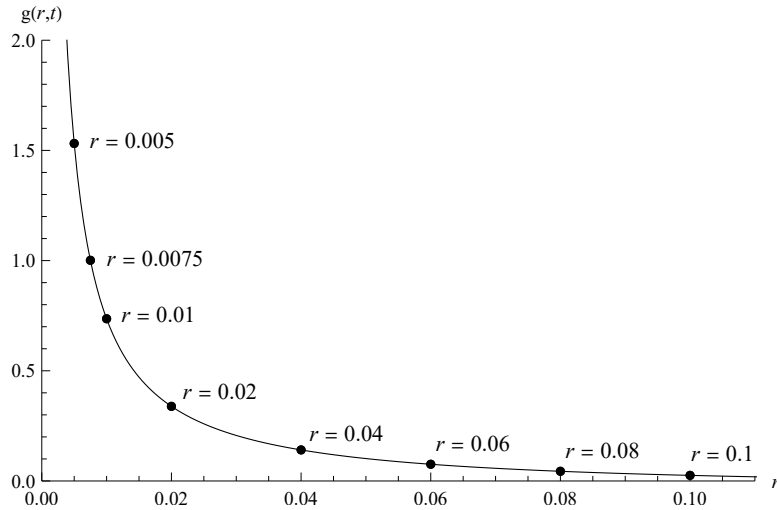


Figure 11: Comparison of spatial profiles of function g , corresponding to model $I^+ID.ID$, obtained according to numerical Laplace transform inversion (solid line) and by analytical expression (dots) at time instant $t = 0.1$.

given by (34) and (42), which are expressed through the corresponding relaxation moduli $\sigma_{sr}^{(c)}$ and $\sigma_{sr}^{(s)}$, such that their initial values, i.e., glass moduli, can be either finite or infinite implying two different cases (36) and (38) for the compressive wave equation (35), as well as two different cases (44) and (45) for the shear wave equation (43). Therefore, in this approach, two wave equations (35) and (43), expressed in terms of scalar and vector fields φ and $\mathbf{\Omega}$, defined by (35)₂ and (43)₂, are obtained as generalizations of classical wave equations (6) and (7), rather than a single wave equation expressed in terms of displacement field, which would be generalization of classical wave equation (1), or equivalently (5). After the expressions (49) and (50) for the scalar and vector fields φ and $\mathbf{\Omega}$ are found dependent on Green's functions $G^{(c)}$ and $G^{(s)}$, the displacement field is expressed by (51), accounting for four possibilities due to Green's functions $G^{(c)}$ and $G^{(s)}$ taking two different forms: (68), which holds for $r < c_x t$ and zero otherwise, and (72), where the first one is valid in the case of finite glass modulus and therefore wave propagation speed c_x , $x \in \{c, s\}$, as well, while the second one is valid in the case of infinite glass modulus and therefore wave propagation speed as well.

Since complex and demanding calculations are required in the first approach, in the second one, the use of resolvent tensor $\hat{\mathbf{R}}$ is found to be more convenient to determine the displacement field, so that the wave equation of viscoelastic body in Fourier and Laplace domain (32) is rewritten in matrix representation (52), yielding the displacement field in Laplace and Fourier domain (54), i.e., yielding the expression (55) for the displacement field as the solution to the system of equations (25) - (27), subject to (28), after performing the inverse Laplace and Fourier transforms of the resolvent tensor (56), implying that the displacement field is simply determined as the application of resolvent tensor in the form (61) to the already known initial conditions (28). For the resolvent tensor, besides the expression (61) consisting of Green's functions $G^{(c)}$ and $G^{(s)}$, given by (68) and (72), as well as of functions $g^{(c)}$ and $g^{(s)}$, obtained as (74), each of them calculated in Appendix, one also obtains expression (62) for the resolvent tensor, clearly showing that the compressive wave progresses in the direction of a radius vector, while the shear wave progresses in the plane perpendicular to the direction of a radius vector.

Finally, the qualitative properties of spatial profiles corresponding to Green's function $G^{(x)}$, $x \in \{c, s\}$, are investigated through the graphical presentation of numerical calculations. Fractional anti-Zener and Zener model $I^+ID.ID$, given by (77), as well as fractional Burgers model VII, given by (80), are respectively chosen as representatives of models describing viscoelastic materials with infinite and finite wave propagation speed, being $c_x = \frac{1}{\sqrt{e}} \sqrt{\frac{b_2}{a_3}}$, in order to plot time evolution of spatial profiles of Green's function $G^{(x)}$, as well as to plot its short and large time asymptotic behavior. Regardless of the fact whether the wave propagation speed is infinite or finite, the spatial profiles of Green's function are positive and display decreasing character for smaller distances r from the origin, see Figures 1, 4, and 8. However, if wave propagation speed is infinite, the tails of spatial profiles either asymptotically tend to zero as distance r tends to infinity, as in Figures 1 and 4a, or, if wave propagation speed is finite, the spatial profiles tend to infinity as r reaches the point $r = c_x t$, forming the peak centered at $r = c_x t$, see Figure 8a, which can actually be observed in Figures 8b and 10, where the plots corresponding to the regularized Green's function are presented. More precisely, if wave propagation speed is infinite, there is a single peak for medium values of r , which carries the information about the initial disturbance, translates towards the higher values of r as time increases, while reducing in height and gaining in width, and resembles to the Dirac delta peak in the case of classical wave propagation, as it is shown in Figures 1 and 4, while, if wave propagation speed is finite, according to the short time asymptotics of Green's

function (63), there is the Dirac delta distribution centered at point $r = c_x t$, and therefore for any time instant one expects the peak forming at point $r = c_x t$, which cannot be completely displayed in Figure 8a, since the analytical expression (68) holds true only for $r < c_x t$. In the case when there are no zeros of functions ϕ_σ and Φ_σ , given by (81) and (99)₁, which respectively refer to the model I⁺ID.ID and fractional Burgers model VII, describing a viscoelastic material with infinite and finite wave propagation speed, i.e., in the case when Green's function in Laplace domain $\tilde{G}^{(x)}$ has no other branch points besides $s = 0$, the spatial profiles do not exhibit an oscillatory character, while if functions ϕ_σ and Φ_σ have a pair of complex conjugated zeros, i.e., if Green's function in Laplace domain $\tilde{G}^{(x)}$ has a pair of complex conjugated branch points s_0 and \bar{s}_0 besides $s = 0$, on one hand, the tails of spatial profiles in the case of model I⁺ID.ID have the damped oscillatory character, as shown in Figure 4b, and on the other hand, an additional negative peak, preceding the peak forming at $r = c_x t$, appears in spatial profiles in the case of fractional Burgers model VII, as obvious from Figure 10. Moreover, asymptotic profiles are compared with spatial profiles of Green's function in Figures 2, 6, and 9 for short times, as well as in Figures 3 and 7 for large times, displaying good agreement, which is also found if the profiles obtained by the numerical Laplace transform inversion of Green's function in the Laplace domain are compared with the profiles corresponding to analytical expression, as it is obvious from Figures 1b, 4a, and 8a.

A Asymptotics of memory function \tilde{c}_x

In order to examine both short- and large-time asymptotic behavior of Green's functions, as done in Section 2.3, it is necessary to find the asymptotics of memory function \tilde{c}_x , $x \in \{c, s\}$, corresponding to the compressive and shear waves. Starting from defining relations (34) and (42) for memory function \tilde{c}_x and by taking into account the expression (16) for the relaxation modulus in Laplace domain, for the memory function one has

$$\tilde{c}_x(s) = \sqrt{\frac{s\tilde{\sigma}_{sr}^{(x)}(s)}{\varrho}} = \frac{1}{\sqrt{\varrho}} \sqrt{\frac{\Phi_\varepsilon(s)}{\Phi_\sigma(s)}}, \quad (82)$$

with functions Φ_ε and Φ_σ given by (15). Memory function \tilde{c}_x , taken in the form (82), corresponds to the fractional linear models having orders in interval $(0, 1)$, given by (19), if functions Φ_ε and Φ_σ are given by (85) below, as well as to the fractional Burgers models (24), if functions Φ_ε and Φ_σ are given by (91) and (97) below, while in the case of fractional anti-Zener and Zener models, listed in Table 1, the memory function takes the form

$$\tilde{c}_x(s) = \frac{1}{\sqrt{\varrho}} \sqrt{s^\xi \frac{\phi_\varepsilon(s)}{\phi_\sigma(s)}}, \quad x \in \{c, s\}, \quad (83)$$

with functions ϕ_ε and ϕ_σ , as well as with exponent ξ given in Table 4, due to the form of complex modulus

$$\tilde{E}(s) = \frac{\Phi_\varepsilon(s)}{\Phi_\sigma(s)} = s^\xi \frac{\phi_\varepsilon(s)}{\phi_\sigma(s)},$$

see also (14)₂, specific for the fractional anti-Zener and Zener models.

Further analysis of the asymptotics of memory function \tilde{c}_x , see (82) and (83), is reduced to finding the asymptotic expressions of functions Φ_σ and Φ_ε , respectively ϕ_σ and ϕ_ε , whose explicit forms are given below and obtained as consequences of the operators acting on stress and strain in the constitutive equation in time domain (10) using the Laplace transform of the constitutive equation, generally yielding (14)₁, according to the Laplace transforms of fractional integral and Riemann-Liouville fractional derivative (12) and (13). It is demonstrated in the sequel that the asymptotic behavior of memory function \tilde{c}_x , given by (82) or (83), is governed by the expression

$$\tilde{c}_x(s) \sim \begin{cases} \kappa, \\ \kappa s^{\frac{\delta}{2}}, \end{cases} \quad \delta \in (0, 1), \quad \text{for both } s \rightarrow \infty \quad \text{and} \quad s \rightarrow 0, \quad (84)$$

for all considered linear fractional-order constitutive models of viscoelastic body, where constants κ and δ are given in the Tables 5 and 6 for linear fractional-order models containing only Riemann-Liouville fractional derivatives of orders in interval $(0, 1)$, see (19), as well as for thermodynamically consistent fractional Burgers models, see (24), while Tables 7 and 8 present constants κ and δ for symmetric and asymmetric fractional anti-Zener and Zener models, see Table 1.

	Function ϕ_σ	Function ϕ_ε	Model	Order ξ	Order λ	Order κ
Symmetric models	$a_1 + a_2 s^{\alpha+\beta}$	$b_1 + b_2 s^{\alpha+\beta}$	ID.ID	$\alpha - \mu$	-	-
			ID.DD ⁺	$\alpha + \mu < 1$	-	-
	$a_1 + a_2 s^\lambda + a_3 s^{\alpha+\gamma}$	$b_1 + b_2 s^\lambda + b_3 s^{\alpha+\gamma}$	IID.IID	$\eta - \gamma$	$\alpha - \beta$	-
			IDD.IDD	$\alpha - \mu$	$\alpha + \beta < 1$	-
			IID.IDD	$\alpha - \mu$	$\mu + \nu < 1$	$\alpha - \beta$
	$a_1 + a_2 s^{\frac{1+\alpha+\gamma}{2}} + a_3 s^{1+\alpha+\gamma}$	$b_1 + b_2 s^{\frac{1+\alpha+\gamma}{2}} + b_3 s^{1+\alpha+\gamma}$	I ⁺ ID.I ⁺ ID	$\alpha - \mu$	-	-
			IDD ⁺ .IDD ⁺	$\eta - \gamma$	-	-
			I ⁺ ID.IDD ⁺	$1 - (\gamma - \eta)$	-	-
			IID.ID	$\beta - \gamma$	$(\alpha + \beta) - (\nu + \gamma)$	$\alpha + \beta < 1$
	Asymmetric models	$a_1 + a_2 s^\lambda + a_3 s^\kappa$	$b_1 + b_2 s^{\alpha+\beta}$	IDD.DD ⁺	$\alpha + \mu < 1$	$\alpha + \beta < 1$
I ⁺ ID.ID				$\beta + \nu < 1$	-	-
$a_1 + a_2 s^{\alpha+\beta} + a_3 s^{2(\alpha+\beta)}$		$b_1 + b_2 s^\lambda + b_3 s^\kappa$	IDD ⁺ .DD ⁺	$\alpha + \mu < 1$	-	-
			ID.IDD	$\alpha - \mu$	$\mu + \nu < 1$	$\alpha + \beta < 1$
			ID.DDD ⁺	$\alpha + \mu < 1$	$\nu - \mu$	$\alpha + \nu - (\mu - \beta)$
$a_1 + a_2 s^{\alpha+\beta}$		$b_1 + b_2 s^{\alpha+\beta} + b_3 s^{2(\alpha+\beta)}$	ID.IDD ⁺	$\nu - \beta$	-	-

Table 4: Summary of constitutive functions ϕ_σ and ϕ_ε , along with the order ξ , corresponding to the thermodynamically consistent fractional anti-Zener and Zener models. The notation * means that the orders $\alpha + \beta$ and $\alpha + \gamma$ belong either to the interval $(0, 1)$ or interval $(1, 2)$.

The functions Φ_σ and Φ_ε , in the case of linear fractional-order models containing only Riemann-Liouville fractional derivatives of orders in interval $(0, 1)$, are obtained by applying the Laplace transform to the unified constitutive equation (19) in the form

$$\Phi_\sigma(s) = \sum_{i=1}^n a_i s^{\alpha_i} \quad \text{and} \quad \Phi_\varepsilon(s) = \sum_{j=1}^m b_j s^{\beta_j}, \quad \text{with} \quad (85)$$

$$0 \leq \alpha_1 < \dots < \alpha_n < \beta_1 < \dots < \beta_m < 1, \quad (86)$$

originating from thermodynamical considerations, respectively reducing to

$$\Phi_\sigma(s) = \sum_{i=1}^n a_i s^{\alpha_i} \quad \text{and} \quad \Phi_\varepsilon(s) = \sum_{i=1}^n b_i s^{\alpha_i}, \quad (87)$$

$$\Phi_\sigma(s) = \sum_{i=1}^n a_i s^{\alpha_i} \quad \text{and} \quad \Phi_\varepsilon(s) = \sum_{i=1}^n b_i s^{\alpha_i} + \sum_{i=n+1}^m b_i s^{\beta_i}, \quad (88)$$

$$\Phi_\sigma(s) = \sum_{i=1}^{n-m} a_i s^{\alpha_i} + \sum_{i=n-m+1}^n a_i s^{\alpha_i} \quad \text{and} \quad \Phi_\varepsilon(s) = \sum_{j=1}^m b_j s^{\alpha_{n-m+j}}, \quad (89)$$

$$\Phi_\sigma(s) = \sum_{i=1}^n a_i s^{\alpha_i} \quad \text{and} \quad \Phi_\varepsilon(s) = \sum_{j=1}^m b_j s^{\beta_j} \quad (90)$$

for models belonging to Case I, II, III, and IV, see (20) - (23) and also Supplementary material. The asymptotics of memory function \tilde{c}_x is governed by (84), with constants κ and δ presented in Table 5 and obtained according to (82) using functions Φ_σ and Φ_ε , see (87) - (90), and property (86) of fractional differentiation orders.

Linear fractional models	Models	asymptotics of \tilde{c}_x as $s \rightarrow \infty$		asymptotics of \tilde{c}_x as $s \rightarrow 0$	
		κ	δ	κ	δ
		Case I	$\frac{1}{\sqrt{\varrho}} \sqrt{\frac{b_n}{a_n}}$	0	$\frac{1}{\sqrt{\varrho}} \sqrt{\frac{b_1}{a_1}}$
Case II	$\frac{1}{\sqrt{\varrho}} \sqrt{\frac{b_m}{a_n}}$	$\beta_m - \alpha_n$	0		
Case III		0	α_{n-m}		
Case IV		$\beta_m - \alpha_n$	$\beta_1 - \alpha_1$		

Table 5: Asymptotics of memory function $\tilde{c}_x(s) = \frac{1}{\sqrt{\varrho}} \sqrt{\frac{\Phi_\varepsilon(s)}{\Phi_\sigma(s)}} \sim \kappa s^{\frac{\delta}{2}}$ for both $s \rightarrow \infty$ and $s \rightarrow 0$ in the case of linear fractional models having highest differentiation order in interval $(0, 1)$.

In the case of fractional Burgers models, listed in Supplementary material, grouping into two thermodynamically consistent classes and represented by the unified constitutive equations (24), functions Φ_σ and Φ_ε , for models of the first class take the form

$$\Phi_\sigma(s) = 1 + a_1 s^\alpha + a_2 s^\beta + a_3 s^\gamma \quad \text{and} \quad \Phi_\varepsilon(s) = b_1 s^\mu + b_2 s^{\mu+\eta}, \quad (91)$$

with model parameters as in Introduction, reducing to

$$\Phi_\sigma(s) = 1 + a_1 s^\alpha + a_2 s^\beta + a_3 s^\gamma \quad \text{and} \quad \Phi_\varepsilon(s) = b_1 s^\mu + b_2 s^{\mu+\eta}, \quad (92)$$

$$\Phi_\sigma(s) = 1 + a_1 s^\alpha + a_2 s^\beta + a_3 s^{2\alpha} \quad \text{and} \quad \Phi_\varepsilon(s) = b_1 s^\mu + b_2 s^{\mu+\alpha}, \quad (93)$$

$$\Phi_\sigma(s) = 1 + a_1 s^\alpha + a_2 s^\beta + a_3 s^{\alpha+\beta} \quad \text{and} \quad \Phi_\varepsilon(s) = b_1 s^\mu + b_2 s^{\mu+\alpha}, \quad (94)$$

$$\Phi_\sigma(s) = 1 + a_1 s^\alpha + a_2 s^\beta + a_3 s^{\alpha+\beta} \quad \text{and} \quad \Phi_\varepsilon(s) = b_1 s^\mu + b_2 s^{\mu+\beta}, \quad (95)$$

$$\Phi_\sigma(s) = 1 + a_1 s^\alpha + a_2 s^\beta + a_3 s^{2\beta} \quad \text{and} \quad \Phi_\varepsilon(s) = b_1 s^\mu + b_2 s^{\mu+\beta}, \quad (96)$$

for Models I, II, III, IV, and V, respectively, while for models of the second class, functions Φ_σ and Φ_ε are given by

$$\Phi_\sigma(s) = 1 + a_1 s^\alpha + a_2 s^\beta + a_3 s^{\beta+\eta} \quad \text{and} \quad \Phi_\varepsilon(s) = b_1 s^\beta + b_2 s^{\beta+\eta}, \quad (97)$$

with model parameters as in Introduction, reducing to

$$\Phi_\sigma(s) = 1 + a_1 s^\alpha + a_2 s^\beta + a_3 s^{\alpha+\beta} \quad \text{and} \quad \Phi_\varepsilon(s) = b_1 s^\beta + b_2 s^{\alpha+\beta}, \quad (98)$$

$$\Phi_\sigma(s) = 1 + a_1 s^\alpha + a_2 s^\beta + a_3 s^{2\beta} \quad \text{and} \quad \Phi_\varepsilon(s) = b_1 s^\beta + b_2 s^{2\beta}, \quad (99)$$

$$\Phi_\sigma(s) = 1 + \bar{a}_1 s^\alpha + \bar{a}_2 s^{2\alpha} \quad \text{and} \quad \Phi_\varepsilon(s) = b_1 s^\alpha + b_2 s^{2\alpha}, \quad (100)$$

for Models VI, VII, and VIII, respectively. The asymptotics of memory function \tilde{c}_x is governed by (84), with constants κ and δ presented in Table 6 and obtained according to (82) using functions Φ_σ and Φ_ε , see (92) - (96), in the case of models belonging to the first class, as well as using functions Φ_σ and Φ_ε , see (98) - (100), in the case of models belonging to the second class.

Fractional Burgers models		Models	asymptotics of \tilde{c}_x as $s \rightarrow \infty$		asymptotics of \tilde{c}_x as $s \rightarrow 0$		
			κ	δ	κ	δ	
		First class	Model I*	$\frac{1}{\sqrt{\varrho}} \sqrt{\frac{b_2}{a_3}}$	$\mu + \eta - \gamma$	$\mu - \alpha$	μ
Model II	$\mu - \alpha$						
Model III	$\mu - \beta$						
Model IV	$\mu - \alpha$						
Model V	$\mu - \beta$						
Second class	Model VI	0	0	0	β	0	
	Model VII						
	Model VIII						$\frac{1}{\sqrt{\varrho}} \sqrt{\frac{b_2}{\bar{a}_2}}$

Table 6: Asymptotics of memory function $\tilde{c}_x(s) = \frac{1}{\sqrt{\varrho}} \sqrt{\frac{\Phi_\varepsilon(s)}{\Phi_\sigma(s)}} \sim \kappa s^{\frac{\delta}{2}}$ for both $s \rightarrow \infty$ and $s \rightarrow 0$ in the case of fractional Burgers models, where * is used to emphasize that $\eta \in \{\alpha, \beta, \gamma\}$.

The functions ϕ_σ and ϕ_ε , as well as exponent ξ , appearing in the expression (83) for memory function \tilde{c}_x , in the case of symmetric and asymmetric fractional anti-Zener and Zener models, listed in Table 1 and in Supplementary material, are given in Table 4, and therefore the asymptotics of memory function \tilde{c}_x is governed by (84), with constants κ and δ presented in Table 7 for symmetric and in Table 8 for asymmetric fractional anti-Zener and Zener models.

B Calculation of Green's function, its asymptotics, and function $\mathfrak{g}^{(x)}$

Green's functions $G^{(x)}$, along with their asymptotics, as well as functions $g^{(x)}$, with $x \in \{c, s\}$, appearing in the resolvent tensor (61) and (62) and discussed about in Section 2.3, are calculated by the application of inverse Laplace transform definition, using the contour integration and Cauchy integral theorem.

B.1 Calculation of Green's function

Green's function in Laplace domain, given by (58), can be rewritten as

$$\tilde{G}^{(x)}(r, s) = \frac{1}{4\pi r \tilde{c}_x^2(s)} e^{-\frac{rs}{\tilde{c}_x(s)}} = \frac{\varrho}{4\pi r} \frac{\Phi_\sigma(s)}{\Phi_\varepsilon(s)} e^{-\sqrt{\varrho} r s \sqrt{\frac{\Phi_\sigma(s)}{\Phi_\varepsilon(s)}}}, \quad (101)$$

using the memory function \tilde{c}_x expressed in the form (82), so that Green's function in Laplace domain (101) and hence (58) as well, has a branch point $s = 0$, due to the terms in functions Φ_σ and Φ_ε containing s^ξ , $\xi \in (0, 2)$, as well as a pair of complex conjugated branch points $s_0 = \rho_0 e^{i\varphi_0}$ and \bar{s}_0 , with $\varphi_0 \in (\frac{\pi}{2}, \pi)$, in the case when s_0 and \bar{s}_0 are zeros of function Φ_σ , while if s_0 and \bar{s}_0 are zeros of function Φ_ε , then these points are also the poles of Green's function in Laplace domain. Note, instead of complex conjugated zeros s_0 and \bar{s}_0 , either of the functions Φ_σ and Φ_ε may have a negative real zero as well, and certainly no zeros at all.

Symmetric anti-Zener/Zener models	Models	asymptotics of \tilde{c}_x as $s \rightarrow \infty$		asymptotics of \tilde{c}_x as $s \rightarrow 0$	
		κ	$\delta = \xi$	κ	$\delta = \xi$
		ID.ID	$\frac{1}{\sqrt{\varrho}} \sqrt{\frac{b_2}{a_2}}$	$\alpha - \mu$	$\frac{1}{\sqrt{\varrho}} \sqrt{\frac{b_1}{a_1}}$
ID.DD ⁺	$\alpha + \mu < 1$	$\alpha + \mu < 1$			
IID.IID	$\frac{1}{\sqrt{\varrho}} \sqrt{\frac{b_3}{a_3}}$	$\eta - \gamma$	$\eta - \gamma$		
IDD.IDD		$\alpha - \mu$	$\alpha - \mu$		
IID.IDD					
I ⁺ ID.I ⁺ ID	$\frac{1}{\sqrt{\varrho}} \sqrt{\frac{b_3}{a_3}}$	$\eta - \gamma$	$\eta - \gamma$		
IDD ⁺ .IDD ⁺		$1 - (\gamma - \eta)$	$1 - (\gamma - \eta)$		
I ⁺ ID.IDD ⁺					

Table 7: Asymptotics of memory function $\tilde{c}_x(s) = \frac{1}{\sqrt{\varrho}} \sqrt{s \xi \frac{\phi_\varepsilon(s)}{\phi_x(s)}} \sim \kappa s^{\frac{\delta}{2}}$ for both $s \rightarrow \infty$ and $s \rightarrow 0$ in the case of symmetric fractional anti-Zener/Zener models.

Asymmetric anti-Zener/Zener models	Models	asymptotics of \tilde{c}_x as $s \rightarrow \infty$		asymptotics of \tilde{c}_x as $s \rightarrow 0$	
		κ	δ	κ	$\delta = \xi$
		IID.ID	$\frac{1}{\sqrt{\varrho}} \sqrt{\frac{b_2}{a_3}}$	$\beta - \gamma = \xi$	$\frac{1}{\sqrt{\varrho}} \sqrt{\frac{b_1}{a_1}}$
IDD.DD ⁺	$\alpha + \beta < 1$	$\alpha + \mu < 1$			
I ⁺ ID.ID	$\nu - \alpha$	$\beta + \nu < 1$			
IDD ⁺ .DD	$\mu - \beta$	$\alpha + \mu < 1$			
ID.IDD	$\frac{1}{\sqrt{\varrho}} \sqrt{\frac{b_3}{a_2}}$	$\alpha - \mu = \xi$	$\alpha - \mu$		
ID.DDD ⁺		$\alpha + \nu < 1$	$\alpha + \mu < 1$		
ID.IDD ⁺			$\nu - \beta$		

Table 8: Asymptotics of memory function $\tilde{c}_x(s) = \frac{1}{\sqrt{\varrho}} \sqrt{s \xi \frac{\phi_\varepsilon(s)}{\phi_x(s)}} \sim \kappa s^{\frac{\delta}{2}}$ for both $s \rightarrow \infty$ and $s \rightarrow 0$ in the case of asymmetric fractional anti-Zener/Zener models.

In the case of linear fractional-order models containing only Riemann-Liouville fractional derivatives of orders in interval $(0, 1)$, given by the constitutive equation (19), there are no zeros of functions Φ_σ and Φ_ε , according to Lemma 4.2. in [18], since all differentiation orders are in interval $(0, 1)$, see (85). On the other hand, in the case of thermodynamically consistent fractional Burgers models, given by (24), the function Φ_σ may have a pair of complex conjugated zeros, or a negative real zero, or no zeros at all, as proved in Appendix A of [25], since function Φ_σ is a polynomial function having the highest differentiation order in interval $(1, 2)$, see (91) and (97) for models of the first and second class respectively. Regarding the fractional anti-Zener and Zener models, listed in Table 1, it is shown in Section 6. of [14] that both functions ϕ_σ and ϕ_ε may have a pair of complex conjugated zeros, or a negative real zero, or no zeros at all, since both functions are polynomial functions having the highest order in interval $(1, 2)$, see Table 4.

In the Cauchy integral theorem

$$\oint_{\Gamma} \tilde{G}_\varepsilon^{(x)}(r, s) e^{st} ds = 0,$$

the integration is performed along the contour Γ , depicted in Figure 12 and taken so that the singular points $s = 0$, s_0 , and \bar{s}_0 lie outside the contour Γ , in order to obtain the regularized Green's function in time domain by the inversion of Laplace transform of Green's function in Laplace domain, regularized by the smooth approximation of Dirac delta distribution, yielding

$$G_\varepsilon^{(x)}(r, t) = \frac{1}{2\pi i} \int_{Br} \tilde{G}_\varepsilon^{(x)}(r, s) e^{st} ds = \mathcal{L}^{-1} \left[\tilde{G}_\varepsilon^{(x)}(r, s) \tilde{\delta}_\varepsilon(s) \right] (r, t) = \mathcal{L}^{-1} \left[\frac{1}{4\pi r \tilde{c}_x^2(s)} e^{-\frac{rs}{\tilde{c}_x(s)}} e^{-\varepsilon\sqrt{s}} \right] (r, t),$$

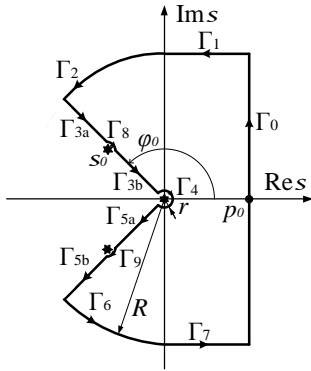
see also (65), where integration is performed along the Bromwich contour Br , i.e., along the contour Γ_0 in the limit when $R \rightarrow \infty$, having Γ_0 as a part of the closed contour Γ from Figure 12, so that the Cauchy integral theorem reduces to

$$2\pi i G_\varepsilon^{(x)}(r, t) = - \lim_{\substack{R \rightarrow \infty \\ \tilde{r} \rightarrow 0}} (I_{\Gamma_{3a} \cup \Gamma_{3b}} + I_{\Gamma_{5a} \cup \Gamma_{5b}}), \quad (102)$$

where $I_{\Gamma_{3a} \cup \Gamma_{3b}}$ and $I_{\Gamma_{5a} \cup \Gamma_{5b}}$ are integrals along contours $\Gamma_{3a} \cup \Gamma_{3b}$ and $\Gamma_{5a} \cup \Gamma_{5b}$ having non-zero contribution, since for the left-hand-side of Cauchy integral theorem one has

$$\oint_{\Gamma} \tilde{G}_\varepsilon^{(x)}(r, s) e^{st} ds = \sum_{i=0}^9 I_{\Gamma_i}, \quad \text{with} \quad I_{\Gamma_i} = \int_{\Gamma_i} \frac{1}{4\pi r \tilde{c}_x^2(s)} e^{-\frac{rs}{\tilde{c}_x(s)}} e^{-\varepsilon\sqrt{s}} e^{st} ds, \quad (103)$$

where the integrals I_{Γ_1} , I_{Γ_2} , I_{Γ_4} , I_{Γ_6} , I_{Γ_7} , I_{Γ_8} , and I_{Γ_9} have zero contribution in the limit when $R \rightarrow \infty$ and $\tilde{r} \rightarrow 0$.



Γ_0 :	Bromwich path,	
Γ_1 :	$s = p + iR$,	$p \in [0, p_0]$, $p_0 \geq 0$ arbitrary,
Γ_2 :	$s = Re^{i\varphi}$,	$\varphi \in [\frac{\pi}{2}, \varphi_0]$,
$\Gamma_{3a} \cup \Gamma_{3b}$:	$s = \rho e^{i\varphi_0}$,	$\rho \in [\tilde{r}, R]$,
Γ_4 :	$s = \tilde{r} e^{i\varphi}$,	$\varphi \in [-\varphi_0, \varphi_0]$,
$\Gamma_{5a} \cup \Gamma_{5b}$:	$s = \rho e^{-i\varphi_0}$,	$\rho \in [\tilde{r}, R]$,
Γ_6 :	$s = Re^{i\varphi}$,	$\varphi \in [-\varphi_0, -\frac{\pi}{2}]$,
Γ_7 :	$s = p - iR$,	$p \in [0, p_0]$, $p_0 \geq 0$ arbitrary,
Γ_8 :	$s = s_0 + \tilde{r} e^{i\varphi}$,	$\varphi \in [-\pi + \varphi_0, \varphi_0]$,
Γ_9 :	$s = \bar{s}_0 + \tilde{r} e^{i\varphi}$,	$\varphi \in [-\varphi_0, \pi - \varphi_0]$.

Table 9: Parametrization of integration contour Γ .

Figure 12: Integration contour Γ .

By the use of parametrization given in Table 9, the integrals in (102) are calculated as

$$\begin{aligned} 2\pi i G_\varepsilon^{(x)}(r, t) &= -\frac{1}{4\pi r} \left(\int_{\infty}^0 \frac{1}{|\tilde{c}_x^2(\rho e^{i\varphi_0})| e^{i \arg \tilde{c}_x^2(\rho e^{i\varphi_0})}} e^{-\frac{r\rho e^{i\varphi_0}}{|\tilde{c}_x(\rho e^{i\varphi_0})| e^{i \arg \tilde{c}_x(\rho e^{i\varphi_0})}}} e^{-\varepsilon\sqrt{\rho e^{i\varphi_0}}} e^{\rho t e^{i\varphi_0}} e^{i\varphi_0} d\rho \right. \\ &\quad \left. + \int_0^{\infty} \frac{1}{|\tilde{c}_x^2(\rho e^{i\varphi_0})| e^{-i \arg \tilde{c}_x^2(\rho e^{i\varphi_0})}} e^{-\frac{r\rho e^{-i\varphi_0}}{|\tilde{c}_x(\rho e^{i\varphi_0})| e^{-i \arg \tilde{c}_x(\rho e^{i\varphi_0})}}} e^{-\varepsilon\sqrt{\rho e^{-i\varphi_0}}} e^{\rho t e^{-i\varphi_0}} e^{-i\varphi_0} d\rho \right) \\ &= \frac{1}{4\pi r} \int_0^{\infty} \frac{1}{|\tilde{c}_x^2(\rho e^{i\varphi_0})|} \left(e^{-\frac{r\rho}{|\tilde{c}_x(\rho e^{i\varphi_0})|} e^{i(\varphi_0 - \arg \tilde{c}_x(\rho e^{i\varphi_0}))}} e^{-\varepsilon\sqrt{\rho e^{i\frac{\varphi_0}{2}}} e^{\rho t e^{i\varphi_0}} e^{i(\varphi_0 - \arg \tilde{c}_x^2(\rho e^{i\varphi_0}))} \right. \end{aligned}$$

$$\begin{aligned}
& - e^{-\frac{r\rho}{|\tilde{c}_x(\rho e^{i\varphi_0})|}} e^{-i(\varphi_0 - \arg \tilde{c}_x(\rho e^{i\varphi_0}))} e^{-\varepsilon\sqrt{\rho e^{-i\varphi_0}}} e^{\rho t e^{-i\varphi_0}} e^{-i(\varphi_0 - \arg \tilde{c}_x^2(\rho e^{i\varphi_0}))} \Big) d\rho \\
&= \frac{1}{4\pi r} \int_0^\infty \frac{1}{|\tilde{c}_x^2(\rho e^{i\varphi_0})|} e^{-\frac{r\rho}{|\tilde{c}_x(\rho e^{i\varphi_0})|} \cos(\varphi_0 - \arg \tilde{c}_x(\rho e^{i\varphi_0}))} e^{-\varepsilon\sqrt{\rho} \cos \frac{\varphi_0}{2}} e^{\rho t \cos \varphi_0} \\
&\quad \times \left(e^{-i\frac{r\rho}{|\tilde{c}_x(\rho e^{i\varphi_0})|} \sin(\varphi_0 - \arg \tilde{c}_x(\rho e^{i\varphi_0}))} e^{-i\varepsilon\sqrt{\rho} \sin \frac{\varphi_0}{2}} e^{i\rho t \sin \varphi_0} e^{i(\varphi_0 - \arg \tilde{c}_x^2(\rho e^{i\varphi_0}))} \right. \\
&\quad \left. - e^{i\frac{r\rho}{|\tilde{c}_x(\rho e^{i\varphi_0})|} \sin(\varphi_0 - \arg \tilde{c}_x(\rho e^{i\varphi_0}))} e^{i\varepsilon\sqrt{\rho} \sin \frac{\varphi_0}{2}} e^{-i\rho t \sin \varphi_0} e^{-i(\varphi_0 - \arg \tilde{c}_x^2(\rho e^{i\varphi_0}))} \right) d\rho \\
&= 2i \frac{1}{4\pi r} \int_0^\infty \frac{1}{|\tilde{c}_x^2(\rho e^{i\varphi_0})|} e^{\frac{\rho t \cos \varphi_0 - \frac{r\rho}{|\tilde{c}_x(\rho e^{i\varphi_0})|} \cos(\varphi_0 - \arg \tilde{c}_x(\rho e^{i\varphi_0})) - \varepsilon\sqrt{\rho} \cos \frac{\varphi_0}{2}} \\
&\quad \times \sin \left(\rho t \sin \varphi_0 - \frac{r\rho}{|\tilde{c}_x(\rho e^{i\varphi_0})|} \sin(\varphi_0 - \arg \tilde{c}_x(\rho e^{i\varphi_0})) + \varphi_0 - \arg \tilde{c}_x^2(\rho e^{i\varphi_0}) - \varepsilon\sqrt{\rho} \sin \frac{\varphi_0}{2} \right) d\rho,
\end{aligned}$$

representing the expression (68) for the regularized Green's function $G_\varepsilon^{(x)}$. It is left to prove that the remaining integrals in (103)₁ have zero contributions.

The integral along the contour Γ_1 , with the parametrization given in Table 9, becomes

$$\begin{aligned}
I_{\Gamma_1} &= \frac{1}{4\pi r} \int_{p_0}^0 \frac{1}{\tilde{c}_x^2(p+iR)} e^{-\frac{r(p+iR)}{\tilde{c}_x(p+iR)}} e^{-\varepsilon\sqrt{p+iR}} e^{(p+iR)t} dp, \text{ i.e.,} \\
&= \frac{1}{4\pi r} \int_{p_0}^0 \frac{1}{\tilde{c}_x^2(p+iR)} e^{-\frac{irR(1+\frac{p}{iR})}{\tilde{c}_x(p+iR)}} e^{-\varepsilon\sqrt{iR(1+\frac{p}{iR})}} e^{pt} e^{iRt} dp \\
&\sim \frac{1}{4\pi r} \int_{p_0}^0 \frac{1}{\kappa^2 R^\delta e^{i\frac{\delta\pi}{2}}} e^{-\frac{irR}{\kappa R^{\frac{\delta}{2}} e^{i\frac{\delta\pi}{4}}}} e^{-\varepsilon\sqrt{R} e^{i\frac{\pi}{4}}} e^{pt} e^{iRt} dp, \text{ as } R \rightarrow \infty,
\end{aligned}$$

since $\tilde{c}_x(p+iR) \sim \kappa R^{\frac{\delta}{2}} e^{i\frac{\delta\pi}{4}}$ as $R \rightarrow \infty$ with $\delta \in [0, 1)$, see (84) with κ and δ given in Tables 5, 6, 7, and 8, so that

$$\begin{aligned}
|I_{\Gamma_1}| &\leq \frac{1}{4\pi r} \int_0^{p_0} \frac{1}{\kappa^2 R^\delta} e^{-\frac{r}{\kappa} R^{1-\frac{\delta}{2}} \cos(\frac{\pi}{2} - \frac{\delta\pi}{4})} e^{-\varepsilon\sqrt{R} \cos \frac{\pi}{4}} e^{pt} dp \\
&\leq \frac{1}{4\pi r} \int_0^{p_0} \frac{1}{\kappa^2 R^\delta} e^{-R\left(\frac{r}{\kappa R^{\frac{\delta}{2}}} \sin \frac{\delta\pi}{4} + \frac{\sqrt{2}}{2} \frac{\varepsilon}{\sqrt{R}}\right)} e^{pt} dp \rightarrow 0, \text{ as } R \rightarrow \infty.
\end{aligned}$$

Note, when $\delta = 0$, the previous expression becomes

$$|I_{\Gamma_1}| \leq \frac{1}{4\pi r \kappa^2} \int_0^{p_0} e^{-\frac{\sqrt{2}}{2} \varepsilon \sqrt{R}} e^{pt} dp \rightarrow 0, \text{ as } R \rightarrow \infty,$$

due to the regularization of Greens' function in Laplace domain introduced by (67). Similar argumentation yields that integral I_{Γ_7} also tends to zero when $R \rightarrow \infty$.

The integral along the contour Γ_2 , with the parametrization given in Table 9, becomes

$$\begin{aligned}
I_{\Gamma_2} &= \frac{1}{4\pi r} \int_{\frac{\pi}{2}}^{\varphi_0} \frac{1}{\tilde{c}_x^2(Re^{i\varphi})} e^{-\frac{rRe^{i\varphi}}{\tilde{c}_x(Re^{i\varphi})}} e^{-\varepsilon\sqrt{Re^{i\varphi}}} e^{Rte^{i\varphi}} Re^{i\varphi} i d\varphi \\
&\sim \frac{1}{4\pi r} \int_{\frac{\pi}{2}}^{\varphi_0} \frac{1}{\kappa^2 R^\delta e^{i\frac{\delta\varphi}{2}}} e^{-\frac{rRe^{i\varphi}}{\kappa R^{\frac{\delta}{2}} e^{i\frac{\delta\varphi}{2}}}} e^{-\varepsilon\sqrt{R} e^{i\frac{\varphi}{2}}} e^{Rte^{i\varphi}} Re^{i\varphi} i d\varphi, \text{ as } R \rightarrow \infty,
\end{aligned}$$

since $\tilde{c}_x(Re^{i\varphi}) \sim \kappa R^{\frac{\delta}{2}} e^{i\frac{\delta\varphi}{2}}$ as $R \rightarrow \infty$ with $\delta \in [0, 1)$, see (84) with κ and δ given in Tables 5, 6, 7, and 8, so that

$$\begin{aligned}
|I_{\Gamma_2}| &\leq \frac{1}{4\pi r} \int_{\frac{\pi}{2}}^{\varphi_0} \frac{1}{\kappa^2} R^{1-\delta} e^{-\frac{r}{\kappa} R^{1-\frac{\delta}{2}} \cos((1-\frac{\delta}{2})\varphi)} e^{-\varepsilon\sqrt{R} \cos \frac{\varphi}{2}} e^{-Rt|\cos \varphi|} d\varphi \\
&\leq \frac{1}{4\pi r} \int_{\frac{\pi}{2}}^{\varphi_0} \frac{1}{\kappa^2} R^{1-\delta} e^{-R\left(t|\cos \varphi| + \frac{\varepsilon}{\sqrt{R}} \cos \frac{\varphi}{2} + \frac{r}{\kappa R^{\frac{\delta}{2}}} \cos((1-\frac{\delta}{2})\varphi)\right)} d\varphi \rightarrow 0, \text{ as } R \rightarrow \infty.
\end{aligned}$$

Note, when $\delta = 0$, the previous expression becomes

$$|I_{\Gamma_2}| \leq \frac{1}{4\pi r \kappa^2} \int_{\frac{\pi}{2}}^{\varphi_0} R e^{-R(t-\frac{r}{\kappa})|\cos \varphi|} e^{-\varepsilon\sqrt{R} \cos \frac{\varphi}{2}} d\varphi \rightarrow 0, \text{ as } R \rightarrow \infty, \text{ for } r < \kappa t.$$

The condition $r < \kappa t$ implies the finite wave propagation speed $c_x = \kappa$. Similar argumentation yields that integral I_{Γ_6} also tends to zero when $R \rightarrow \infty$.

The integral along the contour Γ_4 , with the parametrization given in Table 9, becomes

$$\begin{aligned} I_{\Gamma_4} &= \frac{1}{4\pi r} \int_{\varphi_0}^{-\varphi_0} \frac{1}{\tilde{c}_x^2(\check{r}e^{i\varphi})} e^{-\frac{r\check{r}e^{i\varphi}}{\tilde{c}_x(\check{r}e^{i\varphi})}} e^{-\varepsilon\sqrt{\check{r}e^{i\varphi}}} e^{\check{r}te^{i\varphi}} \check{r}e^{i\varphi} i d\varphi \\ &= \frac{1}{4\pi r} \int_{\varphi_0}^{-\varphi_0} \frac{1}{\kappa^2 \check{r}^\delta e^{i\delta\varphi}} e^{-\frac{r\check{r}e^{i\varphi}}{\kappa \check{r}^{\frac{\delta}{2}} e^{i\frac{\delta\varphi}{2}}} e^{-\varepsilon\sqrt{\check{r}e^{i\frac{\varphi}{2}}} e^{\check{r}te^{i\varphi}} \check{r}e^{i\varphi} i d\varphi \\ &= \frac{1}{4\pi r} \int_{\varphi_0}^{-\varphi_0} \frac{1}{\kappa^2} \check{r}^{1-\delta} e^{i(1-\delta)\varphi} e^{-\frac{\check{r}}{\kappa} \check{r}^{1-\frac{\delta}{2}} e^{i(1-\frac{\delta}{2})\varphi}} e^{-\varepsilon\sqrt{\check{r}e^{i\frac{\varphi}{2}}} e^{\check{r}te^{i\varphi}} i d\varphi, \\ &= \frac{1}{4\pi r} \int_{\varphi_0}^{-\varphi_0} \frac{1}{\kappa^2} \check{r}^{1-\delta} e^{i(1-\delta)\varphi} i d\varphi \rightarrow 0, \quad \text{as } \check{r} \rightarrow 0, \end{aligned}$$

since $\tilde{c}_x(\check{r}e^{i\varphi}) \sim \kappa \check{r}^{\frac{\delta}{2}} e^{i\frac{\delta\varphi}{4}}$ as $\check{r} \rightarrow 0$ with $\delta \in (0, 1)$, see (84) with κ and δ given in Tables 5, 6, 7, and 8.

The integral along the contour Γ_8 , according to parametrization given in Table 9 and memory function (82), becomes

$$I_{\Gamma_8} = \frac{\varrho}{4\pi r} \int_{\varphi_0}^{-\pi+\varphi_0} \frac{\Phi_\sigma(s_0 + \check{r}e^{i\varphi})}{\Phi_\varepsilon(s_0 + \check{r}e^{i\varphi})} e^{-\sqrt{\varrho r}(s_0 + \check{r}e^{i\varphi})} \sqrt{\frac{\Phi_\sigma(s_0 + \check{r}e^{i\varphi})}{\Phi_\varepsilon(s_0 + \check{r}e^{i\varphi})}} e^{-\varepsilon\sqrt{s_0 + \check{r}e^{i\varphi}}} e^{(s_0 + \check{r}e^{i\varphi})t} \check{r}e^{i\varphi} i d\varphi,$$

so if $\Phi_\sigma(s_0) = 0$, then, in the limit when $\check{r} \rightarrow 0$, the integral I_{Γ_8} tends to zero according to the previous expression, while if $\Phi_\varepsilon(s_0) = 0$, then, in the limit when $\check{r} \rightarrow 0$, the integral I_{Γ_8} behaves as

$$\begin{aligned} I_{\Gamma_8} &\sim \frac{\varrho}{4\pi r} \int_{\varphi_0}^{-\pi+\varphi_0} \frac{\Phi_\sigma(s_0)}{\Phi'_\varepsilon(s_0) \check{r}e^{i\varphi} + O(\check{r}^2)} e^{-\sqrt{\varrho r}s_0} \frac{\sqrt{\Phi_\sigma(s_0)}}{\sqrt{\Phi'_\varepsilon(s_0) \check{r}e^{i\varphi} + O(\check{r}^2)}} e^{-\varepsilon\sqrt{s_0}} e^{s_0 t} \check{r}e^{i\varphi} i d\varphi \\ &\sim i \frac{\varrho}{4\pi r} \Phi_\sigma(s_0) e^{-\varepsilon\sqrt{s_0}} e^{s_0 t} \int_{\varphi_0}^{-\pi+\varphi_0} \frac{1}{\Phi'_\varepsilon(s_0) + O(\check{r})} e^{-\sqrt{\varrho r}s_0} \sqrt{\frac{\Phi_\sigma(s_0)}{\Phi'_\varepsilon(s_0)} \frac{1}{\sqrt{\check{r}e^{i\frac{\varphi}{2}}} + O(\sqrt{\check{r}})}} d\varphi \rightarrow 0, \quad \text{as } \check{r} \rightarrow 0, \end{aligned}$$

due to

$$\Phi_\varepsilon(s_0 + \check{r}e^{i\varphi}) = \Phi_\varepsilon(s_0) + \Phi'_\varepsilon(s_0) \check{r}e^{i\varphi} + O(\check{r}^2) = \Phi'_\varepsilon(s_0) \check{r}e^{i\varphi} + O(\check{r}^2), \quad \text{as } \check{r} \rightarrow 0,$$

and

$$\begin{aligned} \frac{1}{\sqrt{\Phi_\varepsilon(s_0 + \check{r}e^{i\varphi})}} &= \frac{1}{\sqrt{\Phi'_\varepsilon(s_0) \check{r}e^{i\varphi} + O(\check{r}^2)}} = \frac{1}{\sqrt{\Phi'_\varepsilon(s_0)} \sqrt{\check{r}e^{i\frac{\varphi}{2}}}} \sqrt{1 + O(\check{r})} \\ &= \frac{1}{\sqrt{\Phi'_\varepsilon(s_0)} \sqrt{\check{r}e^{i\frac{\varphi}{2}}}} + O(\sqrt{\check{r}}), \quad \text{as } \check{r} \rightarrow 0, \end{aligned}$$

if

$$\operatorname{Re} \left(s_0 \sqrt{\frac{\Phi_\sigma(s_0)}{\Phi'_\varepsilon(s_0)}} e^{-i\frac{\varphi}{2}} \right) > 0 \quad \text{for } \varphi \in (-\pi + \varphi_0, \varphi_0),$$

transforming into

$$\begin{aligned} \varphi_0 + \frac{1}{2} \arg \Phi_\sigma(s_0) - \frac{1}{2} \arg \Phi'_\varepsilon(s_0) - \frac{\varphi}{2} &\in \left(-\frac{\pi}{2}, \frac{\pi}{2} \right), \quad \text{i.e.,} \\ \varphi_0 + \arg \Phi_\sigma(s_0) - \arg \Phi'_\varepsilon(s_0) &\in (-2\pi, \pi). \end{aligned}$$

B.2 Calculation of function $\tilde{\mathfrak{g}}^{(x)}$

The function $\tilde{\mathfrak{g}}^{(x)}$, given by (75)₂, takes the form

$$\tilde{\mathfrak{g}}^{(x)}(r, s) = \frac{1}{4\pi r} \frac{1}{s} e^{-\frac{rs}{\tilde{c}_x(s)}} = \frac{1}{4\pi r} \frac{1}{s} e^{-\sqrt{\varrho r} s} \sqrt{\frac{\Phi_\sigma(s)}{\Phi_\varepsilon(s)}},$$

due to the memory function \tilde{c}_x , given by (82), see also (34) and (42), so that function $\tilde{\mathfrak{g}}^{(x)}$ has $s = 0$ as a pole, as well as a branch point, due to the terms in functions Φ_σ and Φ_ε containing s^ξ , $\xi \in (0, 2)$. Moreover, function $\tilde{\mathfrak{g}}^{(x)}$ has a pair of complex conjugated branch points $s_0 = \rho_0 e^{i\varphi_0}$ and \bar{s}_0 , with $\varphi_0 \in (\frac{\pi}{2}, \pi)$, in the case when s_0 and \bar{s}_0 are zeros of function Φ_σ (function Φ_ε), with the possibility that instead of complex conjugated zeros s_0 and \bar{s}_0 , the function Φ_σ (function Φ_ε) may have a negative real zero or no zeros at all.

Therefore, in the Cauchy integral theorem

$$\oint_{\Gamma} \tilde{\mathbf{g}}^{(x)}(r, s) e^{st} ds = 0,$$

the integration is performed along the contour Γ , depicted in Figure 12 and taken so that the singular points $s = 0, s_0$, and \bar{s}_0 lie outside the contour Γ , in order to obtain the function $\mathbf{g}^{(x)}$ in time domain by the inversion of Laplace transform of function $\tilde{\mathbf{g}}^{(x)}$ in Laplace domain, yielding

$$\mathbf{g}^{(x)}(r, t) = \frac{1}{2\pi i} \int_{Br} \tilde{\mathbf{g}}^{(x)}(r, s) e^{st} ds = \mathcal{L}^{-1} \left[\frac{1}{4\pi r} \frac{1}{s} e^{-\frac{rs}{\tilde{c}_x(s)}} \right] (r, t),$$

where the integration is performed along the Bromwich contour Br , i.e., along the contour Γ_0 in the limit when $R \rightarrow \infty$, having Γ_0 as a part of the closed contour Γ from Figure 12, so that the Cauchy integral theorem reduces to

$$2\pi i \mathbf{g}^{(x)}(r, t) = - \lim_{\substack{R \rightarrow \infty \\ \tilde{r} \rightarrow 0}} (I_{\Gamma_{3a} \cup \Gamma_{3b}} + I_{\Gamma_{5a} \cup \Gamma_{5b}}) - \lim_{\tilde{r} \rightarrow 0} I_{\Gamma_4}, \quad (104)$$

where $I_{\Gamma_{3a} \cup \Gamma_{3b}}$, $I_{\Gamma_{5a} \cup \Gamma_{5b}}$, and I_{Γ_4} are integrals along contours $\Gamma_{3a} \cup \Gamma_{3b}$, $\Gamma_{5a} \cup \Gamma_{5b}$, and Γ_4 having non-zero contribution, since for the left-hand-side of the Cauchy integral theorem one has

$$\oint_{\Gamma} \tilde{\mathbf{g}}^{(x)}(r, s) e^{st} ds = \sum_{i=0}^9 I_{\Gamma_i}, \quad \text{with} \quad I_{\Gamma_i} = \int_{\Gamma_i} \frac{1}{4\pi r} \frac{1}{s} e^{-\frac{rs}{\tilde{c}_x(s)}} e^{st} ds, \quad (105)$$

where the integrals $I_{\Gamma_1}, I_{\Gamma_2}, I_{\Gamma_6}, I_{\Gamma_7}, I_{\Gamma_8}$, and I_{Γ_9} have zero contribution in the limit when $R \rightarrow \infty$ and $\tilde{r} \rightarrow 0$.

By the use of parametrization given in Table 9, the integrals in (104) are calculated as

$$\begin{aligned} 2\pi i \mathbf{g}^{(x)}(r, t) &= -\frac{1}{4\pi r} \left(\int_{\infty}^0 \frac{1}{\rho e^{i\varphi_0}} e^{-\frac{r\rho e^{i\varphi_0}}{|\tilde{c}_x(\rho e^{i\varphi_0})| e^{i \arg \tilde{c}_x(\rho e^{i\varphi_0})}}} e^{\rho t e^{i\varphi_0}} e^{i\varphi_0} d\rho \right. \\ &\quad \left. + \int_0^{\infty} \frac{1}{\rho e^{-i\varphi_0}} e^{-\frac{r\rho e^{-i\varphi_0}}{|\tilde{c}_x(\rho e^{-i\varphi_0})| e^{-i \arg \tilde{c}_x(\rho e^{-i\varphi_0})}}} e^{\rho t e^{-i\varphi_0}} e^{-i\varphi_0} d\rho + \lim_{\tilde{r} \rightarrow 0} \int_{\varphi_0}^{-\varphi_0} \frac{1}{\tilde{r} e^{i\varphi}} e^{-\frac{r\tilde{r} e^{i\varphi}}{\tilde{c}_x(\tilde{r} e^{i\varphi})}} e^{\tilde{r} t e^{i\varphi}} \tilde{r} e^{i\varphi} i d\varphi \right) \\ &= \frac{1}{4\pi r} \int_0^{\infty} \frac{1}{\rho} \left(e^{-\frac{r\rho}{|\tilde{c}_x(\rho e^{i\varphi_0})|}} e^{i(\varphi_0 - \arg \tilde{c}_x(\rho e^{i\varphi_0}))} e^{\rho t e^{i\varphi_0}} \right. \\ &\quad \left. - e^{-\frac{r\rho}{|\tilde{c}_x(\rho e^{i\varphi_0})|}} e^{-i(\varphi_0 - \arg \tilde{c}_x(\rho e^{i\varphi_0}))} e^{\rho t e^{-i\varphi_0}} \right) d\rho - \frac{1}{4\pi r} \lim_{\tilde{r} \rightarrow 0} \int_{\varphi_0}^{-\varphi_0} e^{-\frac{r\tilde{r} e^{i\varphi}}{\tilde{c}_x(\tilde{r} e^{i\varphi})}} e^{\tilde{r} t e^{i\varphi}} i d\varphi \\ &= \frac{1}{4\pi r} \int_0^{\infty} \frac{1}{\rho} e^{-\frac{r\rho}{|\tilde{c}_x(\rho e^{i\varphi_0})|} \cos(\varphi_0 - \arg \tilde{c}_x(\rho e^{i\varphi_0}))} e^{-\rho t |\cos \varphi_0|} \\ &\quad \times \left(e^{-i \frac{r\rho}{|\tilde{c}_x(\rho e^{i\varphi_0})|} \sin(\varphi_0 - \arg \tilde{c}_x(\rho e^{i\varphi_0}))} e^{i\rho t \sin \varphi_0} \right. \\ &\quad \left. - e^{i \frac{r\rho}{|\tilde{c}_x(\rho e^{i\varphi_0})|} \sin(\varphi_0 - \arg \tilde{c}_x(\rho e^{i\varphi_0}))} e^{-i\rho t \sin \varphi_0} \right) d\rho - \frac{1}{4\pi r} \int_{\varphi_0}^{-\varphi_0} i d\varphi \\ &= 2i \frac{1}{4\pi r} \int_0^{\infty} \frac{1}{\rho} e^{-\left(\rho t |\cos \varphi_0| + \frac{r\rho}{|\tilde{c}_x(\rho e^{i\varphi_0})|} \cos(\varphi_0 - \arg \tilde{c}_x(\rho e^{i\varphi_0})) \right)} \\ &\quad \times \sin \left(\rho t \sin \varphi_0 - \frac{r\rho}{|\tilde{c}_x(\rho e^{i\varphi_0})|} \sin(\varphi_0 - \arg \tilde{c}_x(\rho e^{i\varphi_0})) \right) d\rho + \frac{1}{4\pi r} 2i\varphi_0, \end{aligned}$$

representing the expression (74), where the behavior $\tilde{c}_x(\tilde{r} e^{i\varphi}) \sim \kappa \tilde{r}^{\frac{\delta}{2}} e^{i \frac{\delta\varphi}{4}}$ as $\tilde{r} \rightarrow 0$ with $\delta \in (0, 1)$, see (84) with κ and δ given in Tables 5, 6, 7, and 8, is used. One can prove that the remaining integrals in (105)₁ have zero contribution as in the case of calculation of Green's function in Section B.1.

B.3 Calculation of short-time asymptotics of Green's function

The expression for short-time asymptotics of Green's function takes the form (63) if wave propagation speed is finite, i.e., if glass modulus $\sigma_{sr/g}^{(x)}$ attains a finite value, which can be further justified by taking into account the asymptotics of regularization of Green's function in Laplace domain

$$\tilde{G}_{\varepsilon}^{(x)}(r, s) \sim \tilde{G}_{\varepsilon, \text{asy}}^{(x)}(r, s) = \frac{1}{4\pi r \kappa^2} e^{-\frac{rs}{\kappa}} e^{-\varepsilon \sqrt{s}}, \quad \text{for } s \rightarrow \infty, \quad (106)$$

that follows from the regularized Green's function in Laplace domain (64), with (58) and (66), due to the asymptotics (84) of memory functions \tilde{c}_x and parameters κ and δ given in Tables 5 and 6, so that the asymptotics (106) implies

$$\begin{aligned} G_\varepsilon^{(x)}(r, s) &\sim G_{\varepsilon, \text{asy}}^{(x)}(r, t) = \frac{1}{4\pi r \kappa^2} \mathcal{L}^{-1} \left[e^{-\varepsilon \sqrt{s}} \right] \left(t - \frac{r}{\kappa} \right) \\ &= \frac{1}{4\pi r \kappa^2} \frac{\varepsilon}{2t' \sqrt{\pi t'}} e^{-\frac{\varepsilon^2}{4t'}} \Big|_{t'=t-\frac{r}{\kappa}} \\ &= \frac{1}{4\pi r \kappa^2} \delta_\varepsilon \left(t - \frac{r}{\kappa} \right), \quad \text{for } t \rightarrow 0, \end{aligned} \quad (107)$$

according to (66), yielding

$$G^{(x)}(r, s) \sim G_{\text{asy}}^{(x)}(r, t) = \lim_{\varepsilon \rightarrow 0} G_{\varepsilon, \text{asy}}^{(x)}(r, t) = \frac{1}{4\pi r \kappa^2} \delta \left(t - \frac{r}{\kappa} \right), \quad \text{for } t \rightarrow 0,$$

which confirms Green's function short-time asymptotics (63).

The integral representation of the asymptotics of regularized Green's function (107) is obtained as the Laplace inversion of (106), being of the form

$$G_{\varepsilon, \text{asy}}^{(x)}(r, t) = \frac{1}{2\pi i} \int_{Br} \tilde{G}_{\varepsilon, \text{asy}}^{(x)}(r, s) e^{st} ds = \mathcal{L}^{-1} \left[\frac{1}{4\pi r \kappa^2} e^{-\frac{rs}{\kappa}} e^{-\varepsilon \sqrt{s}} \right] (r, t),$$

where the integration is performed along the Bromwich contour Br , i.e., along the contour Γ_0 in the limit when $R \rightarrow \infty$, having Γ_0 as a part of the closed contour Γ from Figure 13, which follows from the Cauchy integral theorem

$$\oint_{\Gamma} \tilde{G}_{\varepsilon, \text{asy}}^{(x)}(r, s) e^{st} ds = 0,$$

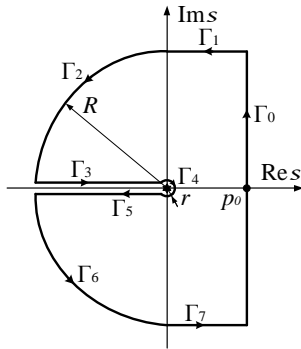
with integration performed along the contour Γ , depicted in Figure 13, yielding

$$2\pi i G_{\varepsilon, \text{asy}}^{(x)}(r, t) = - \lim_{\substack{R \rightarrow \infty \\ \check{r} \rightarrow 0}} (I_{\Gamma_3} + I_{\Gamma_5}), \quad (108)$$

where I_{Γ_3} and I_{Γ_5} are integrals along contours Γ_3 and Γ_5 having non-zero contribution, since for the left-hand-side of Cauchy integral theorem one has

$$\oint_{\Gamma} \tilde{G}_{\varepsilon, \text{asy}}^{(x)}(r, s) e^{st} ds = \sum_{i=0}^7 I_{\Gamma_i}, \quad \text{with } I_{\Gamma_i} = \int_{\Gamma_i} \frac{1}{4\pi r \kappa^2} e^{-\frac{rs}{\kappa}} e^{-\varepsilon \sqrt{s}} e^{st} ds, \quad (109)$$

where the integrals I_{Γ_1} , I_{Γ_2} , I_{Γ_4} , I_{Γ_6} , and I_{Γ_7} have zero contribution in the limit when $R \rightarrow \infty$ and $\check{r} \rightarrow 0$.



Γ_0 :	Bromwich path,	
Γ_1 :	$s = p + iR,$	$p \in [0, p_0], p_0 \geq 0$ arbitrary,
Γ_2 :	$s = R e^{i\varphi},$	$\varphi \in [\frac{\pi}{2}, \pi],$
Γ_3 :	$s = \rho e^{i\pi},$	$\rho \in [\check{r}, R],$
Γ_4 :	$s = \check{r} e^{i\varphi},$	$\varphi \in [-\pi, \pi],$
Γ_5 :	$s = \rho e^{-i\pi},$	$\rho \in [\check{r}, R],$
Γ_6 :	$s = R e^{-i\varphi},$	$\varphi \in [-\pi, -\frac{\pi}{2}],$
Γ_7 :	$s = p - iR,$	$p \in [0, p_0], p_0 \geq 0$ arbitrary.

Table 10: Parametrization of integration contour Γ .

Figure 13: Integration contour Γ .

By the use of parametrization given in Table 10, the integrals in (108) are calculated as

$$\begin{aligned} 2\pi i G_{\varepsilon, \text{asy}}^{(x)}(r, t) &= - \frac{1}{4\pi r \kappa^2} \left(\int_{\infty}^0 e^{-\frac{r\rho e^{i\pi}}{\kappa}} e^{-\varepsilon \sqrt{\rho e^{i\pi}}} e^{\rho t e^{i\pi}} e^{i\pi} d\rho + \int_0^{\infty} e^{-\frac{r\rho e^{-i\pi}}{\kappa}} e^{-\varepsilon \sqrt{\rho e^{-i\pi}}} e^{\rho t e^{-i\pi}} e^{-i\pi} d\rho \right) \\ &= \frac{1}{4\pi r \kappa^2} \int_0^{\infty} e^{-\rho(t-\frac{r}{\kappa})} \left(e^{i\varepsilon \sqrt{\rho}} - e^{-i\varepsilon \sqrt{\rho}} \right) d\rho \\ &= 2i \frac{1}{4\pi r \kappa^2} \int_0^{\infty} e^{-\rho(t-\frac{r}{\kappa})} \sin(\varepsilon \sqrt{\rho}) d\rho, \end{aligned}$$

yielding the integral representation of the asymptotics of regularized Green's function (107), given by (69). One can prove that the remaining integrals in (109)₁ have zero contributions as in the case of calculation of Green's function in Section B.1.

If wave propagation speed is infinite, i.e., if glass modulus $\sigma_{sr/g}^{(x)}$ attains a infinite value, then the asymptotic expression takes the form (71), which is obtained using the Cauchy integral theorem

$$\oint_{\Gamma} \tilde{G}_{\text{asy}}^{(x)}(r, s) e^{st} ds = 0,$$

where integration is performed along the contour Γ , depicted in Figure 13, since

$$\tilde{G}^{(x)}(r, s) \sim \tilde{G}_{\text{asy}}^{(x)}(r, s) = \frac{1}{4\pi r \kappa^2} \frac{1}{s^\delta} e^{-\frac{r}{\kappa} s^{1-\frac{\delta}{2}}}, \quad \text{for } s \rightarrow \infty, \quad (110)$$

being short-time asymptotics of Green's function in Laplace domain, see also (70), and originating from the expression of Green's functions in Laplace domain (58) with asymptotics (84) of memory functions \tilde{c}_x and parameters κ and δ given in Tables 5, 6, 7, and 8, has a branch point $s = 0$, due to the term s^δ , $\delta \in (0, 1)$.

Therefore, in order to obtain the asymptotic behavior of Green's function in time domain, the Laplace inversion of Green's function asymptotics (110) is carried out, yielding

$$G_\varepsilon^{(x)}(r, s) \sim G_{\text{asy}}^{(x)}(r, t) = \frac{1}{2\pi i} \int_{Br} \tilde{G}_{\text{asy}}^{(x)}(r, s) e^{st} ds = \mathcal{L}^{-1} \left[\frac{1}{4\pi r \kappa^2} \frac{1}{s^\delta} e^{-\frac{r}{\kappa} s^{1-\frac{\delta}{2}}} \right] (r, t),$$

where integration is performed along the Bromwich contour Br , i.e., along the contour Γ_0 in the limit when $R \rightarrow \infty$, having Γ_0 as a part of the closed contour Γ from Figure 13, so that the Cauchy integral theorem reduces to

$$2\pi i G_{\text{asy}}^{(x)}(r, t) = - \lim_{\substack{R \rightarrow \infty \\ \check{r} \rightarrow 0}} (I_{\Gamma_3} + I_{\Gamma_5}), \quad (111)$$

where I_{Γ_3} and I_{Γ_5} are integrals along contours Γ_3 and Γ_5 having non-zero contribution, since for the left-hand-side of Cauchy integral theorem one has

$$\oint_{\Gamma} \tilde{G}_{\text{asy}}^{(x)}(r, s) e^{st} ds = \sum_{i=0}^7 I_{\Gamma_i}, \quad \text{with } I_{\Gamma_i} = \int_{\Gamma_i} \frac{1}{4\pi r \kappa^2} \frac{1}{s^\delta} e^{-\frac{r}{\kappa} s^{1-\frac{\delta}{2}}} e^{st} ds, \quad (112)$$

where the integrals I_{Γ_1} , I_{Γ_2} , I_{Γ_4} , I_{Γ_6} , and I_{Γ_7} have zero contribution in the limit when $R \rightarrow \infty$ and $\check{r} \rightarrow 0$.

By the use of parametrization given in Table 10, the integrals in (111) are calculated as

$$\begin{aligned} 2\pi i G_{\text{asy}}^{(x)}(r, t) &= -\frac{1}{4\pi r \kappa^2} \left(\int_{\infty}^0 \frac{1}{\rho^\delta e^{i\delta\pi}} e^{-\frac{r}{\kappa} \rho^{1-\frac{\delta}{2}}} e^{i(1-\frac{\delta}{2})\pi} e^{\rho t e^{i\pi}} e^{i\pi} d\rho + \int_0^{\infty} \frac{1}{\rho^\delta e^{-i\delta\pi}} e^{-\frac{r}{\kappa} \rho^{1-\frac{\delta}{2}}} e^{-i(1-\frac{\delta}{2})\pi} e^{\rho t e^{-i\pi}} e^{-i\pi} d\rho \right) \\ &= -\frac{1}{4\pi r \kappa^2} \int_0^{\infty} \frac{1}{\rho^\delta} \left(e^{\frac{r}{\kappa} \rho^{1-\frac{\delta}{2}}} e^{-i\frac{\delta\pi}{2}} e^{-i\delta\pi} - e^{\frac{r}{\kappa} \rho^{1-\frac{\delta}{2}}} e^{i\frac{\delta\pi}{2}} e^{i\delta\pi} \right) e^{-\rho t} d\rho \\ &= \frac{1}{4\pi r \kappa^2} \int_0^{\infty} \frac{1}{\rho^\delta} e^{\frac{r}{\kappa} \rho^{1-\frac{\delta}{2}} \cos \frac{\delta\pi}{2}} e^{-\rho t} \left(e^{i\left(\frac{r}{\kappa} \rho^{1-\frac{\delta}{2}} \sin \frac{\delta\pi}{2} + \delta\pi\right)} - e^{-i\left(\frac{r}{\kappa} \rho^{1-\frac{\delta}{2}} \sin \frac{\delta\pi}{2} + \delta\pi\right)} \right) d\rho \\ &= 2i \frac{1}{4\pi r \kappa^2} \int_0^{\infty} \frac{1}{\rho^\delta} e^{-\rho \left(t - \frac{r}{\kappa} \rho^{-\frac{\delta}{2}} \cos \frac{\delta\pi}{2} \right)} \sin \left(\frac{r}{\kappa} \rho^{1-\frac{\delta}{2}} \sin \frac{\delta\pi}{2} + \delta\pi \right) d\rho, \end{aligned}$$

yielding the expression (71) for short-time asymptotic behavior of Green's functions $G_{\text{asy}}^{(x)}$ in the case when wave propagation speed is infinite. One can prove that the remaining integrals in (112)₁ have zero contributions as in the case of calculation of Green's function in Section B.1.

C Validity of condition needed for Fourier transform inversion

In order to obtain Green's function in Laplace domain $\tilde{G}^{(x)}$, see (58), the inverse Fourier transform can be applied to Green's function in Fourier and Laplace domain $\tilde{\tilde{G}}^{(x)}$, see (47)₂ and (48)₂, provided that the condition

$$\text{Re} \frac{s^2}{\tilde{c}_x^2(s)} > 0 \quad \text{for } \text{Re } s > 0, \quad (113)$$

is satisfied, as noted in Section 2.2. The condition (113) is equivalent to the request that the function

$$s^2 + k^2 \tilde{c}_x^2(s) = \tilde{c}_x^2(s) \left(k^2 + \frac{s^2}{\tilde{c}_x^2(s)} \right) \neq 0, \quad \text{for } k \in \mathbb{R}, \text{Re } s > 0, \quad (114)$$

since $\tilde{c}_x^2(s) = \frac{1}{\varrho} \frac{\Phi_\varepsilon(s)}{\Phi_\sigma(s)}$, see (82), has neither zeros nor poles for $\text{Re } s > 0$, while the term in brackets is non-zero if $\text{Re } \frac{s^2}{\tilde{c}_x^2(s)} > 0$ for $\text{Re } s > 0$.

The validity of condition (113), through its equivalent form (114), is checked in Section 4 of [18] for linear fractional-order models having differentiation orders up to one, given by (19), while condition's validity in the case of thermodynamically consistent fractional Burgers models, given by (24), is proved in Appendix A of [27].

In the case of fractional anti-Zener and Zener models, listed in Table 1, the condition (114) reads

$$s^2 + \frac{k^2}{\varrho} s^\xi \frac{\phi_\varepsilon(s)}{\phi_\sigma(s)} \neq 0, \quad \text{for } k \in \mathbb{R}, \text{Re } s > 0, \quad (115)$$

according to (83), with functions ϕ_ε and ϕ_σ listed in Table 4. Considering the model I⁺ID.ID, used in numerical examples in Section 3 and given by (77), one finds that condition (115) becomes

$$s^2 + \frac{k^2}{\varrho} s^{\beta+\nu} \frac{b_1 + b_2 s^{\alpha+\beta}}{a_1 + a_2 s^{\alpha+\beta} + a_3 s^{2(\alpha+\beta)}} \neq 0, \quad \text{for } k \in \mathbb{R}, \text{Re } s > 0, \quad (116)$$

so that, using the substitution $s = \rho e^{i\varphi}$, $\rho > 0$, $\varphi \in [-\frac{\pi}{2}, \frac{\pi}{2}]$, and by separating real and imaginary parts, condition's imaginary part takes the form

$$F(\rho, \varphi) = \rho^2 \sin(2\varphi) + \frac{k^2}{\varrho} \frac{\rho^{\beta+\nu}}{|a_1 + a_2 s^{\alpha+\beta} + a_3 s^{2(\alpha+\beta)}|^2} f(\rho, \varphi) \neq 0, \quad (117)$$

with

$$\begin{aligned} f(\rho, \varphi) &= a_1 b_1 \sin((\beta + \nu)\varphi) + a_1 b_2 \rho^{\alpha+\beta} \sin((\alpha + 2\beta + \nu)\varphi) \\ &\quad + a_2 b_1 \rho^{\alpha+\beta} \sin((\nu - \alpha)\varphi) + a_2 b_2 \rho^{2(\alpha+\beta)} \sin((\beta + \nu)\varphi) \\ &\quad - a_3 b_1 \rho^{2(\alpha+\beta)} \sin((2\alpha + \beta - \nu)\varphi) + a_3 b_2 \rho^{3(\alpha+\beta)} \sin((\nu - \alpha)\varphi). \end{aligned} \quad (118)$$

Note, if $\varphi \rightarrow -\varphi$, then function F , defined in (117), satisfies $F(\rho, \varphi) = -F(\rho, \varphi)$ and therefore it is sufficient to consider the interval $\varphi \in [0, \frac{\pi}{2}]$. Moreover, if $\varphi = 0$, then $s = \rho$ and hence

$$\rho^2 + \frac{k^2}{\varrho} \rho^{\beta+\nu} \frac{b_1 + b_2 \rho^{\alpha+\beta}}{a_1 + a_2 \rho^{\alpha+\beta} + a_3 \rho^{2(\alpha+\beta)}} > 0, \quad \text{for } \rho > 0,$$

by (116), so that one considers the interval $\varphi \in (0, \frac{\pi}{2}]$.

If function $f(\rho, \varphi) > 0$ for $\rho > 0$ and $\varphi \in (0, \frac{\pi}{2}]$, then one has that function $F(\rho, \varphi) > 0$ and hence different from zero, since all other terms in F are positive. Rewriting the function f , given by (118), as

$$\begin{aligned} f(\rho, \varphi) &= a_1 b_1 \sin((\beta + \nu)\varphi) + a_1 b_2 \rho^{\alpha+\beta} \sin((\alpha + 2\beta + \nu)\varphi) \\ &\quad + a_2 b_1 \rho^{\alpha+\beta} \sin((\nu - \alpha)\varphi) + a_3 b_2 \rho^{3(\alpha+\beta)} \sin((\nu - \alpha)\varphi) \\ &\quad + a_3 b_2 \rho^{2(\alpha+\beta)} \sin((2\alpha + \beta - \nu)\varphi) \left(\frac{a_2}{a_3} \frac{\sin((\beta + \nu)\varphi)}{\sin((2\alpha + \beta - \nu)\varphi)} - \frac{b_1}{b_2} \right) \end{aligned}$$

one has that $f(\rho, \varphi) > 0$ for $\rho > 0$ and $\varphi \in (0, \frac{\pi}{2}]$ if

$$\frac{b_1}{b_2} < \frac{a_2}{a_3} \frac{\sin((\beta + \nu)\varphi)}{\sin((2\alpha + \beta - \nu)\varphi)}, \quad (119)$$

since all other terms are non-negative according to the thermodynamical restrictions (78). In order to prove (119), becoming

$$\frac{b_1}{b_2} \leq \frac{a_2}{a_3} \frac{\sin \frac{(\beta+\nu)\pi}{2}}{\sin \frac{(2\alpha+\beta-\nu)\pi}{2}} < \frac{a_2}{a_3} \frac{\sin((\beta + \nu)\varphi)}{\sin((2\alpha + \beta - \nu)\varphi)},$$

due to the thermodynamical restrictions (79) and property of function g . Namely, one considers function g and its first derivative g' :

$$g(\varphi) = \frac{\sin(\zeta\varphi)}{\sin(\xi\varphi)} > 0 \quad \text{and} \quad g'(\varphi) = \frac{\xi\varphi\zeta\varphi \cos(\xi\varphi) \cos(\zeta\varphi)}{\varphi \sin^2(\xi\varphi)} \left(\frac{\tan(\xi\varphi)}{\xi\varphi} - \frac{\tan(\zeta\varphi)}{\zeta\varphi} \right) < 0,$$

with $0 < \xi < \zeta < 1$ on the interval $\varphi \in (0, \frac{\pi}{2}]$, for which one has

$$g(\varphi) > g\left(\frac{\pi}{2}\right), \quad \text{for } \varphi \in \left(0, \frac{\pi}{2}\right],$$

since function $g(\varphi)$ is a decreasing function for $\varphi \in (0, \frac{\pi}{2}]$, due to the function $\frac{\tan x}{x}$ being monotonically increasing for $x \in (0, \frac{\pi}{2}]$.

Note, the same procedure can be followed for proving the condition (114) in the case of all other fractional anti-Zener and Zener models, listed in Table 1.

Acknowledgements

The work is supported by the Ministry of Science, Technological Development and Innovation of the Republic of Serbia under grant 451-03-47/2023-01/200125 (SJ and DZ).

References

- [1] J. Abate and P. P. Valkó. Multi-precision Laplace transform inversion. *International Journal for Numerical Methods in Engineering*, 60:979–993, 2004.
- [2] J. Archenbach. *Wave Propagation in Elastic Solids*. North Holland, Amsterdam, 1973.
- [3] T. M. Atanackovic, S. Konjik, Lj. Oparnica, and D. Zorica. Thermodynamical restrictions and wave propagation for a class of fractional order viscoelastic rods. *Abstract and Applied Analysis*, 2011:ID975694–1–32, 2011.
- [4] M. V. Ayzenberg-Stepanenko, E. N. Sherb, G. G. Osharovich, and Z. Sh. Yanovitskaya. Numerical simulation of shock wave processes in elastic media and structures. Part II: Application results. *Journal of Mining Science*, 48:84–103, 2012.
- [5] F. Broucke and Lj. Oparnica. Micro-local and qualitative analysis of the fractional Zener wave equation. *Journal of Differential Equations*, 321:217–257, 2022.
- [6] F. Broucke and Lj. Oparnica. Distributed-order time-fractional wave equations. *Zeitschrift für angewandte Mathematik und Physik*, 74:19–1–25, 2023.
- [7] A. Callejas, J. Melchor, I. H. Faris, and G. Rus. Viscoelastic model characterization of human cervical tissue by torsional waves. *Journal of the mechanical behavior of biomedical materials*, 115:104261–1–15, 2021.
- [8] L. Cardoso and S. C. Cowin. Role of structural anisotropy of biological tissues in poroelastic wave propagation. *Mechanics of Materials*, 44:174–188, 2012.
- [9] A. Chen, Y. Wang, G. Yu, Y. Guo, and Z. Wang. Elastic wave localization in two-dimensional phononic crystals with one-dimensional quasi-periodicity and random disorder. *Acta Mechanica Solida Sinica*, 21:517–528, 2008.
- [10] C. Dorn and D. M. Kochmann. Ray theory for elastic wave propagation in graded metamaterials. *Journal of the Mechanics and Physics of Solids*, 168:105049–1–21, 2022.
- [11] W. J. Drugan. Wave propagation effects possible in solid composite materials by use of stabilized negative-stiffness components. *Journal of the Mechanics and Physics of Solids*, 136:103700–1–13, 2020.
- [12] Y. Hayati and M. E. Ghadi. Three-dimensional coupled thermoelastodynamic stress and flux induced wave propagation for isotropic half-space with scalar potential functions. *Zeitschrift für angewandte Mathematik und Physik*, 69:1–32, 2018.
- [13] S. Jelić and D. Zorica. Fractional Burgers wave equation on a finite domain. *Chaos, Solitons, and Fractals*, 154:111632–1–26, 2022.
- [14] S. Jelić and D. Zorica. Energy balance for fractional anti-Zener and Zener models in terms of relaxation modulus and creep compliance. *Applied Mathematical Modelling*, 123:688–728, 2023.
- [15] S. Jelić and D. Zorica. Fractionalization of anti-Zener and Zener models via rheological analogy. *Acta Mechanica*, 234:313–354, 2023.
- [16] S. Jelić and D. Zorica. Stress and power as a response to harmonic excitation of a fractional anti-Zener and Zener type viscoelastic body. *arXiv:2311.09798*, pages 1–29, 2023.
- [17] A. A. Kilbas, H. M. Srivastava, and J. J. Trujillo. *Theory and Applications of Fractional Differential Equations*. Elsevier B.V., Amsterdam, 2006.

- [18] S. Konjik, Lj. Oparnica, and D. Zorica. Distributed-order fractional constitutive stress-strain relation in wave propagation modeling. *Zeitschrift für angewandte Mathematik und Physik*, 70:51–1–21, 2019.
- [19] X. Liu. Difference methods for time discretization of spectral fractional stochastic wave equation. *Communications in Nonlinear Science and Numerical Simulation*, 116:106863–1–17, 2023.
- [20] Y. Luchko. Fractional wave equation and damped waves. *Journal of Mathematical Physics*, 54:031505–1–16, 2013.
- [21] F. Mainardi. *Fractional Calculus and Waves in Linear Viscoelasticity*. Imperial College Press, London, 2010.
- [22] J. Meng, Z. Deng, X. Xu, K. Zhang, and X. Hou. A precise method for solving wave propagation in hollow sandwich cylinders with prismatic cores. *Acta Mechanica Solida Sinica*, 28:360–374, 2015.
- [23] S. P. Näsholm and S. Holm. On a fractional Zener elastic wave equation. *Fractional Calculus and Applied Analysis*, 16:26–50, 2013.
- [24] A. S. Okuka and D. Zorica. Formulation of thermodynamically consistent fractional Burgers models. *Acta Mechanica*, 229:3557–3570, 2018.
- [25] A. S. Okuka and D. Zorica. Fractional Burgers models in creep and stress relaxation tests. *Applied Mathematical Modelling*, 77:1894–1935, 2020.
- [26] Lj. Oparnica and E. Süli. Well-posedness of the fractional Zener wave equation for heterogenous viscoelastic materials. *Fractional Calculus and Applied Analysis*, 23:126–166, 2020.
- [27] Lj. Oparnica, D. Zorica, and A. S. Okuka. Fractional Burgers wave equation. *Acta Mechanica*, 230:4321–4340, 2019.
- [28] F. Pled and C. Desceliers. Review and recent developments on the perfectly matched layer (PML) method for the numerical modeling and simulation of elastic wave propagation in unbounded domains. *Archives of Computational Methods in Engineering*, 29:471–518, 2022.
- [29] P. Ponnusamy and M. Rajagopal. Wave propagation in a transversely isotropic thermoelastic solid cylinder of arbitrary cross-section. *Acta Mechanica Solida Sinica*, 24:527–538, 2011.
- [30] S. G. Pshenichnov. Nonstationary dynamic problems of nonlinear viscoelasticity. *Mechanics of Solids*, 48:83–95, 2013.
- [31] K. Ryuzono, S. Yashiro, S. Onodera, and N. Toyama. Performance evaluation of crack identification using density-based topology optimization for experimentally visualized ultrasonic wave propagation. *Mechanics of Materials*, 172:104406–1–16, 2022.
- [32] I. Sarkar, S. Banerjee, and S. Shaw. Memory-dependent generalized thermoelasticity with finite wave speeds. *Mechanics of Materials*, 153:103655–1–10, 2021.
- [33] K. Shukla, J. M. Carcione, R. C. Pestana, P. Jaiswal, and T. Özdenvar. Modeling the wave propagation in viscoacoustic media: An efficient spectral approach in time and space domain. *Computers and Geosciences*, 126:31–40, 2019.
- [34] W. J. Sim and S. H. Lee. Finite element analysis of transient dynamic viscoelastic problems in time domain. *Journal of Mechanical Science and Technology*, 19:61–71, 2005.
- [35] J. Singh and S. K. Tomar. Plane waves in thermo-elastic material with voids. *Mechanics of Materials*, 39:932–940, 2007.
- [36] P. Singh, A. K. Singh, and A. Chattopadhyay. Reflection of three-dimensional plane waves at the free surface of a rotating triclinic half-space under the context of generalized thermoelasticity. *Applied Mathematics and Mechanics*, 42:1363–1378, 2021.
- [37] N. H. Sweilam, M. M. Abou Hasan, and S. A. Alkhatib. Time fractional of nonlinear heat-wave propagation in a rigid thermal conductor: Numerical treatment. *Alexandria Engineering Journal*, 61:10153–10159, 2022.
- [38] P. Tandel, H. Patel, and T. Patel. Tsunami wave propagation model: A fractional approach. *Journal of Ocean Engineering and Science*, 7:509–520, 2022.
- [39] B. Tripathi, D. Espíndola, and G. F. Pinton. Modeling and simulations of two dimensional propagation of shear shock waves in relaxing soft solids. *Journal of Computational Physics*, 395:205–222, 2019.

- [40] C. Wang, X. Chena, P. Wei, and Y. Li. Reflection of elastic waves at the elastically supported boundary of a couple stress elastic half-space. *Acta Mechanica Solida Sinica*, 30:154–164, 2017.
- [41] N. Wang, G. Xing, T. Zhu, H. Zhou, and Y. Shi. Propagating seismic waves in VTI attenuating media using fractional viscoelastic wave equation. *Journal of Geophysical Research: Solid Earth*, 127:e2021JB023280–1–31, 2022.
- [42] Y. Wang and M. F. Insana. Wave propagation in viscoelastic materials. In I. Nenadic, M. Urban, J. Greenleaf, J-L. Gennisson, M. Bernal, and M. Tanter, editors, *Ultrasound Elastography for Biomedical Applications and Medicine*, chapter 9. John Wiley & Sons, Hoboken, 2019.
- [43] L. Xu, H. Fan, and Y. Zhou. Torsional wave in a circular micro-tube with clogging attached to the inner surface. *Acta Mechanica Solida Sinica*, 30:299–305, 2017.
- [44] W. Zhang. A numerical method for wave propagation in viscoelastic stratified porous media. *Transport in Porous Media*, 61:15–24, 2005.
- [45] Y. Zhou, Q. Wang, and Z. Zhang. Physical properties preserving numerical simulation of stochastic fractional nonlinear wave equation. *Communications in Nonlinear Science and Numerical Simulation*, 99:105832–1–20, 2021.
- [46] D. Zorica and Lj. Oparnica. Energy dissipation for hereditary and energy conservation for non-local fractional wave equations. *Philosophical Transactions of the Royal Society A*, 378:20190295–1–24, 2020.